Doklady Physics, Vol. 46, No. 10, 2001, pp. 687–689. Translated from Doklady Akademii Nauk, Vol. 380, No. 4, 2001, pp. 469–471.

PHYSICS

Magnonic Crystals and Spin Waves in Periodic Structures

Academician Yu. V. Gulyaev and S. A. Nikitov

Received April 5, 2001

We study the propagation of spin waves through a periodic structure consisting of ferromagnetic layers of equal thickness but different magnetization. The wave spectrum contains forbidden zones determined by the parameters of both the structure and external magnetic field. The wave propagation in such a structure is impossible if its frequency lies in a forbidden zone. In the presence of a layer with different thickness and magnetization, the structure symmetry is violated; this leads to the possibility of spin-mode localization on a structure defect. The coefficients of wave reflection from a periodic structure of finite thickness and of wave propagation through such a structure are calculated. By analogy with the known photonic crystals, in which non-transmission zones arise in the spectrum when light propagates through a crystal, such magnetic superlattices can be termed magnonic crystals.

In recent years, the problem associated with controlling and manipulating the optical properties of crystals has received much attention. In particular, materials in which light can propagate only in certain directions or generally can be localized in certain areas are designed, constructed, and investigated. Since the properties of light propagating in them closely resemble those of electrons in actual crystals, these materials have come to be known as photonic crystals [1]. In its basis, a photonic crystal represents a material whose index of light refraction varies periodically. The most simple example of a photonic crystal, also called a one-dimensional photonic crystal, is a one-dimensional multilayered periodic structure [2]. The spectrum of optical radiation propagating through such a structure has forbidden frequency gaps. Light with frequencies lying in a forbidden gap cannot propagate in the direction perpendicular to the plane of such a structure. Afterwards, two- and three-dimensional photonic crystals were also modeled and obtained [3]. Three-dimensional crystals, in addition, can have an absolutely forbidden gap. This implies that the light in such crystals has no possibility of propagating along any direction. Recently it was demonstrated that even a one-dimensional photonic crystal can have an absolutely forbidden gap [4, 5] if a proper choice of layers is performed in a multilayered structure. By analogy with photonic crystals, phononic crystals [in which acoustic waves (phonons) exhibit properties similar to those of light] were also modeled and obtained [6]. The properties of certain photonic crystals can be governed by varying the external magnetic field if one or all layers in a periodic structure are made of a magnetic material [7].

It is possible to create materials similar to photonic and phononic crystals in which information is transferred by spin waves. Such materials possess forbidden gaps for propagating spin waves and can be termed *magnonic crystals* by analogy with photonic crystals. Over the past decade, multilayered magnetic structures are extensively studied for investigating giant magnetoresistance. In investigating their properties, the ferromagnetic and spin-wave resonance methods were applied, but an idea related to using similar structures as systems similar to photonic crystals was not previously considered.

In this study, we analyze the dispersion properties of spin waves in a one-dimensional periodic multilayered structure (a one-dimensional magnonic crystal) and present the results of investigations on the reflection and transmission of these waves through such a structure.

The investigated periodic structure consists of isotropic ferromagnetic layers with the same thickness d but with different magnetization, M_1 and M_2. The system energy can be written in the form

$$U = M_0^2 \int_{V_f} dv \left(\frac{\alpha}{2} (\nabla m)^2 - \frac{1}{2} m h_0 \right), \qquad (1)$$

where $M_0 = \sqrt{M_1^2 + M_2^2}$ is the average saturation magnetization, α is the nonuniform exchange interaction constant, V_f is the volume of the system, and $h_0 = \dfrac{H_0}{M_0}$ and $m = \dfrac{M}{M_0}$. Solving the Landau–Lifshitz equation in the circular variables

Institute of Radio Engineering and Electronics, Russian Academy of Sciences, Mokhovaya ul. 18, Moscow, 103907 Russia

1028-3358/01/4610-0687$21.00

$$m^{\pm} = \frac{1}{2}(m_x \pm i m_y),$$

$$\frac{\partial m^{\pm}}{\partial t} = \gamma[m^{\pm} \times H_{\text{eff}}], \qquad (2)$$

$$H_{\text{eff}} = -\frac{\delta U}{\delta m^{\pm}},$$

we arrive at the following differential equation:

$$\frac{\partial^2 m^{\pm}}{\partial z^2} + f^2(z) m^{\pm} = 0, \qquad (3)$$

where

$$f^2(z) = \frac{\dfrac{\omega}{\omega_0} - h_0 + 4\pi m(z) - \alpha q_z^2}{\alpha}, \qquad (4)$$

and $\omega_0 = \gamma M_0$. Having described the solution for the magnetization in a harmonic form

$$m^{\pm} = A_0^{\pm} \exp[\pm i(q_y y + q_z z - \omega t)] \qquad (5)$$

and having set the periodic boundary-value conditions (similarly to the Kronig–Penning model that describes the motion of electrons in a periodic potential), we obtain the following dispersion equation:

$$\cos\kappa_1 d \cos\kappa_2 d + \left(\frac{\kappa_1}{2\kappa_2} + \frac{\kappa_2}{2\kappa_1}\right)\sin\kappa_1 d \sin\kappa_2 d = \cosh(2q_z d). \qquad (6)$$

Here, κ_1 and κ_2 are the propagation constants defined by Eq. (4), and q_z is the wave number of the spin wave propagating along an axis perpendicular to the structure surface. Note that the presence of forbidden zones is a characteristic feature of the dispersion curves (Fig. 1). If the wave frequency lies in this zone, the propagation of waves in such a structure is impossible. However, the situation changes under conditions when the symmetry of a system is broken. If a structure contains a layer with different magnetization or thickness, there appear conditions in which a wave can penetrate the structure even when its frequency lies in the forbidden zone. The dispersion equation of spin waves in the structure with broken symmetry (one of the layers has a thickness l) has the following form:

$$\cos\kappa_3 l \cos\kappa_2(l+d)\cos\kappa_2 l \cos\kappa_1(l-d) + \left(\frac{\kappa_1}{2\kappa_3} + \frac{\kappa_3}{2\kappa_1}\right)\sin\kappa_3 l \sin\kappa_1(l-d)\cos\kappa_2 l + \left(\frac{\kappa_1}{2\kappa_2} + \frac{\kappa_2}{2\kappa_1}\right)\sin\kappa_2 d \sin\kappa_1(l-d)\cos\kappa_3 l - \left(\frac{\kappa_2}{2\kappa_3} + \frac{\kappa_3}{2\kappa_2}\right)\sin\kappa_3 l \sin\kappa_2 d \cos\kappa_1(l-d) = \cosh(2q_z d). \qquad (7)$$

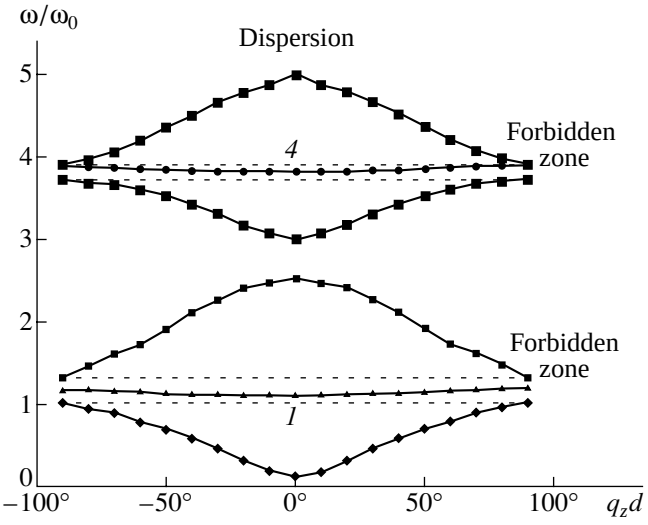

Fig. 1. Dispersion of spin waves (the reduced frequency $\frac{\omega}{\omega_0}$ as a function of $q_z d$) propagating through a periodic multilayered ferromagnetic structure (curves *1* and *4* correspond to the localized modes).

Figure 1 also shows the dispersion curve for spin waves propagating in a periodic structure with broken symmetry (curves *1* and *4* correspond to the modes localized on defects).

We now consider the reflection of spin waves from a periodic structure with a finite number of periods and their propagation through such a structure. First, we calculate the reflection of spin waves from a semi-infinite periodic structure. If the coefficients of reflection from and transmission through a single boundary separating two ferromagnetic materials are known for a wave, then the coefficient of reflection from a semi-infinite structure can be represented similarly to that of a quantum-mechanical particle from a semi-infinite potential [8]:

$$R_{\infty}^{(\rightarrow)} = \frac{\left[(R^{(\rightarrow)}+1)^2 - T^{(\rightarrow)^2}\right]^{1/2} - \left[(R^{(\rightarrow)}-1)^2 - T^{(\rightarrow)^2}\right]^{1/2}}{\left[(R^{(\rightarrow)}+1)^2 - T^{(\rightarrow)^2}\right]^{1/2} + \left[(R^{(\rightarrow)}-1)^2 - T^{(\rightarrow)^2}\right]^{1/2}}. \qquad (8)$$

Here, $R^{(\rightarrow)}$ and $T^{(\rightarrow)}$ are the corresponding coefficients of reflection and transmission of spin waves through a single boundary. In the case of spin waves, the boundary value condition with partially fixed spins at the

interface between the two ferromagnetics has the form:

$$\frac{\partial m^{\pm}}{\partial n} \pm \xi m = 0, \quad (9)$$

where ξ is the spin fixation parameter. Hence,

$$R^{(\rightarrow)} = \frac{i\kappa_1 + \xi}{ik_1 - \xi}\frac{2e^{i\kappa_1 d} - 2e^{-i\kappa_2 d} - e^{2i\kappa_1 d} + e^{-2i\kappa_2 d}}{2e^{-i\kappa_2 d} - 2e^{i\kappa_1 d} - e^{-2i\kappa_1 d} + e^{-2i\kappa_2 d}}, \quad (10)$$

$$T^{(\rightarrow)} = \frac{i\kappa_1 + \xi}{i\kappa_2 + \xi}\frac{(e^{-i\kappa_1 d} - e^{-i\kappa_2 d})(e^{-2i\kappa_2 d} - e^{-2i\kappa_1 d}) - (e^{-i\kappa_1 d} - e^{-i\kappa_2 d})(e^{2i\kappa_1 d} - e^{-2i\kappa_2 d})}{2i\sin\kappa_2 d[2(e^{-i\kappa_1 d} - e^{-i\kappa_2 d}) + (e^{-2i\kappa_1 d} - e^{-2i\kappa_2 d})]}. \quad (11)$$

In order to describe the coefficients of reflection and transmission for a finite-length lattice (for a wave incident onto a structure from the left), it is necessary to note that to the left of the structure there are both incident and reflected waves, whereas to the right, there is only the transmitted wave. Inside the structure itself, there are waves propagating from the right to the left and vice versa. Satisfying these end conditions, we obtain the coefficients of reflection and transmission of a wave from a lattice of the finite length L:

$$R = R_{\infty}^{(\rightarrow)}\frac{1 - e^{i\Delta L}}{1 - |R_{\infty}^{(\rightarrow)}|^2 e^{i\Delta L}}, \quad (12)$$

$$T = \frac{(1 - |R_{\infty}^{(\rightarrow)}|^2)e^{i\Delta L/2}}{1 - |R_{\infty}^{(\rightarrow)}|^2 e^{i\Delta L}}, \quad (13)$$

where $\Delta = \kappa_1 + \kappa_2$. The plots for the coefficient of transmission of spin waves through the periodic structure consisting of 100 periods are shown in Fig. 2 as a function of the wave number $\frac{q_z d}{\pi}$. In the calculations, we used a periodic structure composed of nickel and iron layers with a thickness of 0.1 μm, and the other parameters were chosen in accordance with the experimental study [9] devoted to investigating the spin-wave resonance in layered ferromagnetic structures. It is seen that there are peaks of almost total transmission and total reflection (corresponding to the forbidden zones). The peaks *2* and *3* correspond to the modes localized on defects. The thickness of a defective layer was taken to be 0.15 μm.

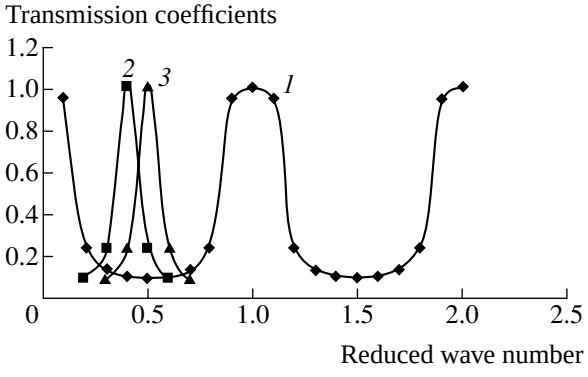

Fig. 2. Transmission coefficients for spin waves propagating through a periodic structure containing 100 periods of ferromagnetic nickel and iron layers (peaks *2* and *3* correspond to the modes localized on defects).

Thus, we considered the propagation of spin waves through a periodic multilayered structure consisting of ferromagnetic layers with the same thickness but different magnetization. The wave spectrum contains the forbidden zones. The transmission coefficients of waves having the frequencies within these zones are virtually equal to zero; i.e., such waves are almost totally reflected. By analogy with photonic crystals, such structures may be termed one-dimensional magnonic crystals. As with the photonic crystals, it is possible to work out and investigate both two- and three-dimensional magnonic crystals.

ACKNOWLEDGMENTS

This work was supported by the International Scientific and Technical Center, project no. 1522, and the Russian Foundation for Basic Research, project no. 99-02-17660.

REFERENCES

1. J. D. Joannopoulos, R. D. Meade, and J. N. Winn, *Photonic Crystals: Molding the Flow of Light* (Princeton Univ. Press, Princeton, 1995).
2. M. Jacoby, Chem. Eng. News **76** (47), 38 (1998).
3. B. Grant, Photonics Spectra **33** (5), 33 (1999).
4. Y. Fink, J. N. Winn, S. Fan, *et al.*, Science **282**, 1679 (1998).
5. E. Yablonovitch, Opt. Lett. **23**, 1648 (1998).
6. I. E. Psarobas, N. Stefanou, and A. Modinos, Phys. Rev. B **62**, 5536 (2000).
7. M. Inoue, K. I. Arai, M. Abe, *et al.*, J. Magn. Soc. Jpn. **23**, 1861 (1999).
8. V. K. Ignatovich, Usp. Fiz. Nauk **150**, 145 (1986) [Sov. Phys. Usp. **29**, 880 (1986)].
9. R. Kordecki, R. Meckenstock, J. Pelzl, *et al.*, J. Appl. Phys. **70**, 6418 (1991).

Translated by Yu. Vishnyakov

Doklady Physics, Vol. 46, No. 10, 2001, pp. 690–693. Translated from Doklady Akademii Nauk, Vol. 380, No. 4, 2001, pp. 472–475.

PHYSICS

The Physical Nature of the Electric-Conduction Law for Metals

Yu. V. Kornev, V. V. Sidorenkov, and S. L. Timchenko

Presented by Academician Yu. A. Osip'yan April 24, 2001

Received April 26, 2001

The process of electric conduction was studied on the basis of experimental results for current–voltage characteristics (CVCs) of metallic conductors (copper wire with a length L_0 = 50 mm and diameter d = 0.1 mm) for a direct current up to its maximum density (at $j_{max} \sim 2 \times 10^9$ A/m^2 samples collapse) under near-isothermal conditions (cooling by running water at $T \simeq$ 290 K). It was established (Fig. 1) that CVCs of conductors under the indicated conditions can be approximated by the dependence

$$E(j) = \rho(j)j = aj + bj^2, \quad (1)$$

where $a \equiv \rho_0$ is the resistivity of the material for $j \longrightarrow 0$ and b is a positive constant [experimental values for copper are: $\rho_0 = (1.98 \pm 0.04) \times 10^{-8}$ Ω m, $b = (3.84 \pm 0.24) \times 10^{-18}$ V m^3/A^2]. Analogous measurements under similar conditions were carried out [1] for nickel foils ($\delta \sim 5$ μm) whose CVCs had the same shape as those displayed here.

A nonlinear behavior of the CVCs (for $j > 3 \times 10^8$ A/m^2) is accompanied by conductor deformations (elongation) $\Delta L(j)$, which, like the resistivity of the sample material $\rho(j) = \dfrac{E(j)}{j}$ (Fig. 2), are temperature-dependent: $\Delta L(T) = L_0\alpha_T\Delta T$ and $\rho(T) = \rho_0(1 + \alpha_\rho\Delta T)$. From here, we obtain the relation

$$\rho(e_j) = \rho_0\left(1 + \frac{\alpha_\rho}{\alpha_T}e_j\right), \quad (2)$$

where α_ρ and α_T are, respectively, the coefficients of the resistivity and of the linear elongation for a conductor and $e_j \equiv e(j) = \dfrac{\Delta L(j)}{L_0}$ are the relative conductor strains caused by the action of the electric current.

Comparing relationships (1) and (2), we obtain that the indicated relative strains should be defined as

$$e(j) = \gamma j, \quad (3)$$

where the coefficient γ will be referred to as the galvanomechanical coefficient. Correspondingly, according to (3), the current dependences of resistivity and temperature must also be linear:

$$\Delta\rho(j) = \rho_0\frac{\alpha_\rho\gamma}{\alpha_T}j, \quad \Delta T(j) = \frac{\gamma}{\alpha_T}j. \quad (4)$$

It can be seen that, under the condition of intense cooling of a sample, the Joule law of heat release, which is quadratic with respect to the electric current, does not manifest itself explicitly in the form of current dependences $e(j)$, $\Delta\rho(j)$, and $\Delta T(j)$. Therefore, expressions (3) and (4) describe the nonthermal action of the electric current on the conductor parameters.

It is of interest that the first experimental investigations of this nonthermal effect of the electric current on the physical properties of a metal were carried out as early as 1844 by Wertheim [2]. From the elongation of wire samples of various metals subjected to constant mechanical loading under conditions of the electric-current conductance $j \sim 10^7$–10^8 A/m^2 or only under

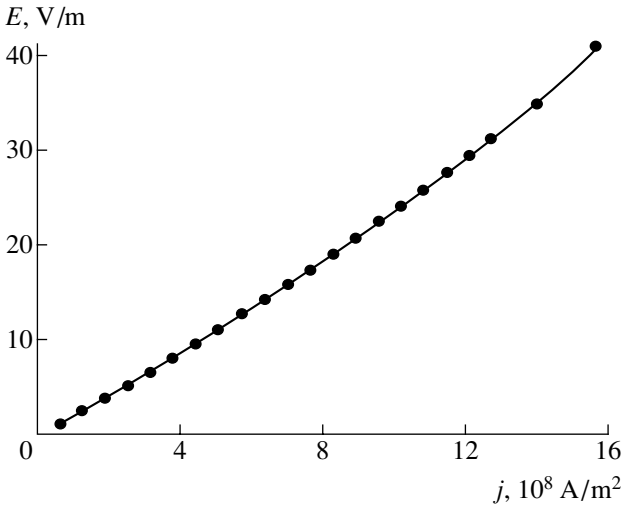

Fig. 1. Current–voltage characteristics $E(j)$ for copper-wire samples (with the length L_0 = 50 mm and diameter d = 0.1 mm): the circles are experimental data, and the solid line represents the approximation. $E(j) = aj + bj^2$; $a = 1.98 \times 10^{-8}$, $sd = 3.86 \times 10^{-10}$; $b = 3.84 \times 10^{-18}$, $sd = 2.41 \times 10^{-19}$; $R = 0.999$.

Bauman State Technical University,
Vtoraya Baumanskaya ul. 5, Moscow, 107005 Russia

1028-3358/01/4610-0690$21.00

thermal action, the Young elastic moduli G_1 and G_2 of the studied material were determined at a fixed sample temperature. The obtained difference $\Delta G = |G_1 - G_2|$ served as an evidence for the nonthermal effect of the electric current on the value of the elastic modulus of a metal. These investigations are a unique physical experiment, and a priority in the discovery of the phenomenon of mechanically stressed states under the action of electric current belongs to Wertheim. Unfortunately, this phenomenon was not appropriately perceived at that time. Only after a lapse of 125 years it was rediscovered by Troitskiĭ [3].

Nowadays, the mechanically stressed state of a metal conductor induced by a high-density electric current ($j \sim 10^8$–10^9 A/m^2) is vigorously studied (see, for example, [1, 4–8]), in particular, with the purpose of practical applications. However, in our opinion, the key physical problem considered in this paper has yet not been posed.

Following formula (4) for $\Delta\rho(j)$, we find, as a result, the specific analytical expression for the CVC specified by physical parameters of the metal conductor

$$E(j) = \rho_0 j + \frac{\rho_0 \alpha_\rho \gamma}{\alpha_T} j^2. \quad (5)$$

This expression agrees qualitatively and quantitatively with the experiment (Fig. 1) [for copper with $\gamma = (7.7 \pm 0.4) \times 10^{-13}$ m^2/A].

Correspondingly, we can write out the relation between the electric-field strength in a metal and its galvanomechanical strains:

$$E(e_j) = \frac{\rho_0}{\gamma} e_j + \frac{\rho_0 \alpha_\rho}{\gamma \alpha_T} e_j^2. \quad (6)$$

Here, a certain analogy is noted with the piezoelectric effect in dielectrics; however, contrary to the piezoelectric effect that exists only in crystals without a center of symmetry, the effect described by expression (6) is observed in metals of an arbitrary crystal system. This phenomenon can be conventionally named the electroelastic effect.

Numerical estimates of coefficients ahead of e_j show that, for elastic strains in a metal ($e \le 10^{-4}$), the first term in (6) is at least by two orders of magnitude larger than the second term. Therefore, for routine values of current density ($j \le 10^7$ A/m^2), the dependence $E(e_j)$ is linear (for copper, the coefficient $\frac{\rho_0}{\gamma} \approx 2.6 \times 10^4$ V/m).

As can be seen, the presence of an electric field in a metal is related to the mechanically stressed state of a conductor under the action of electric current. From the equality $\frac{ED}{2} = \frac{Ge^2}{2}$ of the densities of electric and elastic energies (G is the elastic Young modulus), we find the electric induction in the conductor, which can be written for the linear part of expression (6) as

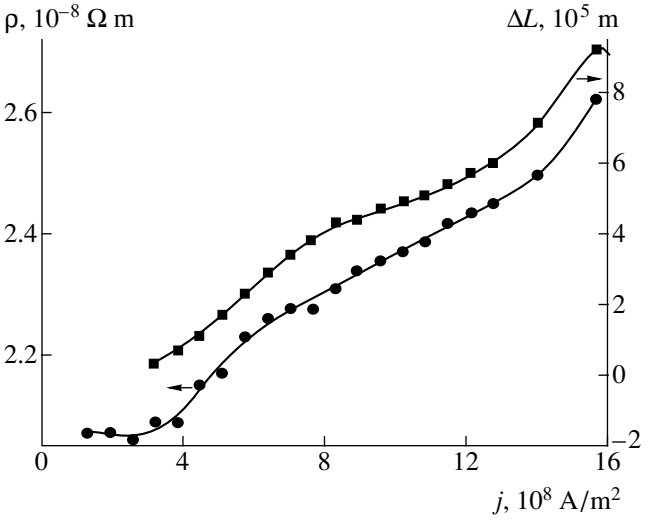

Fig. 2. Resistivity $\rho(j)$ and absolute elongation $\Delta L(j)$ of copper wires as a function of the electric-current density j.

$$D(j) = \frac{G\gamma^2}{\rho_0} j = \tau j. \quad (7)$$

Here, the coefficient τ has the dimension of time and is equal to 3.8×10^{-6} s for copper. Thus, the electric field in a metal is the consequence of the electric polarization of the conductor material in the process of passing the electric current.

An expression similar to formula (7) can also be obtained from the material relationships of electrodynamics as applied to an electrically conducting medium:

$$\mathbf{D} = \varepsilon\varepsilon_0 \mathbf{E} = \varepsilon\varepsilon_0 \rho \mathbf{j} = \tau' \mathbf{j}.$$

Here ε is the relative permittivity of the medium, and ε_0 is the dielectric constant. The physical meaning of the coefficient $\tau' = \varepsilon\varepsilon_0\rho$ can be understood from the continuity equation $\mathrm{div}\mathbf{j} + \frac{\partial \rho_q}{\partial t} = 0$ $\left(\text{in our case, } \mathbf{j} = \frac{\mathbf{D}}{\tau'}\right)$ and the Gauss theorem $\mathrm{div}\mathbf{D} = \rho_q$ (ρ_q is the space-charge density at a given point). Upon integrating this equation, we obtain $\rho_q(t) = \rho_q(0)\exp\left(-\frac{t}{\tau'}\right)$, where τ' is the relaxation time for a charge in a conducting medium.

It should be noted that the estimate of τ, which is obtained from the electroelastic effect, correlates in the order of magnitude with the value of the relaxation time for a charge in a metal ($\tau' \sim 10^{-6}$ s as was reported in [9]). Taking $\tau \equiv \tau'$, we estimate the order of magnitude of the relative permittivity for a normal (nonsuperconducting) metal (under the condition of passing the direct electric current) by expressing permittivity in

terms of the material parameters of the metal: $\varepsilon = \frac{\tau}{\rho_0 \varepsilon_0} \sim 10^{13}$–$10^{14}$. In our opinion, such a value of ε is physically reasonable, because, in the case of a flowing electric current, the electric field in a normal conductor is very weak but nonzero, in contrast to the essentially zero electrostatic field of a conductor.

The additional experiments intended to verify the electroelastic effect in metals were carried out with the indicated wire samples without their intense cooling, i.e., in conditions of considerable heating ($T \simeq 400$–600 K) by the electric current ($j < 1 \times 10^8$ A/m^2) in the ambient air. In this experiment, the CVCs $E(j)$ and the current dependences of the absolute elongation $\Delta L(j)$ and the resistivity $\rho(j)$ were found to be substantially nonlinear; however, the strain dependence $E(e_j)$ remained linear.

Thus, it was established that the electric-field strength $E(j)$ in an electrically conductive metal in the process of passing an electric current and its mechanical strains e_j caused by the action of the electric current of a standard value ($j \le 10^7$ A/m^2) are connected by a linear dependence. It is physically logical to assume that the indicated phenomenon of the galvanomechanical strain $E(e_j)$ is characteristic of arbitrary conductors and can be observed at all temperatures of the condensed state of matter (above the temperature of superconducting transition).

The electroelastic effect $E(e_j)$ makes it possible to alternatively define the difference in electric potentials (electric voltage)

$$U = \int_L E(e_j)dL = \frac{\rho}{\gamma}\Delta L(j)$$

in a metal as the work of extraneous forces (for deformation of the crystal lattice of the conductor per unit charge) in the process of passing an electric current. As a result, the electric field in a conductor is caused by scattering of the drift pulse of current carriers on heterogeneities of the conductor crystal lattice. This scattering leads to the relative shift of the centers of mass for positive and negative charges, which is responsible for the electric polarization of the medium. In this case, in order to create the electric field in a metal under the action of an electric current, the energy of the electromotive-force source must be permanently spent for heating the conductor. Therefore, the process of passing the electric current without the energy dissipation in the case of superconductivity proceeds essentially without a drop of the electric voltage in the conductor.

The character of dependence (3) for $e(j)$, which follows formally from the analysis of the experimental CVC (Fig. 1), can be physically explained by an excess pressure of the conduction-electron gas in the metal crystal lattice in the case of passing an electric current. This pressure is induced by the overheating temperature of the electron gas, $\Delta T(j) = T_{el} - T_{latt}$, with respect to the lattice temperature [10]. In this case, due to the presence of $\Delta T(j)$, the resistivity $\rho(j)$ of the material must essentially depend on the electric-current density, and it increases with the current even for a sample maintained, in one way or another, at a constant temperature. As estimates show, according to relation (4), the dependence $\Delta\rho(j)$ for a copper conductor manifests itself markedly only for the currents $j > 2 \times 10^8$ A/m^2 when $\Delta T(j) \ge 10$ K; i.e., this dependence has a threshold character with respect to the current. This fact is also confirmed by the results of our experiment (Fig. 2).

Using the value of the galvanomechanical coefficient ($\gamma = 7.7 \times 10^{-13}$ m^2/A) obtained experimentally for a copper conductor, we can estimate the ultimate strength σ_u for a copper whisker (1 μm in diameter and 10 μm in length), whose explosive collapse occurred, according to [11], under conditions of intense cooling for the current densities $j > j_{cr} \simeq 1.5 \times 10^{11}$ A/m^2. In this case, $\sigma_u = Ge_j = G\gamma j_{cr} \sim 2 \times 10^{10}$ N/m^2, which corresponds to the theoretical value of the ultimate strength for a metal ($\sim G/10$).

For such currents, the volume density of electric energy in a metal, $\frac{ED}{2} = \frac{1}{2}\rho j^2\tau \simeq 10^9$ J/m^3, is on the order of the thermal-energy density for an actual thermoionic cathode $q_T = c\rho_m T$ (ρ_m and c are the density and specific heat capacity of the material, and $T = 2 \times 10^3$ K). Using (4) for $\Delta T(j)$, we obtain that, for $j \sim 5 \times 10^{10}$ A/m^2, the temperature of overheating for the conduction-electron gas above the lattice temperature in the process of passing the electric current is $\Delta T \simeq 3 \times 10^3$ K. Therefore, under such conditions, the thermoionic emission must occur from the surface of a cold metal ($T_{latt} \ll T_{el}$). In fact, this emission was observed in [11] when, for $j \simeq 1 \times 10^{11}$ A/m^2, the emission current was detected from the surface of a copper single crystal whose temperature T_{latt} did not exceed 373 K. It is interesting that the anomalously high electron emission from thermoionic cathodes at the heating current density $j \sim 10^{11}$ A/m^2 has long been known [12]; however, there was no satisfactory explanation for this fact.

Thus, we can conclude that the existence of the electric field in a conductor is caused by the mechanically stressed state of the medium under the action of electric current. Therefore, the Ohm law $E(j)$ for electric conduction is the formal generalization of two physical phenomena: the galvanomechanical strain e_j of a conductor caused by scattering of a drift pulse of current carriers in the crystal lattice, and the electric polarization arising in this case, which is a source of the electric field $E(e_j)$ in the conductor. It is essential that the resistivity $\rho(j)$ of the conductor material depends on the density of the electric current and increases with current not only due to the Joule-heat release but also due to the current dependence of the temperature $\Delta T(j)$ of the heating of the electron gas with respect to the lattice

temperature. Introducing a new material characteristic for a conducting medium, the galvanomechanical coefficient γ, which is of the same importance as the resistivity ρ, makes it possible to refine and extend our notion about the range of physical phenomena accompanying the process of passing an electric current.

REFERENCES

1. V. V. Sidorenkov, Dokl. Akad. Nauk SSSR **308**, 870 (1989) [Sov. Phys. Dokl. **34**, 926 (1989)].
2. G. Wertheim, Ann. Phys. Chem. **11**/**11**, 1 (1848).
3. O. A. Troitskiĭ, Pis'ma Zh. Éksp. Teor. Fiz. **10**, 18 (1969) [JETP Lett. **10**, 11 (1969)].
4. V. I. Spitsyn and O. A. Troitskiĭ, *Electroplastic Deformation of Metals* (Nauka, Moscow, 1985).
5. V. M. Kontorovich, in *Conduction Electrons*, Ed. by M. I. Kaganov and V. S. Édel'man (Nauka, Moscow, 1985), pp. 44–100.
6. H. Conrad, N. Karam, S. Mannan, and A. F. Sprecher, Scr. Metall. **22**, 235 (1988).
7. V. V. Sidorenkov, D. I. Sementsov, and Yu. V. Kornev, Dokl. Akad. Nauk SSSR **310**, 1371 (1990) [Sov. Phys. Dokl. **35**, 188 (1990)].
8. V. V. Sidorenkov and S. L. Timchenko, Inventor's Certificate No. 1770399, Byull. Izobret., No. 39 (1992).
9. A. Sommerfeld, *Electrodynamics* (Academic, New York, 1952; Inostrannaya Literatura, Moscow, 1958).
10. P. G. Borzyak and Yu. A. Kulyupin, *Electron Processes in Island Metallic Films* (Naukova Dumka, Kiev, 1980).
11. E. E. Vdovin and A. I. Kasumov, Fiz. Tverd. Tela (Leningrad) **30**, 311 (1988) [Sov. Phys. Solid State **30**, 180 (1988)].
12. V. L. Ginzburg and V. P. Shabanskiĭ, Dokl. Akad. Nauk SSSR **100**, 445 (1955).

Translated by V. Bukhanov

Doklady Physics, Vol. 46, No. 10, 2001, pp. 694–696. Translated from Doklady Akademii Nauk, Vol. 380, No. 5, 2001, pp. 607–609.

PHYSICS

Self-Similar Solution to Equations of Magnetic Hydrodynamics for a Pinch of an Elliptic Cross Section

N. D. Naumov

Presented by Academician A. F. Andreev June 25, 2001

Received February 28, 2001

The construction of exact unsteady solutions to equations of magnetic hydrodynamics is of doubtless interest. To achieve this purpose, it turns out to be efficient to use the self-similar approach [1], whose merit consists in the possibility to pass from solving a set of partial differential equations to integrating a set of ordinary differential equations, which is a simpler problem. Such solutions to equations of magnetic hydrodynamics were previously obtained for unsteady plasma motions rated in the class of continuum motions for which velocities are proportional to the distance to the center of symmetry [2–6].

However, these studies dealt with the one-dimensional motion of plasma. Here, we construct an exact solution to the two-dimensional problem for motion with a homogeneous strain. This unsteady solution to equations of magnetic hydrodynamics describes the time dependence of the transverse size for the pinch of elliptic cross section as the external magnetic field varies.

The set of equations of magnetic hydrodynamics is used for the macroscopic description of plasma in the context of a model of a perfect conducting fluid [7]:

$$\mathrm{div}\mathbf{B} = 0, \quad \frac{\partial \mathbf{B}}{\partial t} = \mathrm{rot}[V\mathbf{B}], \tag{1}$$

$$\frac{\partial \rho}{\partial t} + \mathrm{div}\rho\mathbf{V} = 0, \tag{2}$$

$$\frac{d\mathbf{V}}{dt} \equiv \frac{\partial \mathbf{V}}{\partial t} + (\mathbf{V}\nabla)\mathbf{V} = -\frac{1}{\rho}\nabla p - \frac{1}{4\pi\rho}[\mathbf{B}\mathrm{rot}\mathbf{B}]. \tag{3}$$

Here, ρ, $\mathbf{V}$, and p are the density, velocity, and pressure of plasma, respectively.

The steady solution to Eqs. (1)–(3) for a plasma cylinder of elliptic cross section was obtained in [8]:

$$\mathbf{B} = \frac{4I}{abc(\lambda^2 + 1)}(-y, \lambda^2 x, 0), \tag{4}$$

$$p = \frac{1}{2}\rho Q\left(1 - \frac{x^2}{a^2} - \frac{y^2}{b^2}\right). \tag{5}$$

Here, I is the strength of electric current flowing along the pinch, $\lambda = \frac{b}{a}$, a and b are the semiaxes in the pinch cross section, and Q is the constant.

In this case, the magnetic field represents a superposition of the confining external magnetic field of the quadrupole type and the magnetic field generated by the pinch [9]:

$$\mathbf{B} = \mathbf{B}_0 + \mathbf{B}_1, \quad \mathbf{B}_0 = k(y, x, 0), \tag{6}$$

$$\mathbf{B}_1 = \frac{4I}{abc(\lambda + 1)}(-y, \lambda x, 0). \tag{7}$$

To characterize a value of the external-field gradient k, it is convenient to use the value J of the strength of a certain effective current assuming $k = \frac{4J}{abc}$. Expressions (5) and (7) lead to a different form of representation of the external field:

$$\mathbf{B}_0 = \frac{4I}{abc}\frac{\lambda(\lambda - 1)}{(\lambda + 1)(\lambda^2 + 1)}(y, x, 0). \tag{8}$$

Thus, from the comparison of expressions (6) and (8), we obtain the following relationship:

$$I\lambda(\lambda - 1) = J(\lambda + 1)(\lambda^2 + 1). \tag{9}$$

If relationship (9) is considered as an equation with respect to λ, then this equation has positive roots under the condition

$$I \geq I_{\mathrm{cr}} = J\sqrt{22 + 10\sqrt{5}}.$$

Thus, the steady state of the pinch is possible in the case when the intensity of the current flowing along it is not lower than the critical value I_{cr} specified by the external-field gradient. Otherwise, the external field tears the pinch apart.

Before passing to the construction of an unsteady solution to equations (1)–(3), we obtain a useful consequence from the condition of the freezing-in of magnetic-field lines. Let S be a certain value that is conserved during the plasma motion. If Eq. (1) is multi-

1028-3358/01/4610-0694$21.00

plied by ∇S, the resulting equation can be transformed to the following form:

$$\nabla S\frac{\partial \mathbf{B}}{\partial t} = \nabla S\mathrm{rot}[\mathbf{VB}] = -\mathrm{div}[\nabla S[\mathbf{VB}]]$$

$$= \mathbf{B}\mathrm{grad}(\mathbf{V}\nabla S) - \mathbf{V}\mathrm{grad}(\mathbf{B}\nabla S) - (\mathbf{B}\nabla S)\mathrm{div}\mathbf{V}.$$

With allowance for equations

$$\mathbf{V}\nabla S = -\frac{\partial S}{\partial t}, \quad \mathrm{div}\mathbf{V} = -\frac{1}{\rho}\frac{d\rho}{dt},$$

we finally obtain the following result:

$$\frac{d}{dt}\left(\frac{\mathbf{B}\nabla S}{\rho}\right) = 0; \tag{10}$$

i.e., $\frac{\mathbf{B}\nabla S}{\rho}$ is also the quantity being conserved during the plasma motion.

In the case of motions with a homogeneous strain, the plasma density is $\rho = \frac{\rho_0 a_0 a_0}{ab}$, and the expression for plasma velocity has the form:

$$\mathbf{V} = (\dot{a}\xi, \dot{b}\eta, 0),$$

where $\xi = \frac{x}{a}$ and $\eta = \frac{y}{b}$ are self-similar variables. For the class of motions under consideration, these variables are the conserved quantities: $\frac{d\xi}{dt} = \frac{d\eta}{dt} = 0$. Assuming subsequently $S_1 = \eta$ and $S_2 = \xi$ in (10), we find the following conditions:

$$a^2\left[k + \frac{4I}{ac(a+b)}\right] = C_1,$$
$$b^2\left[\frac{4I}{bc(a+b)} - k\right] = C_2, \tag{11}$$

where C_i are the constants determined from the initial conditions.

From conditions (11), it follows that, in the general case, the unsteady motions with a homogeneous strain are possible if the gradient of the external magnetic field and the strength of the current flowing along the pinch depend on time:

$$k = \frac{1}{a+b}\left(\frac{C_1}{a} - \frac{C_2}{b}\right),$$
$$I = \frac{c}{4}\left(C_1\frac{b}{a} + C_2\frac{a}{b}\right). \tag{12}$$

To specify these dependences, it is necessary to integrate a set of ordinary differential equations obtained from Euler equation (3):

$$a\ddot{a} = \alpha, \quad b\ddot{b} = \beta. \tag{13}$$

Here, we introduce the following notation:

$$\alpha = Q - \mu IC_1, \quad \beta = Q - \mu IC_2, \quad \mu = \frac{1}{\pi c a_0 b_0 \rho_0},$$

where the current strength I is defined by expression (12).

The analytical solution to equations (13) can be constructed in the case when α and β are independent of time, i.e., for a constant strength of the current flowing along the pinch. As can be seen from (12), this condition is met if the ratio $\lambda = \frac{b}{a}$ of semiaxes in the pinch cross section remains invariable in the process of the plasma motion.

The simplest result is obtained in the case $\alpha = \beta = 0$, i.e., for the linear time dependence of the cross section size:

$$a = a_0 + \dot{a}_0 t, \quad b = b_0 + \lambda\dot{a}_0 t. \tag{14}$$

This solution describes the self-similar motion of the pinch as the gradient of the external magnetic field varies according to the law

$$k = \frac{4I\lambda(\lambda-1)}{abc(\lambda+1)(\lambda^2+1)}. \tag{15}$$

This dependence follows from the fact that the condition $C_1 = C_2$ leads to relationship (9). Accordingly, expression (14) passes to the above steady solution to Eqs. (1)–(3) for $\dot{a}_0 = 0$.

As is easy to understand, the analytical expression for the nonlinear law of variation of the transverse pinch sizes can be obtained as the condition $\alpha = \beta\lambda^2$ is met. In this case, λ is independent of time if $a = a_0 f$ and $b = b_0 f$, where the function f, as it follows from (11) and (13), satisfies the equation

$$f\ddot{f} = \kappa. \tag{16}$$

Here, we use the following notation:

$$\kappa = \frac{1}{2}\left[\frac{Q}{\lambda a_0 b_0}(1+\lambda^2) - \omega^2\right], \quad \omega^2 = \frac{1}{\pi\rho_0}\left(\frac{2I}{a_0 b_0 c}\right)^2.$$

Equation (16) describes the self-similar pinch expansion for positive values of κ and its contraction for negative values. The contraction can be preceded by a certain preliminary expansion of the pinch provided that $\dot{f}_0 = u > 0$:

$$t = \tau F\sqrt{\pi}[\mathrm{erf}(u\tau) - \mathrm{erf}(\sqrt{u^2\tau^2 - \ln f})].$$

This result can be obtained from Eq. (16) if we put $\kappa = -\frac{1}{2\tau^2}$. The maximum increase in the transverse size of the pinch is characterized by the quantity $f = F =$

$\exp(u^2\tau^2)$ and is attained at the time moment $t = t_k = \tau\sqrt{\pi}F\,\mathrm{erf}(u\tau)$. Then, at $t \geq t_k$, the contraction begins:

$$t = t_k + \tau F\sqrt{\pi}\,\mathrm{erf}(\sqrt{u^2\tau^2 - \ln f}).$$

When $\dot{f}_0 = -u \leq 0$, the pinch contraction occurs at once:

$$t = \tau F\sqrt{\pi}[\mathrm{erf}(\sqrt{u^2\tau^2 - \ln f}) - \mathrm{erf}(u\tau)].$$

Here, $\mathrm{erf}(x)$ is the probability integral [10].

The solution obtained corresponds to the time dependence of the external-field gradient, which is similar to (15):

$$k = \frac{2I}{abc}\left[\frac{1-\lambda}{\lambda+1} + \left(1 - \frac{1}{\omega^2\tau^2}\right)\frac{\lambda^2-1}{\lambda^2+1}\right].$$

This dependence coincides with (15) as $\tau \longrightarrow \infty$. For arbitrary initial conditions, the solution to the set of differential equations (13) can be obtained by numerical methods.

REFERENCES

1. L. I. Sedov, *Similarity and Dimensional Methods in Mechanics* (Nauka, Moscow, 1981; Academic, New York, 1959).
2. A. G. Kulikovskiĭ, Dokl. Akad. Nauk SSSR **114**, 984 (1957) [Sov. Phys. Dokl. **2**, 269 (1958)]; Dokl. Akad. Nauk SSSR **120**, 984 (1958) [Sov. Phys. Dokl. **2**, 507 (1959)].
3. I. M. Yavorskaya, Dokl. Akad. Nauk SSSR **114**, 988 (1957) [Sov. Phys. Dokl. **2**, 273 (1958)].
4. V. P. Korobeĭnikov, Dokl. Akad. Nauk SSSR **121**, 613 (1958) [Sov. Phys. Dokl. **2**, 739 (1959)].
5. E. V. Ryazanov, Prikl. Mat. Mekh. **23**, 187 (1959).
6. Yu. P. Ladikov, Dokl. Akad. Nauk SSSR **137**, 303 (1961) [Sov. Phys. Dokl. **6**, 198 (1961)].
7. L. D. Landau and E. M. Lifshitz, *Course of Theoretical Physics*, Vol. 8: *Electrodynamics of Continuous Media* (Nauka, Moscow, 1982; Pergamon, New York, 1984).
8. R. Gajewski, Phys. Fluids **15** (1), 70 (1972).
9. L. E. Zakharov and V. D. Shafranov, in *Reviews of Plasma Physics*, Ed. by M. A. Leontovich (Atomizdat, Moscow, 1982; Consultants Bureau, New York, 1986), Vol. 11.
10. *Handbook of Mathematical Functions*, Ed. by M. Abramowitz and I. A. Stegun (Dover, New York, 1971; Nauka, Moscow, 1979).

Translated by V. Bukhanov

Doklady Physics, Vol. 46, No. 10, 2001, pp. 697–700. Translated from Doklady Akademii Nauk, Vol. 380, No. 5, 2001, pp. 610–613.

PHYSICS

Formation of Dust Vortices in a Nuclear-Excited Plasma

Academician V. E. Fortov*, V. I. Vladimirov*, L. V. Deputatova*, A. P. Nefedov*, V. A. Rykov, and A. V. Khudyakov****

Received April 17, 2001

The purpose of this study is to show the role of the momentum transfer from drifting ions to neutral components of a medium in initiation of a vortex motion of dust particles in a nuclear-excited dust plasma. The vortex motion of dust particles was previously observed in [1].

A characteristic feature of the nuclear excited plasma is its track structure. This implies that the quasineutrality of such a plasma takes place only for volumes that contain a large number of nuclear-particle tracks. Within the tracks themselves, the quasineutrality is violated very rapidly due to the large difference in diffusion coefficients for electrons and ions. In an external field, the track decomposes into clusters of electrons and ions drifting towards the corresponding electrodes. In a homogeneous field, the clusters conserve the cylindrical symmetry. For the high intensity of a radioactive source, the role of direct processes of charging particles increases when an ionizing particle shoots through a dust particle.

In [1], we studied the behavior of dust particles of CeO_2 in the nuclear-excited plasma formed in atmospheric air by both fission fragments and alpha particles from ^{252}Cf. As the strength of an external electric field increased above 20 V/cm, the levitation of particles gave way to a rotational motion that appeared as an equilibrium vortex formation. The particles in the ensemble moved along closed trajectories forming a torus in the volume of the experimental cylindrical chamber, the torus axis being coincided with the axis of the cylinder. Rotational motion was also observed for sole particles, as well as in the absence of walls within the region occupied by vortices.

The vortex motion of macroparticles in air has two characteristic features. The velocity of dust particles near the chamber axis is always directed away from the radioactive source. The angular rotation rate of particles in a vortex increases with the electric-field strength and approaches a constant value similar to the current–voltage characteristic for the flat ionization chamber in which the experiment was carried out (Fig. 1).

First, we consider the process of the electric-charge accumulation by a dust particle with a diameter of 1 μm in air. In the interelectrode space with nuclear-excited

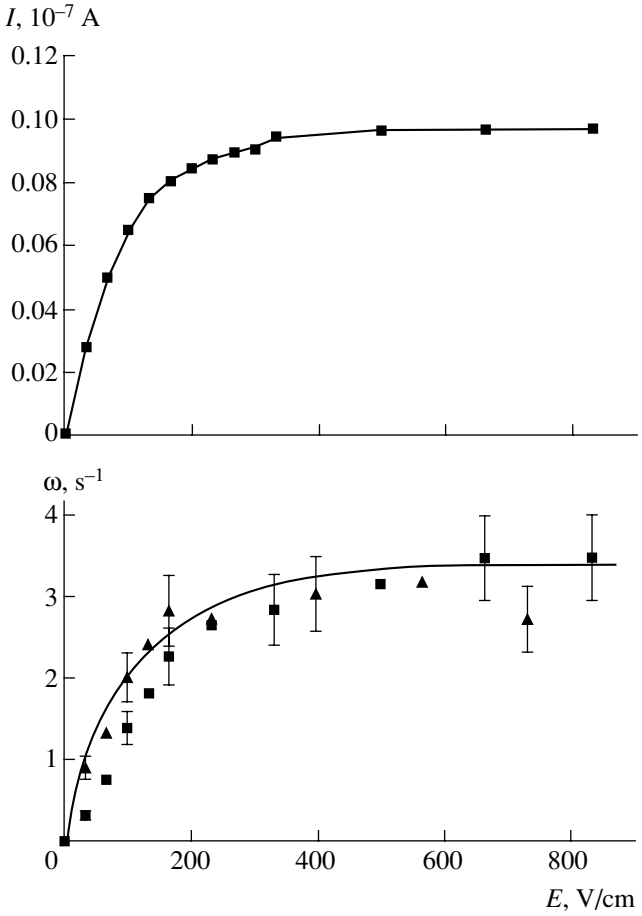

Fig. 1. The current–voltage characteristic of the ionization chamber for the ^{252}Cf source with an intensity of 10^5 fissions/s at a pressure of 10^5 Pa and the angular velocity of a vortex of CeO_2 dust particles with a mean diameter of 1 μm as functions of the electric-field strength. The symbols correspond to experimental data; the lines are the results of calculation.

* *Institute of Thermal Physics of Extremal States (IVTAN), Russian Academy of Sciences, Izhorskaya ul. 13/19, Moscow, 127412 Russia*

** *Institute of Physics and Power Engineering, State Scientific Center, pl. Bondarenko 1, Obninsk, Kaluzhskaya oblast, 249020 Russia*

1028-3358/01/4610-0697$21.00

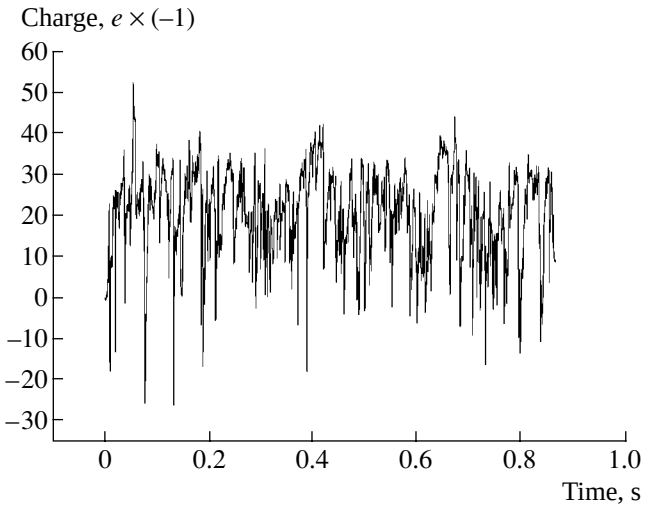

Fig. 2. Inverted charge of a dust particle as a function of time for a distance 1 cm from the source. The mean charge corresponds to 20.6 units of the elementary electric charge *e*.

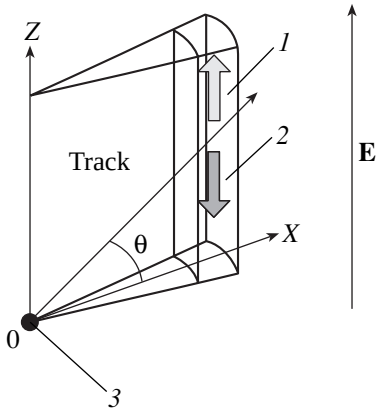

Fig. 3. Geometry of the calculation: the arrows *1* and *2* correspond to drifting ions with opposite signs; (*3*) is the source of fission fragments.

plasma, the clusters of ions drift to the corresponding electrodes under the action of an external electric field. In a homogeneous field, these clusters have a cylindrical shape with the axis of symmetry parallel to the flight direction of the ionizing particle. When entering the drifting cluster, a dust particle acquires a charge from ions that form the cluster. The time dependence of a dust-particle charge was calculated by the Monte Carlo method following [2] for an electric-field strength of 100 V/cm characteristic for the experiment. The results of the calculation are shown in Fig. 2. The value of the charge is below several tens of elementary electric charges. Thus, this charge is too small to induce the observed motion of macroparticles. Fluctuations of the charge are caused by the random nature of interaction between nuclear particles and matter.

Another cause of the charge accumulation can be the motion of ionized air induced by the momentum transfer from ions accelerated in the electric field to the neutral component. Macroparticles make the air motion visible so that we consider this process at the macroscopic level. In the time t of motion, N_i ions acquire the momentum, and, therefore, transfer it to gas molecules. In the linear approximation, the momentum is equal to $\frac{m_i w_i N_i t}{\tau}$, where τ is the average time between collisions and w_i is the drift velocity. To estimate the momentum transferred to a gas mass Δm in the drift time T_d, we easily obtain

$$\frac{\Delta p}{\Delta m} \approx \frac{qET_d}{m_m nV} \approx \frac{m_i w_i N_i T_d/\tau}{m_m nV} \approx \frac{j\langle \nu_T \sigma \rangle T_d}{e}, \qquad (1)$$

where j is the current density, ν_T is the ion thermal velocity, m_m is the mass of a gas molecule, σ is the collision cross section of ions and molecules, V is the gas volume, n is the concentration of gas atoms, q is the total electric charge of ions in the volume V, and E is the field strength. The substitution of the values characteristic for the experiment performed into expression (1) a value of several cm/s for the specific momentum transferred to the gas mass, which agrees with the experimental data of [1]. In addition, it can be seen that the transferred momentum is proportional to the ion current, and this fact explains the form of the dependence of the rotation velocity on the electric-field strength (Fig. 1).

A more accurate calculation of the specific transferred momentum averaged over the time interval T, which takes into account the stochastic nature of the escape of ionizing particles and the track structure of the plasma being formed, was carried out by the Monte Carlo method according to the expression

$$\left\langle \frac{\Delta p}{\Delta m} \right\rangle = \left\{ \frac{1}{\Delta m T} \int F(t)dt \right\} \Delta t, \qquad (2)$$

where Δp is the momentum transferred to the gas mass Δm in the time Δt when a time-averaged force F acts upon the gas. This force is caused by the interaction of the charge of an electron cloud or ion cloud with an external electric field E. Under experimental conditions, due to a limited intensity of the ionizing-particle source, the time dependence of the force F has a pulsed nature:

$$F(t) = \begin{cases} Q_{e,i}E, & \text{if } t \in [t_s, t_e] \\ 0, & \text{if } t \notin [t_s, t_e]. \end{cases} \qquad (3)$$

Here, $Q_{e,i}$ is the charge of an electron cluster or ion cluster, and t_s and t_e are the starting and final instants of time in its motion towards the electrode. The averaging time T can be arbitrary. It is only necessary for this time to correspond to a reasonably large number of events. The time interval Δt is equal to the characteristic time

of variation in the velocity of vortex motion; it is approximately 1 s in the experiment. To simplify the calculation, the field was assumed to be homogeneous.

In Fig. 3, we show opposite drift directions for two ion flows within a single elementary cell. The source of ionizing particles is located at the point $Z = 0$. When considering the entire track, these flows have a cylindrical shape, the cylinder axis being parallel to the initial track. In the Monte Carlo method, the ejection angle θ is a random quantity. The result is averaged over the time corresponding to the passage of 2000 tracks. The cell length along the *Z*-axis is assumed to be equal to the mean free path of fission fragments; along the *X*-axis, each cell has a size equal to a hundredth fraction of the free path for a fission fragment. We calculated a number of ions produced by a fragment within the cells crossed by this fragment. The contribution of ions with opposite charges in every elementary cell, which is cut by a step along the *X*-axis, is taken with the opposite sign.

The calculations were carried out for air at atmospheric pressure and for neon at a pressure of 5×10^4 Pa. The electric-field strength was chosen to be equal to 100 V/cm. The drift velocities required for the calculation were taken from [3–5]. The results are shown in Fig. 4. The drop in the energy loss for the ionization along the track, as well as the decrease in the density of tracks with the removal of ionizing particles from the source, increases the contribution to the transferred momentum of ions moving near the *Z*-axis. In each elementary cell, the number of ion pairs increases with approaching the source. The ions moving towards the upper electrode travel a longer path in gas and transfer a higher momentum. The momentum transfer in air, in accordance with the experimental data, is almost independent of the electric-field direction. In the experiment, the O_2^- ions are formed in a time on the order of several fractions of microsecond as a result of the interactions with oxygen. The mobility of these ions differs only slightly from that of the N_2^+ ions, and the contribution of these ions to the momentum transfer is almost independent of the sense of the field. This leads to the initiation of air motion that is directed away from the source of ionizing particles at an arbitrary polarity of ions. In a volume bounded by walls and electrodes, a vortex motion of gas appears, which becomes visible owing to dust particles.

If the electric field in neon is directed along the *Z*-axis, the positive neon ions move upwards (Fig. 3), and electrons move downwards. In this case, the specific momentum transfer near the *Z*-axis is large, and, in the volume occupied by neon, there appears gas motion directed away from the source. The vortex motion of this kind in neon is actually observed in the experiment for the indicated sense of the field. If the field is directed oppositely to the *Z*-axis, the upward-moving electrons cannot give a large contribution to the transferred momentum due to the very short drift time. A small contribution of ions leads to the momentum transfer towards the source.

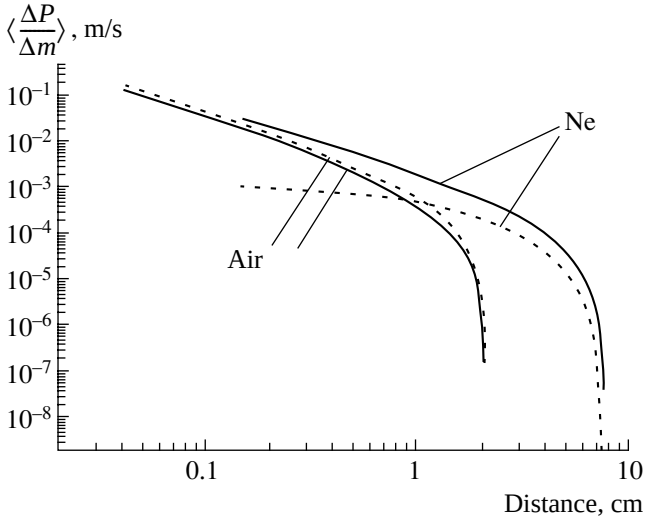

Fig. 4. Results of calculations as functions of a distance along the *X*-axis. The solid and dashed curves correspond to the electric field directed along and opposite to the *Z*-axis, respectively.

The calculations were carried out under the assumption that the ionization chamber operates in the regime of the saturation of the current–voltage characteristic. For lower values of the electric-field strength, the recombination leads to a loss of charges both in the track itself and on the way of ions to electrodes. This effect results in a decrease in both the electric current intensity and the momentum transferred. The proposed model of the appearance of the vortex motion explains the second important experimental fact, namely, the saturation of the rotation rate that attains a plateau in accordance with the current–voltage characteristic. The reason is the same in both cases. Before saturating the rotation rate, both values increase, because the recombination in the tracks decreases, whereas upon reaching the plateau, all the ions produced by the source arrive at the electrodes. Therefore, the velocity of vortex motion depends on the applied voltage in the same way as in the case of the current–voltage characteristic. In fact, according to expression (1), the value of the transferred momentum is proportional to the drift time (inversely proportional to the drift velocity) and to the field strength. In its turn, the drift velocity is proportional to the field strength. Then, under the saturation condition, in the absence of the charge loss, the dependence of the transferred momentum on the field strength disappears.

Thus, the mechanism of the vortex formation proposed in this study explains two characteristic features of the vortex motion in air and in neon, namely, the sense of the rotation and the property of saturation of the rotation velocity. The value of the gas-motion velocity near the axis agrees with experimental data.

The difference between the values of rotation velocity for vortices in air and neon in the case of a change in the sign of the potential can be explained as follows. When the positive potential is applied to an electrode covered by a layer of californium and the negative potential is applied to the opposite electrode, the positive ions formed mainly near the source travel a longer path to the negative electrode and transfer a larger momentum to gas molecules. This is valid for both an electronegative gas and an inert gas. When the sign of potential in the electronegative gas changes, negative ions also form near the source for fractions of a microsecond. While moving to the positive opposite electrode, they travel a long path and transfer a large momentum to the gas. For inert gases, it is electrons that travel a long path to the positive electrode. But since their drift velocity is several orders of magnitude higher than that for ions, they have no time to transfer a noticeable momentum to the gas. Eventually, this fact is associated with a negligible electron-to-molecule mass ratio.

ACKNOWLEDGMENTS

This work was supported by the Russian Foundation for Basic Research, project no. 00-02-17620.

REFERENCES

1. V. E. Fortov, V. I. Vladimirov, L. V. Deputatova, *et al.*, Dokl. Akad. Nauk **366**, 184 (1999) [Dokl. Phys. **44**, 279 (1999)].
2. V. E. Fortov, A. P. Nefedov, V. M. Torchinsky, *et al.*, Phys. Lett. A **258**, 305 (1999).
3. Yu. P. Raĭzer, *Gas Discharge Physics* (Nauka, Moscow, 1987; Springer, Berlin, 1991).
4. L. G. H. Huxley and R. W. Crompton, *The Diffusion and Drift of Electrons in Gases* (Wiley, New York, 1974; Mir, Moscow, 1976).
5. E. W. McDaniel and E. A. Mason, *The Mobility and Diffusion of Ions in Gases* (Wiley, New York, 1973; Mir, Moscow, 1976).

Translated by V. Bukhanov

Doklady Physics, Vol. 46, No. 10, 2001, pp. 701–704. Translated from Doklady Akademii Nauk, Vol. 380, No. 5, 2001, pp. 614–618.

PHYSICS

An Effect of Structural Variations on the Decomposition of Materials under High-Intensity Thermal Actions

O. F. Shlensky

Presented by Academician V. V. Osiko May 22, 2001

Received April 17, 2001

It is well known that substances in the condensed state preserve their thermodynamic stability below the upper temperature of the phase-state boundary. This boundary can be attained as a result of both an intensification of heating and a sharp drop in pressure [1–4]. The description of thermal processes accompanying the decomposition of various materials in macroscopic volumes and under the intense heating of surface layers, in particular heat-resistant coatings [5], is of prime interest for practical applications. Near the phase-state boundary, the frequency of homogeneous nucleation, which is rather low at moderate temperatures, sharply increases (by orders of magnitude). This is explained by a high activation barrier that causes the vaporization rate and substance-thermolysis rate to be enhanced. In addition, the mechanism of chemical thermal-decomposition reactions in nonvolatile materials can change near the phase-state boundary [6, 7]. In this paper, our objective is to develop a mathematical model for the macroscopic (bulk) process of material thermal decomposition. We propose to include into this model parameters of a phase-state boundary and kinetic features of processes occurring in its vicinity.

In thermodynamics, the position of the phase-state boundary is determined from the condition of vanishing the second variation for one of thermodynamic potentials, e.g., $\delta^2 G = 0$, where G is the Gibbs free energy [1]. Since

$$\delta^2 G = \frac{\partial^2 G}{\partial T^2} dT^2 + 2\frac{\partial^2 G}{\partial T \partial p} dT dp + \frac{\partial^2 G}{\partial p^2} dp^2,$$

the partial derivatives $\frac{\partial p}{\partial V}$ or $\frac{\partial T}{\partial V}$ vanish on the stability boundary. This enables us to calculate parameters of a phase-state boundary for both volatile and nonvolatile substances using the equation of state [1–4]. However, the absence of reliable equations of state that would be adequate for the thermodynamic properties of a number of substances has long been an obstacle for determining parameters of the phase-state boundary. It should also be noted that the equation of state, which was proposed recently in [8, 9] and is valid in a wide range of temperature variations, allows us to calculate with a high accuracy the parameters of phase-state boundaries for polymeric and other materials. Moreover, experimental methods of a thermal probe [2–4] and a contact thermal analysis [9–11] were developed recently. These methods make it possible to approach the phase-state boundary as a result of high-rate (up to 10^6 K/s) heating and to obtain information on structural variations and thermolysis kinetics in the vicinity of the phase-state boundary. These methods also enable us to determine the temperatures T_l for the attainable overheating of substances that are lower even by 2 to 5 K than the corresponding temperatures on the phase-state boundary under various given pressures and thermal-decomposition rates.

In Fig. 1, the thermal-decomposition time t_p obtained by contact thermal analysis for certain substances is presented as a function of the inverse absolute temperature near the phase-state boundary. The plots exhibit a specific configuration. The lower branch corresponding to moderate temperatures has a shape similar to a descending straight line; i.e., it can be described by the Arrhenius equation. The left-hand branch is bend up and asymptotically approaches a vertical line with the abscissa equal to $\frac{1}{T_l}$, which does not correspond to Arrhenius kinetics. We use these data in order to construct a mathematical model for the thermal decomposition of a material.

We consider a one-dimensional steady-state process of the thermal decomposition of a half-space, which proceeds in accordance with the equation of thermal conduction:

$$\frac{d}{dx}\lambda\frac{dT}{dx} - F(T) + \rho C_p u\frac{dT}{dx} = 0. \quad (1)$$

Here, u is the velocity of motion for the decomposition front that coincides with the origin of a chosen coordi-

Mendeleev State University of Chemical Technology, Miusskaya pl. 9, Moscow, 125047 Russia

1028-3358/01/4610-0701$21.00

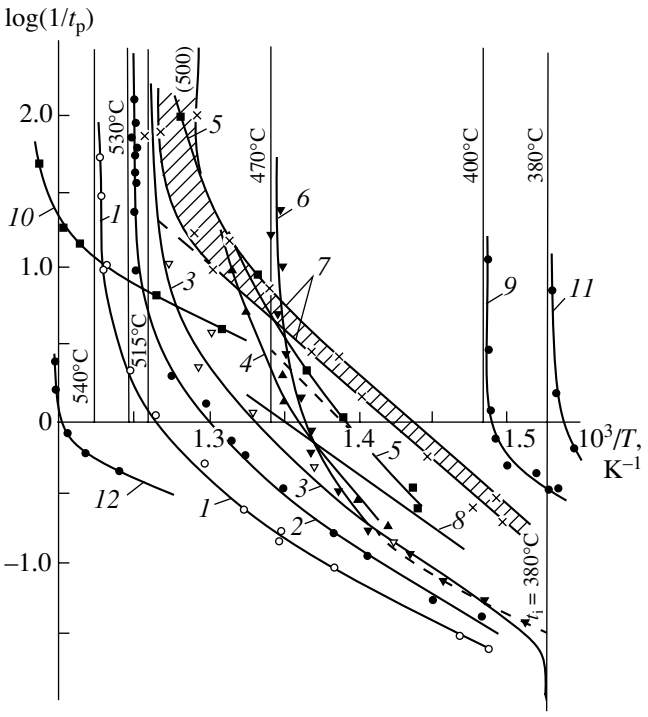

Fig. 1. Data obtained while testing materials by the method of contact thermal analysis; (*1*) UPM-07037 shock-proof polystyrene; (*2*) polystyrene of unit design with a molecular mass of 600000; (*3*) 276-73 high-density polyethylene; (*4*) lavsan; (*5*) 10201-04 low-density polyethylene; (*6*) TUM XII 2898-55 polyvinylchloride film; (*7*) polymethyl methacrylate (technological PMMA, the inclined shaded region corresponds to data spreading for PMMA of different trade marks); (*8*) polycaprolactam obtained by polymerization of α-caprolactam; (*9*) colemanite mineral; (*10*) oil from the Alanin layer; (*11*) polyethylene glycol with the molecular mass of 2000; (*12*) aluminum nitrate.

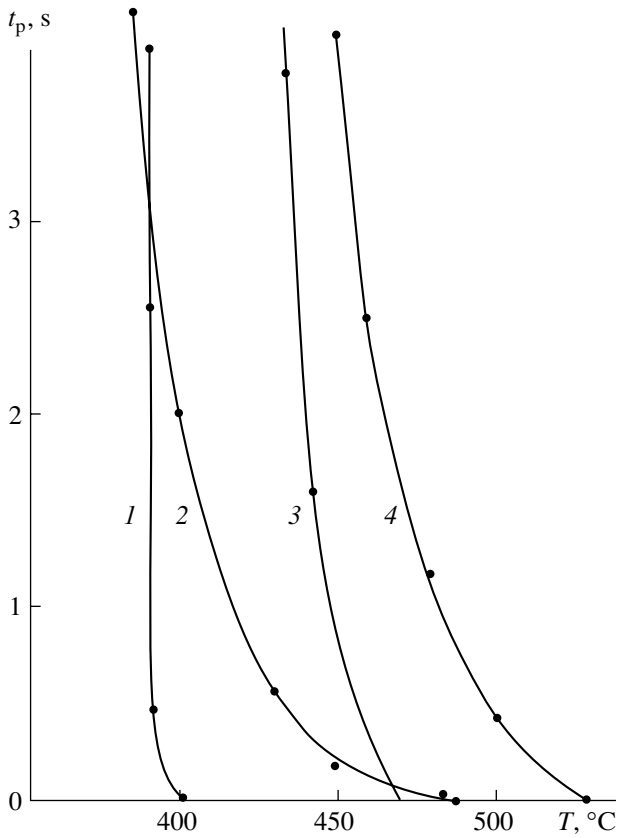

Fig. 2. Duration of the material thermal decomposition as a function of temperature. The data are obtained by the method of contact thermal analysis under short-term heating: (*1*) colemanite mineral; (*2*) polymethyl methacrylate; (*3*) polyvinylchloride; (*4*) polystyrene.

nate system ($x = 0$), and $F(T)$ is the heat-absorption function. The latter is usually written out in the form $F(T) = \rho Q k(T)$ [5] under the assumption that the thermolysis reaction proceeds as a zero-order reaction (Q is the reaction thermal effect) with the reaction constant $k(T)$ and the density ρ. [For these reactions, $k(T) = \frac{1}{t_p}$.]

The last term in formula (1) is usually ignored by virtue of its smallness [5]. Upon integrating Eq. (1) with allowance for the boundary condition $\frac{dT}{dx} = 0$ as $x \longrightarrow \infty$ and assuming the variation of the heat conduction due to the secondary porosity to be proportional to the density variation, i.e., $\lambda(T) = \frac{\lambda_0 \rho(T)}{\rho_0}$ [6], we arrive at the equation

$$\frac{dT}{dx} = -D(J(T))^{1/2}, \qquad (2)$$

where the notation

$$J(T) = \int_{T_0}^{T} k(T)dT, \quad D = \left(\frac{2\rho_0 Q}{\lambda_0}\right)^{1/2}$$

is introduced.

In the case of high-intensity thermal actions that are common for conditions in which heat-resistant coatings are applied [5], the times of heating a substance from the initial temperature T_0 to the surface temperature T_w do not exceed a few seconds. These short times correspond to the upper segments of the plots in Fig. 1. Reconstructing the plots in the linear scale (see Fig. 2) showed that they correspond to the equation of an nth-power parabola, which has the form $t_p = A(T_l - T)^n$, where n is an integer ($n = 3, 4, 5, \ldots$). The function $J(T)$ for two segments can be represented as the sum

$$J(T) = \int_{T_0}^{T_a} k(T)dT + \int_{T_a}^{T} k(T)dT,$$

where T_a is the upper temperature within the Arrhenius

segment. For this segment, thermolysis times t_p attain from several minutes to several hours. In the case of intense heating, these times are virtually not realized. Thus, we may consider that

$$J(T) \simeq \int_{T_a}^{T} k(T)dT = \int_{T_a}^{T} \frac{dT}{A(T_l - T)^n},$$

$$T_a \simeq (0.8\text{–}0.97)T_l.$$

We now equalize the heat inflow q_w to the material surface and the total amount of the thermal energy spent for the heating and decomposition of the material:

$$q_w = -\lambda_w\left(\frac{dT}{dx}\right)_{x=0} = u\rho(C_p(T_w - T_0) + \zeta Q). \quad (3)$$

Here, $\lambda_w = \lambda(T_w) = \kappa\lambda_0$, $\kappa \simeq \dfrac{\rho(T_w)}{\rho_0}$, and ζ is the fraction of the material that has reacted. After substituting the temperature gradient from formula (2) into Eq. (3), we find

$$u = \frac{D\kappa\lambda_0/\rho_0}{C_p(T_w - T_0) + \zeta Q}(J(T_w))^{1/2}, \quad (4)$$

where C_p is the thermal capacity averaged within the temperature range from T_0 to T_w.

We now substitute the value of the integral found above

$$J(T) = \frac{(T_l - T)^{1-n} - (T_l - T_a)^{1-n}}{A(n-1)}$$

into the right-hand side of Eq. (4) for the case of the upper limit $T = T_w$. After simple transformations, we arrive at the expression

$$u = \frac{D\kappa\lambda_0/A^{1/2}(n-1)^{1/2}\rho_0}{C_p(T_w - T_0) + \zeta Q}$$

$$\times((T_l - T_w)^{1-n} - (T_l - T_a)^{1-n})^{1/2}. \quad (5)$$

In this expression, the temperature T_w remains unknown. It can be determined using Eq. (2):

$$q_w = -\lambda_w\frac{dT}{dx} = \lambda_w(DJ(T_w))^{1/2}.$$

Substituting the value of $J(T_w)$ into this formula, we obtain

$$T_w = T_l - \frac{1}{(q_w^2 B - C)^{\frac{1}{n-1}}},$$

where $B = \left(\dfrac{A(n-1)}{\lambda_w D}\right)^2$ and $C = \dfrac{1}{(T_l - T_0)^{n-1}}$.

From this, it follows that as q_w increases the rise in the surface temperature is bounded by the value T_l. This result is consistent with the numerous experimental data [13–15]. For example, in the case of polymethyl methacrylate, while intensifying heating up to values above 0.1–0.7 kW/cm^2 by laser radiation or radiant or convective heating, as well as while burning gas mixtures with a high oxygen content, the surface temperature T_w measured by different methods did not exceed $T_l = 500$°C within an accuracy of ±20 to ±40°C. These observations cannot be described within the framework of traditional mathematical models based on the Arrhenius dependence $k(T)$. Figure 3 shows plots of variations in the velocity $u = f(1/T)$ for polymethyl methacrylate, which were obtained according to the data of [13] in the case of intensely heating the material surface. As was shown in [13], the Arrhenius equation (dashed line) approximates the lower segment of the plots but fails to describe the rise near the phase-state boundary.

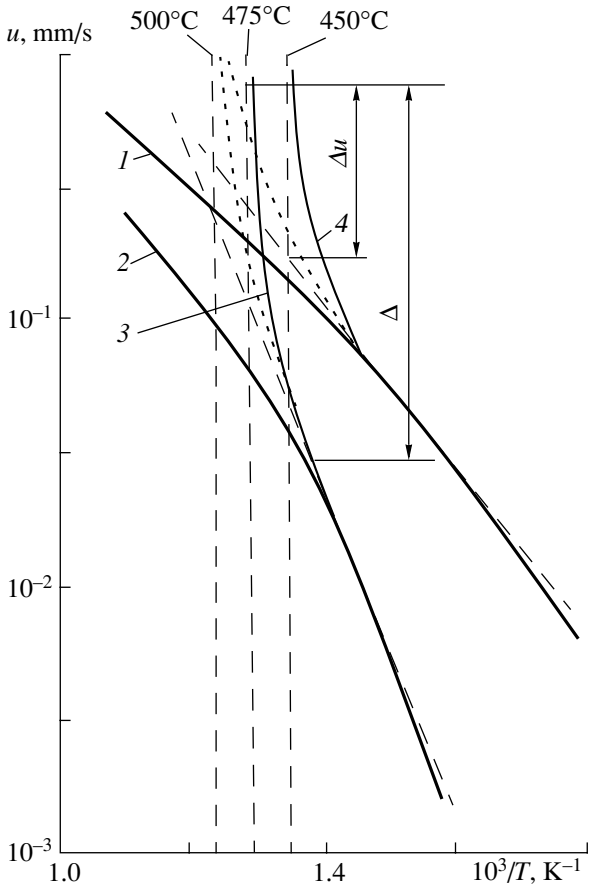

Fig. 3. Data (and their approximation) obtained while testing polymethyl methacrylate by the method of linear pyrolysis [13]. The linear pyrolysis rate: (*2*, *3*) for the transversely sewed PMMA and (*1*, *4*) for the linear PMMA as functions of temperature T_w (the case of a heating element in the form of a metallic plate). The upper numbers 500°C and 475°C, 450°C correspond to the temperature T_l of PMMA and maximum temperatures T_w attained in the experiment, respectively. Dashed and dotted lines correspond to the approximation by the Arrhenius and parabolic equations, respectively. Δ represents the segment of the plot approximated by the proposed mathematical model at temperatures close to T_l (the segment of structural variations); Δu is an error arising while using the Arrhenius approximation.

In accordance with Eq. (6), the calculation using characteristics of polymethyl methacrylate, which were taken from [5], with $\lambda_0 = 0.21$ W/(m K), $\rho_0 = 1000$ kg/m^3, $C_p = 1.9$ kJ/(kg K), $Q = 2100$ kJ/kg, and plots of Fig. 1, makes it possible to provide consistency with the experimental data (see the dotted line in the high-temperature region) and to propose a simple explanation for the similarity of the shapes for the dependence $u(1/T)$ and plots shown in Fig. 1.

The approach under consideration allows us to calculate the variation of the temperature near the surface of the body that is being heated. As a result of integrating Eq. (2), with allowance for the dependence $J(T) \simeq \frac{(T_1 - T)^{1-n}}{A(n-1)}$, which is valid at high temperatures, we arrive at the dependence $T(x)$ in the form

$$T = T_1 - \left(\frac{Dm}{\sqrt{A(n-1)}}x - (T_1 - T_0)^m\right)^{1/m},$$

where $m = \frac{1+n}{2}$. For example, in the case of polymethyl methacrylate, we have $n = 3$ and $m = 2$; therefore

$$T(x) = T_1 - \left(\frac{2D}{\sqrt{2A}}x - (T_1 - T_0)^2\right)^{1/2}.$$

This distribution differs from the Michelson temperature profile [5], which is known in the theory of frontal processes, by higher temperature gradients dependent on the reaction thermal effect Q. In accordance with the dependence $T(x)$, it is easy to calculate the near-surface distribution of the excess pressure for thermolysis gaseous products

$$\Delta p(x) = \frac{x}{P}\int_0^x k(T)dx,$$

which causes the formation of the vapor-droplet zone consisting of particles of the undecomposed material [13–15]. Upon substituting the value of $k(T) = \frac{1}{t_p}$, we obtain for $n = 3$, as a result of integration,

$$\Delta p(x) = \frac{2x/D}{PA(2/N)^{1/2}}\sqrt{Dx + M},$$

where P is the diffusive permeability, $N = (A(n-1))^{1/2}$, and $M = N(T_1 - T_0)^2$. The thickness of the vapor-droplet zone is determined by the coordinate x_1 that corresponds to the maximum value Δp found from $\frac{d(\Delta p)}{dx} = 0$ with allowance for the dependence $P(x)$.

The analysis performed showed that the experimentally observed deviation of the thermal decomposition rate of a material from the Arrhenius dependence at high-intensity heating of the material surface is caused by structural variations near the phase-state boundary of an initially homogeneous medium. The allowance for parameters of structural variations (i.e., the temperature of the attainable overheating, which is determined by the homogeneous-nucleation frequency [2], density variations, heat-conduction variations, and the degree of completing the thermolysis reaction) makes it possible to propose a simple interpretation of experimental data and noticeably improve the accuracy of calculating macroscopic thermal-decomposition phenomena in the process of their mathematical simulation. In light of this, it is especially worth mentioning the necessity of attaining a high accuracy, while calculating the sizes of heat-resistant coating elements. Indeed, the calculation of the heat resistance of a coating material, which is carried out without allowance for the parameters of the phase-state boundary (as was shown by the example of a simple Arrhenius extrapolation) yields a considerably underestimated (by an order of magnitude) thermal-decomposition rate for the material under consideration. A coating thickness chosen in accordance with this calculation is, evidently, insufficient to provide a reliable heat resistance for a given time period.

REFERENCES

1. A. Münster, *Chemische Thermodynamik* (Akademie, Berlin, 1969; Mir, Moscow, 1971).
2. V. P. Skripov, E. N. Sinitsyn, P. A. Pavlov, *et al.*, *Thermophysical Properties of Liquids in the Metastable State* (Atomizdat, Moscow, 1980).
3. P. A. Pavlov, *Boiling-up Dynamics for High-Superheated Liquids* (Akad. Nauk SSSR, Sverdlovsk, 1988).
4. V. P. Skripov, *Metastable Liquids* (Nauka, Moscow, 1972).
5. Yu. V. Polezhaev and F. B. Yurevich, *Thermal Resistance* (Énergiya, Moscow, 1976).
6. O. F. Shlenskiĭ, N. V. Afanas'ev, and A. G. Shashkov, *Thermal Fracture of Materials* (Énergoatomizdat, Moscow, 1996).
7. E. F. Vainstein, G. E. Zaikov, and O. F. Shlensky, Polym.-Plast. Technol. Eng. **35**, 669 (1996).
8. I. V. Lomonosov, V. E. Fortov, and K. V. Khishchenko, Khim. Fiz. **14**, 47 (1995).
9. I. V. Lomonosov, K. V. Khishchenko, E. V. Fortov, and O. F. Shlenskiĭ, Dokl. Akad. Nauk **349**, 322 (1996) [Phys. Dokl. **41**, 304 (1996)].
10. O. F. Shlensky, Zh. Fiz. Khim. **70**, 29 (1996).
11. K. V. Khishchenko, D. A. Rogatkin, D. N. Yundev, *et al.*, Teplofiz. Vys. Temp. **36**, 227 (1998).
12. D. N. Yundev, A. A. Lash, and O. F. Shlenskiĭ, Teplofiz. Vys. Temp. **27**, 369 (1989).
13. A. S. Shteĭnberg, *Linear Pyrolysis*, Preprint, Inst. Khim. Fiz., Chernogolovka, 1977, p. 17.
14. N. P. Novikov and A. A. Kholodilov, Inzh.-Fiz. Zh. **22**, 618 (1972); **22**, 257 (1972).
15. N. P. Novikov and A. A. Kholodilov, Mekh. Polim., No. 1, 124 (1971).

Translated by G. Merzon

Doklady Physics, Vol. 46, No. 10, 2001, pp. 705–707. Translated from Doklady Akademii Nauk, Vol. 380, No. 6, 2001, pp. 754–756.

PHYSICS

Nonlinear Electrodynamic Effect of Ray Bending in the Magnetic-Dipole Field

V. I. Denisov*, I. P. Denisova, and S. I. Svertilov***

Presented by Academician G. T. Zatsepin May 28, 2001

Received May 30, 2001

According to quantum electrodynamics, vacuum has nonlinear properties. For this reason, equations for electromagnetic field in vacuum coincide in their form with the equations of the electrodynamics of continua:

$$\mathrm{rot}\mathbf{H} = \frac{1}{c}\frac{\partial \mathbf{D}}{\partial t}, \quad \mathrm{div}\mathbf{D} = 0,$$

$$\mathrm{rot}\mathbf{E} = -\frac{1}{c}\frac{\partial \mathbf{B}}{\partial t}, \quad \mathrm{div}\mathbf{B} = 0.$$

However, the meaning of the vectors **D** and **H** in these equations is different:

$$\mathbf{D} = \mathbf{E} + \frac{\alpha}{45\pi B_q^2}\{2(\mathbf{E}^2 - \mathbf{B}^2)\mathbf{E} + 7(\mathbf{BE})\mathbf{B}\},$$

$$\mathbf{H} = \mathbf{B} + \frac{\alpha}{45\pi B_q^2}\{2(\mathbf{E}^2 - \mathbf{B}^2)\mathbf{B} - 7(\mathbf{BE})\mathbf{E}\}.$$

Here $B_q = \frac{m^2c^3}{e\hbar} = 4.41 \times 10^{13}$ G is a quantum electrodynamic parameter, and $\alpha = \frac{e^2}{\hbar c} \approx \frac{1}{137}$ is the electromagnetic coupling constant.

For a long time, nonlinear electrodynamics in vacuum had no experimental verification and, therefore, was considered by many researchers as an abstract theoretical model. At present, its status has changed essentially. Experiments [1] on the inelastic scattering of laser photons by gamma photons corroborated that the electrodynamics in vacuum is actually a nonlinear theory. Therefore, its various predictions, which can be verified experimentally, are worthy of the most serious attention.

In the current scientific literature [2–10], a diversity of various experiments was proposed for studying such effects. However, for the fields $B, E \sim 10^6$ G, which are accessible in terrestrial laboratories, the nonlinear corrections to the Maxwell equations in vacuum are so small that it is very difficult to detect the effects they cause. For this reason, it is appropriate to investigate the principal tendencies of nonlinear electrodynamics in vacuum [4] by using astrophysical sources of magnetic fields. In fact, such astrophysical objects as pulsars, for example, have magnetic-dipole fields of $B \sim 10^{13}$ G that are inaccessible under laboratory conditions, and such strong fields stretch for significant distances. Even more intense magnetic fields, $B \sim 10^{15}$ G, are generated by recently discovered magnetars.

The basic channel of incoming information on nonlinear electrodynamic effects that occur in the magnetic-dipole field of astrophysical objects is electromagnetic radiation. This is an electromagnetic wave that passes through the magnetic field of a neutron star and is affected by the nonlinear electrodynamic and gravitational actions of this field. Because the gravitational influence on electromagnetic waves is well studied in the general theory of relativity [11], it is also possible to reveal certain principal tendencies of the nonlinear electrodynamic interaction of electromagnetic fields by analyzing the incoming electromagnetic radiation. It should be noted at once that since pulsars and magnetars have magnetospheres filled with matter, these experiments should be performed with X-rays or gamma-radiation, because the magnetosphere is transparent for such waves.

Now, we turn to studying the nonlinear electrodynamic bending of electromagnetic rays in a pulsar or magnetar field. We consider the magnetic field of a magnetic dipole with the magnetic dipole moment **m**:

$$\mathbf{B}_0 = \frac{3(\mathbf{mr})\mathbf{r} - r^2\mathbf{m}}{r^5}. \quad (1)$$

Using the mathematical approach developed in [7–10], it is possible to show that the eikonal equation for a ray

* *Moscow State University, Vorob'evy gory, Moscow, 119899 Russia*

** *Tsiolkovskiĭ Russian State Technological University, Moscow, 103498 Russia*

1028-3358/01/4610-0705$21.00

passing through the field described by formula (1) takes the form

$$\frac{1}{c^2}\left(\frac{\partial S}{\partial t}\right)^2 - [1 - 4\eta\xi B_0^2](\nabla S)^2 - 4\eta\xi(\mathbf{B}_0\nabla S)^2 = 0. \quad (2)$$

The coefficient η entering into this equation depends on the electromagnetic-wave polarization and takes one of the following values for two mutually perpendicular polarizations:

$$\eta = \frac{\alpha}{45\pi} = 5.1\times 10^{-5} \text{ and } \eta = \frac{7\alpha}{180\pi} = 9.0\times 10^{-5}.$$

The eikonal equation represents a nonlinear differential equation whose solution is not generally known. Therefore, we analyze the behavior of a ray in a particular case when Eq. (2) can be integrated in analytical form.

We denote a plane perpendicular to the magnetic dipole moment **m** as the *XOY* plane. The eikonal equation for an electromagnetic wave polarized along the vector **m** and traveling in the *XOY* plane takes the form

$$\frac{1}{c^2}\left(\frac{\partial S}{\partial t}\right)^2 - \left[1 - \frac{7\alpha|\mathbf{m}|^2}{45\pi B_q^2 r^6}\right]\left[\left(\frac{\partial S}{\partial r}\right)^2 + \frac{1}{r^2}\left(\frac{\partial S}{\partial \varphi}\right)^2\right] = 0.$$

Solving this equation by the method of separation of variables, we arrive at

$$S = E_0 t + M\varphi + \int dr \sqrt{\frac{E_0^2}{c^2}\left[1 + \frac{7\alpha|\mathbf{m}|^2}{45\pi B_q^2 r^6}\right] - \frac{M^2}{r^2}}, \quad (3)$$

where E_0 and M are integration constants that take the following forms for a ray passing near the star at a distance ρ:

$$E_0 = \omega_0, \quad M = \frac{\omega_0\rho}{c}.$$

Because the value of $\frac{\alpha|\mathbf{m}|^2}{B_q^2 r^6}$ is small, we can use here the algorithm developed for the calculation of the gravitational-bending angle for light rays. Using the denotations introduced in monograph [11], we expand the radial part of eikonal (3) in powers of $\frac{\alpha|\mathbf{m}|^2}{B_q^2 r^6}$:

$$S_r = S_r^0 + \frac{7\alpha|\mathbf{m}|^2\omega_0}{720\pi B_q^2 c}\left[\frac{(2\rho^2 + 3r^2)\sqrt{r^2 - \rho^2}}{\rho^4 r^4} + \frac{3}{\rho^5}\arccos\left(\frac{\rho}{r}\right)\right],$$

where S_r^0 describes the rectilinear propagation of the gamma-radiation.

In the case when a wave propagates from a gamma-radiation source located at a large distance R to the point $r = \rho$, which is nearest to the star, and then to the same distance R, the total variation of S_r is

$$\Delta S_r - \Delta S_r^0 = \frac{7\alpha|\mathbf{m}|^2\omega_0}{360\pi B_q^2 c}\left[\frac{(2\rho^2 + 3R^2)\sqrt{R^2 - \rho^2}}{\rho^4 R^4} + \frac{3}{\rho^5}\arccos\left(\frac{\rho}{R}\right)\right].$$

The variation in the polar angle on this path can be obtained by differentiating $\Delta S_r^0 - \Delta S_r$ with respect to $M = \frac{\omega_0\rho}{c}$:

$$\delta\varphi_1 = \frac{7\alpha|\mathbf{m}|^2}{360\pi B_q^2}\left[\frac{15}{\rho^6}\arccos\left(\frac{\rho}{R}\right) + \frac{15R^4 - 2\rho^2R^2 - 5\rho^4}{\rho^5 R^4\sqrt{R^2 - \rho^2}}\right].$$

Passing to the limit $R \gg \rho$, we arrive at

$$\delta\varphi_1 = \frac{7\alpha|\mathbf{m}|^2}{48 B_q^2 \rho^6}. \quad (4)$$

The plus sign in this expression shows that the magnetic-dipole field in the plane of the magnetic equator acts on electromagnetic waves like a convex lens. Quite similarly, it is possible to show that the ray bending angle for an electromagnetic wave polarized in the *XOY* plane is equal to

$$\delta\varphi_2 = \frac{\alpha|\mathbf{m}|^2}{12 B_q^2 \rho^6}. \quad (5)$$

According to the general theory of relativity, together with the nonlinear electrodynamic bending of light rays, the gravitational bending takes place [11]:

$$\delta\varphi_g = \frac{2r_g}{\rho}, \quad (6)$$

where r_g is the gravitational radius of the star.

We now estimate the maximum values of the ray-bending angles in the magnetic and gravitational fields of pulsars and magnetars. In the case of pulsars, the magnetic field can attain a value of $B \sim 10^{13}$ G. In this case, expressions (4) and (5) yield the following estimates: $\delta\varphi_1 = 5.5\times 10^{-5}$ rad and $\delta\varphi_2 = 3.1\times 10^{-5}$ rad.

When the gamma-radiation propagates through the magnetic field of a magnetar, the maximum values for the angles of the nonlinear electrodynamic bending increase significantly: $\delta\varphi_1 = 0.55$ rad and $\delta\varphi_2 = 0.31$ rad.

Because the masses and sizes of pulsars and magnetars are approximately equal, we will use the mean values $r_g = 3$ km and $\rho = 100$ km in order to estimate the maximum value of the gravitational bending of light

rays. In this case, expression (6) leads to the estimate $\delta\varphi_g = 6 \times 10^{-2}$ rad.

Thus, in the cases of pulsars and magnetars, the main contributions to the ray bending are, respectively, due to the gravitational field and nonlinear electrodynamic effects in vacuum. Because the gravitational and nonlinear electrodynamic bendings of a light ray are inversely proportional to the first and sixth powers of the impact parameter ρ, respectively, these two contributions can be separated, provided that the summary bending angle is measured for several values of the impact parameter.

As the detailed analysis shows, the external manifestation of the nonlinear electrodynamic and gravitational bendings of light rays depends on the ratio of the distances from the gamma-radiation source and pulsar (or magnetar) to the Earth. For extragalactic gamma-ray sources, the scattering of their gamma-radiation flux by the magnetic and gravitational fields of a pulsar or magnetar is large. Therefore, the radiation intensity for significantly curved rays should be extremely small in the vicinity of the Earth. In this case, the ray bending manifests itself in a sharp decrease in the radiation intensity, even for vanishingly small bending angles.

If the gamma-radiation originates in the vicinity of a magnetic neutron star (for example, in the case of the star contained in a close binary system, or if the gamma-radiation originates in regions immediately adjoining the surface of the star), the radiation scattering by the magnetic and gravitational fields is not so pronounced. In this case, the radiation intensity detected on the Earth decreases with an increase in the bending angle, but not so abruptly as in the case of an extragalactic source. Therefore, for astrophysical objects containing a neutron star with a magnetic field $B \sim 10^{13}$–10^{15} G, the effects of the nonlinear-electrodynamic and gravitational ray bendings already become observable at the current level of the measurement accuracy for facilities of extraterrestrial astronomy.

REFERENCES

1. D. L. Burke, R. C. Feld, G. Horton-Smith, *et al.*, Phys. Rev. Lett. **79**, 1626 (1997).
2. I. M. Ternov, V. R. Khalilov, and V. N. Rodionov, *Interaction of Charged Particles with Strong Electromagnetic Field* (Mosk. Gos. Univ., Moscow, 1982).
3. E. B. Aleksandrov, A. A. Ansel'm, and A. N. Moskalev, Zh. Éksp. Teor. Fiz. **89**, 1181 (1985) [Sov. Phys. JETP **62**, 680 (1985)].
4. V. L. Ginzburg, *Theoretical Physics and Astrophysics* (Nauka, Moscow, 1987; Pergamon, Oxford, 1979).
5. N. N. Rozanov, Zh. Éksp. Teor. Fiz. **103**, 1996 (1993) [JETP **76**, 991 (1993)].
6. D. Bakalov *et al.*, Quantum Semiclassic. Opt. **10**, 239 (1998).
7. V. I. Denisov, Phys. Rev. D **61**, 036004 (2000).
8. V. I. Denisov, J. Opt. A **2**, 372 (2000).
9. V. I. Denisov and I. P. Denisova, Opt. Spektrosk. **90**, 329 (2001) [Opt. Spectrosc. **90**, 282 (2001)].
10. V. I. Denisov and I. P. Denisova, Opt. Spektrosk. **90**, 1022 (2001) [Opt. Spectrosc. **90**, 928 (2001)].
11. L. D. Landau and E. M. Lifshitz, *The Classical Theory of Fields* (Nauka, Moscow, 1988; Pergamon, Oxford, 1975).

Translated by V. Bukhanov

Doklady Physics, Vol. 46, No. 10, 2001, pp. 708–710. Translated from Doklady Akademii Nauk, Vol. 380, No. 4, 2001, pp. 476–478.

TECHNICAL PHYSICS

Influence of Vacancies on the Surface Tension at the Interface between Two Materials

R. V. Gol'dshtein* and M. E. Sarychev**

Presented by Academician A. Yu. Ishlinskiĭ March 29, 2001

Received April 3, 2001

Various defects of crystal structure dramatically affect the physical and mechanical properties of solids [1, 2]. Above all, such defects are represented by vacancies, interstitials, and dislocations. According to the available concepts [1], vacancies play an important role in the processes of diffusion and related phenomena such as aging, precipitation of secondary phases, and annealing. It was also established, among them theoretically, that nonequilibrium vacancies can change the surface tension of intergrain boundaries (see, e.g., [3]). There are various methods to obtain noticeable concentrations of vacancies in materials, in particular, by irradiating them with nuclear particles or with the help of plastic strains. Varying the vacancy concentration, it is thereby possible to control the corresponding properties of materials, including the surface tension of boundaries.

In this paper, we considered theoretically a possibility of affecting the surface tension of a boundary (an interface) formed as a result of the contact of various crystalline materials by changing the vacancy concentration in them. This problem is of special interest in studying the adhesion properties of multilayer coatings, because, in the case of brittle rupture, the surface energy (in the Griffits sense) coincides with the surface tension at the interface within the accuracy to the coefficient of two if the crack grows along the interface between the materials (an adhesion crack). In a number of experimental studies (for example, in [4]), it was shown that the adhesion and strength of thin-film coatings determined by the value of surface tension at the coating–substrate interface [5] depend substantially on defect concentration. In our consideration, we employed the thermodynamic approach similar to that used in [3] for analysis of the surface tension of intergrain boundaries.

* *Institute of Problems in Mechanics, Russian Academy of Sciences, pr. Vernadskogo 101, Moscow, 117526 Russia*

** *Institute of Physics and Technology, Russian Academy of Sciences, ul. Krasikova 25a, Moscow, 117218 Russia*

We consider an interface between two different homogeneous materials 1 and 2, which is in equilibrium with these materials. As is well known, a change in the surface tension σ_{12} of the interface caused by the variation in the thermodynamic state of materials 1 and 2 is described by the Gibbs equation [3]. If the changes in the states of materials are caused by the deviation of their vacancy concentrations from the equilibrium ones, the Gibbs equation can be written as

$$d\sigma_{12} = -\Gamma_1 d\mu_1 - \Gamma_2 d\mu_2 - s_I dT - v_I dp, \qquad (1)$$

where T and p are the temperature and pressure in materials 1 and 2, $d\mu_1$ and $d\mu_2$ are the changes in the chemical potentials of these materials caused by a change in the concentrations of vacancies, s_I and v_I are the specific (per unit interface area) entropy and specific volume of the interface, and Γ_1 and Γ_2 are the numbers of vacancies from materials 1 and 2 in the interface per its unit area:

$$\Gamma_i = \frac{C_{Ii} b}{\Omega_i}, \quad i = 1, 2. \qquad (2)$$

Here, $G_{Ii} < 1$ is the dimensionless concentration of vacancies of the ith material in the interface, Ω_i is the volume of the corresponding vacancies, and b is the interface thickness.

The chemical potentials of nonequilibrium vacancies, whose variation contributes into Eq. (1), are determined by the expressions [6]

$$\mu_i = kT \ln \frac{C_i}{C_{ie}}, \quad i = 1, 2, \qquad (3)$$

where C_i is the nonequilibrium dimensionless concentration of vacancies in the ith material, C_{ie} is its equilibrium value, and k is the Boltzmann constant.

Furthermore, we assume that the temperature and pressure are constant; i.e., $dT = 0$ and $dp = 0$ in (1). Then, substituting expressions (2) and (3) into (1), we obtain

$$d\sigma_{12} = -bkT\left(\frac{C_{I1}}{\Omega_1}\frac{dC_1}{C_1} + \frac{C_{I2}}{\Omega_2}\frac{dC_2}{C_2}\right). \qquad (4)$$

1028-3358/01/4610-0708$21.00

The concentrations C_{I1} and C_{I2} in (4) are, in general, the functions of C_1 and C_2. To find them, we use a model according to which the interface is considered as a surface absorbing the vacancies [3]. We also assume that the absorption of vacancies in each of the materials 1 and 2 takes place independently. In this case, the kinetics of the variation in C_{I1} and C_{I2} is described by the equations

$$\begin{aligned}\frac{dC_{I1}}{dt} &= k_{a1}(1-C_{I1})C_1 - k_{d1}C_{I1}(1-C_1),\\ \frac{dC_{I2}}{dt} &= k_{a2}(1-C_{I2})C_2 - k_{d2}C_{I2}(1-C_2).\end{aligned} \tag{5}$$

Here, k_{a1} and k_{d1} are, respectively, the constants of adsorption and desorption of vacancies in the process of their exchange between the material 1 and the interface, and k_{a2} and k_{d2} are these constants for material 2. In the steady-state regime $\left(\frac{dC_{Ii}}{dt} = 0\right)$, we obtain from (5):

$$C_{Ii} = \frac{k_{di}C_i}{k_{di} + (k_{ai} - k_{di})C_i}. \tag{6}$$

In its form, dependence (6) represents the known Langmuir isotherm for the surface adsorption [3]. Integrating equation (4), with allowance for (6), yields

$$\sigma_{12} = \sigma_{12}^{(0)} - bkT\left\{\frac{\frac{h_1}{\Omega_1}}{h_1 - 1}\ln\left[\frac{1 + (h_1 - 1)C_1}{1 + (h_1 - 1)C_{1e}}\right] + \frac{\frac{h_2}{\Omega_2}}{h_2 - 1}\ln\left[\frac{1 + (h_2 - 1)C_2}{1 + (h_2 - 1)C_{2e}}\right]\right\}, \tag{7}$$

where $h_i = \frac{k_{ai}}{k_{di}}$ and $\sigma_{12}^{(0)} = \sigma_{12}$ ($C_1 = C_{1e}$, $C_2 = C_{2e}$) is the value of surface tension in the equilibrium state. Formula (7) generalizes the relationship derived in [3] for the dependence of the intergrain–boundary tension on the concentration of nonequilibrium vacancies in the grains of a polycrystalline structure.

It is easy to understand that the character of the dependence of σ_{12} on C_1 and C_2 is unaffected by the value h_i. Both contributions in the braces of (7) increase, respectively, with C_1 and C_2 from negative values for $C_i < C_{ie}$ to positive values for $C_i > C_{ie}$ and vanish for $C_i = C_{ie}$.

At the same time, the value of $\sigma_{12} - \sigma_{12}^{(0)}$ depends rather strongly on the values of h_1 and h_2. We consider, therefore, in more detail what determines these values. The constants k_{ai} and k_{di} of adsorption and desorption depend on temperature in the manner similar to the Arrhenius law, which yields

$$h_i = h_{i0}\exp\left(\frac{\sigma_i^{(ex)}\Omega_i}{kT}\right), \tag{8}$$

where

$$h_{i0} \cong \exp\left\{\frac{\Delta E_i + (\sigma_i^{(in)}\Omega_i - \sigma_I\Omega_I)}{kT}\right\}$$

and $\Delta E_i = E_{di} - E_{ai}$ is the difference in the activation energies for desorption (E_{di}) and adsorption (E_{ai}) of vacancies in the interface, σ_I and σ_i are the mechanical stresses in the interface and in the bulk of the corresponding material (the latter is the sum of external $\sigma_i^{(ex)}$ and internal $\sigma_i^{(in)}$ stresses generated by the interface; i.e., $\sigma_i = \sigma_i^{(in)} + \sigma_i^{(ex)}$), and h_{i0} is the value of h_i without external mechanical loading.

If the interface is a good absorber of vacancies of the given material for $\sigma_i^{(ex)} = 0$, k_{ai} must exceed k_{di} as follows from (5), because this provides $\frac{dC_{Ii}}{dt} > 0$; i.e., $h_{i0} > 1$. Thus, if $\sigma_i^{(ex)} > 0$, we have *a fortiori* that $h_i > 1$. However, in fact, this contribution only slightly affects the relationship between h_i and 1 for real stresses by virtue of the smallness of $\sigma_i^{(ex)}\Omega_i$ in (8) compared to ΔE_i. For example, even for $\sigma_i^{(ex)} \sim 100$ MPa and $\Omega_i \simeq 10^{-29}$ m^3, we have $\sigma_i^{(ex)}\Omega_i \sim 0.01$ eV, whereas $|\Delta E_i| \sim 0.1$ eV.

We now consider the character of the dependence of σ_{12} on concentrations C_1 and C_2. As follows from (7), each of the two contributions into σ_{12} is a monotone function of C_1 and C_2, respectively. In other words, independent of whether the interface is a good ($h_i > 1$) or bad ($h_i < 1$) absorber for the vacancies of the materials used, its surface tension decreases with an increase in the vacancy concentration in each of them separately. In this case, the inequalities $\sigma_{12} - \sigma_{12}^{(0)} < 0$ and $\sigma_{12} - \sigma_{12}^{(0)} > 0$ are realized for $C_i > C_{ie}$ and $C_i < C_{ie}$, respectively.

However, being the function of two variables, $\sigma_{12}(C_1, C_2)$ can also behave in a more complicated fashion. Let C_1 and C_2 vary simultaneously so that C_2 is a certain function of C_1; for example, $C_2 = \varepsilon C_1 + C_{2e} - \varepsilon C_{1e}$ ($\varepsilon > 0$ is a certain coefficient). If the interface effectively absorbs the vacancies from material 1 ($h_1 > 1$) and poorly from material 2 ($h_2 < 1$), the analysis shows

that the dependence of σ_{12} on C_1 can have a maximum at $C_1 = C_1^*$ $\left(\frac{d\sigma_{12}}{dC_1} = 0 \text{ at } C_1 = C_1^*\right)$, where

$$C_1^* = \frac{\frac{bh_1}{\Omega_1} + \frac{\varepsilon h_2}{\Omega_2}}{\varepsilon\left[\frac{h_1}{\Omega_1}(1-h_2) - \frac{h_2}{\Omega_2}(h_1-1)\right]},$$

$$b = 1-(1-h_2)(C_{2e} - \varepsilon C_{1e}),$$

provided that the conditions

$$\varepsilon > \frac{1-(1-h_2)C_{2e}}{1-(1-h_2)C_{1e}}, \quad \frac{\frac{1}{h_2}-1}{1-\frac{1}{h_1}} > \frac{\Omega_1}{\Omega_2},$$

are satisfied for which $0 < C_1^* < 1$ and $\left(\frac{d^2\sigma_{12}}{dC_1^2}\right) < 0$ for $C_1 = C_1^*$.

Thus, when the value of σ_{12} is changed by varying the vacancy concentrations in the bulk of the materials that form the interface, it is possible to realize both the monotonic dependences and those having a maximum. This conclusion can turn out to be useful for the optimization of those characteristics of interfaces, which are related to the surface tension in them.

Finally, using (7), we estimate the order of magnitude for $\Delta\sigma_{12} = \sigma_{12}^{(0)} - \sigma_{12}$. For example, at $T = 300$ K, $b \sim 5$ Å, $\Delta E_1 = 0.35$ eV, $\Delta E_2 = -0.1$ eV, $C_{1e} \simeq 10^{-9}$, $C_{2e} \simeq 10^{-8}$, and $\Omega_1 \sim \Omega_2 \sim 10^{-29}$ m^3, we obtain

$$\Delta\sigma_{12} \sim 0.2\ln(10^6 C_1) \text{ J/m}^2.$$

In this case, $\Delta\sigma_{12} \sim 0.5$ J/m^2 for $C_1 \sim 10^{-5}$ and $\Delta\sigma_{12} \sim 0.1$ J/m^2 for $C_1 \sim 10^{-6}$. These are reasonably high values if we take into account that the surface tension of metals amounts to 1–3 J/m^2 [7]. The tension coefficients for interfaces between two metals must be of the same order of magnitude, because, according to the current theories (see the review in [5]), $|\sigma_1 - \sigma_2| < \sigma_{12}^{(0)} < \sigma_1 + \sigma_2$ (σ_1 and σ_2 are the surface tensions of the metals forming the interface). For example, $\sigma_{Al} \sim 1$ J/m^2 and $\sigma_{Cu} \sim 1.7$ J/m^2 [7]; i.e., 0.7 J/m^2 < $\sigma_{Al-Cu}^{(0)}$ < 2.7 J/m^2 for the Al–Cu interface.

REFERENCES

1. *Physical Metallurgy*, Ed. by R. W. Cahn (North-Holland, Amsterdam, 1965; Mir, Moscow, 1968), Vol. 3.
2. D. S. Rickerby, Thin Solid Films **154**, 125 (1987).
3. B. S. Bokshteĭn, N. V. Konetskiĭ, and P. S. Shvindlerman, *Thermodynamics and Kinetics of Grain Boundaries in Metals* (Metallurgiya, Moscow, 1986).
4. T. Foeke and D. van Heerden, in *Chemistry and Physics of Nanostructures and Related Nonequilibrium Materials*, Ed. by En Ma *et al.* (TMS, Pittsburgh, 1997), pp. 193–199.
5. A. J. Kinloch, *Adhesion and Adhesives: Science and Technology* (Chapman and Hall, London, 1987; Mir, Moscow, 1997).
6. A. M. Kosevich, *Foundations of Crystal-Lattice Mechanics* (Nauka, Moscow, 1972).
7. A. P. Babichev, I. A. Babushkina, A. A. Bratkovskiĭ, *et al.*, *Physical Quantities, Handbook* (Énergoizdat, Moscow, 1991).

Translated by V. Bukhanov

Doklady Physics, Vol. 46, No. 10, 2001, pp. 711–714. Translated from Doklady Akademii Nauk, Vol. 380, No. 4, 2001, pp. 479–483.

TECHNICAL PHYSICS

Thermodynamics of the Ni–Zr Melt: Specific Features of Interatomic Interaction and Transition into an Amorphous State

A. I. Zaitsev and N. E. Zaitseva

Presented by Academician O. A. Bannykh April 9, 2001

Received April 11, 2001

Nickel–zirconium alloys have a high glass-forming ability in a wide range of concentrations and constitute the basis for a variety of bulky amorphous metallic materials [1]. However, until now, there is no information on the Gibbs energy of the Ni–Zr-melt formation. This fact hampers both the analysis of thermodynamic and kinetic parameters of the transition of the Ni–Zr liquid into an amorphous state and the understanding of the reasons why such a transition easily proceeds in a number of transition metal systems.

In the study proposed, we investigated the composition of vapor and thermodynamic properties of the nickel–zirconium alloy within the temperature range between 1357 and 1861 K and in the composition range from 0 to 94.3 at. % Zr using the method of Knudsen mass spectrometry. The saturated-vapor pressure was measured using doubled Knudsen cells manufactured from molybdenum, tantalum, or niobium. To prevent the interaction of the alloys under investigation and a reference sample with the material of effusion cells, we deposited zirconium oxide or zirconium diboride on their inner surface using the plasma method. No effect of the cell material on the vapor composition and partial pressures of components was observed. For comparison, we used ultrapure iron with an impurity content of 10^{-6}% of cobalt of 99.99% purity. For the synthesis of alloys, iodide zirconium (99.98%) and electrolytic nickel (99.99%) were used. The methods of preparation of samples and performing experiments were similar to those described previously [2].

In the mass spectra of saturated vapor, Ni^+ and Zr^+ ions were detected above nickel–zirconium melts, testifying to its simple composition. The values of pressure of saturated-vapor components found were used to calculate their activities with respect to liquid metals. For this purpose, we used the data of [3] on the Gibbs energies for melting Ni and Zr. Because Zr-vapor pressure was measurable only within a very narrow interval of the investigated temperature–concentration range, the activity of vapor was mainly found by integrating the Gibbs–Duhem equation using the nickel α-functions:

$$\alpha(\mathrm{Ni}) = \frac{\ln\{\gamma(\mathrm{Ni})\}}{[1 - x(\mathrm{Ni})]^2}.$$

As a result of the experiments and calculations performed, we obtained a representative data base containing more than 900 values of activities of the components for various compositions and temperatures. A part of them are displayed in the table.

The structure of the phase diagram for the Ni–Zr system [4], an intense interaction between its components (see the table), and the tendency of the melt to amorphization in a wide range of concentrations make it natural [5] to describe its thermodynamic behavior using the conception of association solutions. Previously, it was this approach that made it possible to adequately approximate both the concentration and temperature dependences of thermodynamic functions of liquid alloys for a number of binary and ternary systems of transition metals with metalloids [5, 6]. It turned out that in many cases special features in the behavior of such liquids are close to those for perfect association solutions due to the prevalence of a covalent constituent of the chemical bond between its components. In the case of nickel–zirconium alloys, the presence of a considerable metal constituent of the chemical bond is evident; it must lead to an essential excess interaction in addition to the formation of the associative groups. This interaction can be taken into account in the context of the model [5], according to which the Gibbs energy of the Ni–Zr-melt formation can be represented by the equation

$$\Delta_f G = \sum n(i)\Delta_f G(i) + RT\{n(\mathrm{Ni}_1)\ln x(\mathrm{Ni}_1) + n(\mathrm{Zr}_1)\ln x(\mathrm{Zr}_1) + \sum n(i)\ln x(i)\} + \Delta_f G^E, \quad (1)$$

where $\Delta_f G(i) = -RT\ln K(i) = \Delta_f H(i) - T\Delta_f S(i)$ is the Gibbs energy for the formation of one mole of the asso-

Kurdyumov Institute of Metal Physics and Functional Materials, Bardin Central Research Institute for the Iron and Steel Industry, Vtoraya Baumanskaya ul. 9/23, Moscow, 107005 Russia

1028-3358/01/4610-0711$21.00

Experimental data on activities of Ni–Zr melt components chosen arbitrarily from the experimental data base and the values of a(Ni) and a(Zr) calculated from the model proposed

x(Ni)	T, K	a(Ni)		a(Zr)	
		experiment	model	experiment	model
0.148	1823	0.000305	0.000302	0.760	0.760
0.570	1823	0.0625	0.0620	0.0345	0.0343
0.994	1823	0.991	0.994	1.18×10^{-7}	1.19×10^{-7}
0.199	1773	0.000493	0.000500	0.635	0.640
0.473	1773	0.0082	0.0183	0.104	0.102
0.799	1773	0.462	0.457	0.000283	0.000286
0.242	1723	0.000757	0.000764	0.527	0.531
0.406	1723	0.00705	0.00701	0.187	0.184
0.752	1723	0.308	0.307	0.000783	0.000778
0.303	1673	0.00149	0.00147	0.378	0.378
0.705	1673	0.186	0.187	0.00201	0.00203
0.903	1673	0.779	0.790	5.70×10^{-6}	5.65×10^{-6}
0.351	1623	0.00229	0.00232	0.271	0.268
0.850	1623	0.607	0.607	2.32×10^{-7}	2.29×10^{-5}
0.524	1573	0.0188	0.0186	0.0430	0.0436
0.598	1523	0.407	0.401	0.0121	0.0122
0.903	1473	0.768	0.776	8.22×10^{-7}	8.15×10^{-7}
0.647	1423	0.0570	0.0570	0.00311	0.00313

ciative complex of the type i; $K(i)$ is the constant of equilibrium of the corresponding reaction of formation for the groups of the type i; $n(i)$, $x(i)$, $n(\mathrm{Ni}_1)$, $n(\mathrm{Zr}_1)$, $x(\mathrm{Ni}_1)$, and $x(\mathrm{Zr}_1)$ are the numbers of moles and the mole fractions of components of the association solution; and $\Delta_f G^E$ is the excess Gibbs energy for the solution formation. This excess energy is caused by both the presence of other contributions to the chemical bond between initial components (except the covalent bond), which is responsible for the formation of associative groups, and the presence of a certain residual interaction as well as a distinction in the volumes of monomeric particles and associative groups [4]. The summation in Eq. (1) is accomplished over all the types of associative complexes being formed. For $\Delta_f G^E$, according to [5, 7], we take the expression

$$\Delta_f G^E = \sum L_{ij} n^i(\mathrm{Ni}) n^j(\mathrm{Zr}) / (n(\mathrm{Ni}) + n(\mathrm{Zr}))^{(i+j-1)}, \quad (2)$$

where n(Ni) and n(Zr) are the numbers of moles of initial components. The quantity, type, thermodynamic functions of formation of associative groups, as well as the number of terms and the values of coefficients for the term $\Delta_f G^E$ were found with the help of the optimization procedure. It consisted of varying the model parameters ($\Delta_f H(i)$, $\Delta_f S(i)$, L_{ij}) and finding the minimum of the sum for the squares of residuals between the calculated and experimental activities of the components. In the calculations, we used a complete data base of experimental values. The calculations performed showed that an adequate description of the concentration and temperature dependences for activities of the components with an accuracy better than the experimental error (2–3%) (see the table) can be attained only with allowance for the presence of the associative groups of three types (NiZr, Ni_2Zr, and Ni_3Zr) in the solution and of two terms in the expression for the excess Gibbs energy. Values of parameters ($\Delta_f H$ and L_{ij} expressed in J/mol and $\Delta_f S$ expressed in J/(mol K)) are:

$$\begin{aligned} &\Delta_f H(\mathrm{NiZr}) = -62\,000, \quad \Delta_f S(\mathrm{NiZr}) = -38.4; \\ &\Delta_f H(\mathrm{Ni_2Zr}) = -97\,400, \quad \Delta_f S(\mathrm{Ni_2Zr}) = -40.3; \\ &\Delta_f H(\mathrm{Ni_3Zr}) = -120\,800, \quad \Delta_f S(\mathrm{Ni_3Zr}) = -60.2; \\ &L_{11} = -106\,875, \quad L_{21} = -26\,975. \end{aligned} \quad (3)$$

The concentration dependences found for the integral thermodynamic functions of the Ni–Zr-melt formation are asymmetric (Fig. 1) Their extremes are shifted towards nickel, which agrees well with the form of the phase diagrams of the Ni–Zr system [4]. Until now, only the enthalpy $\Delta_f H$ for the formation of liquid

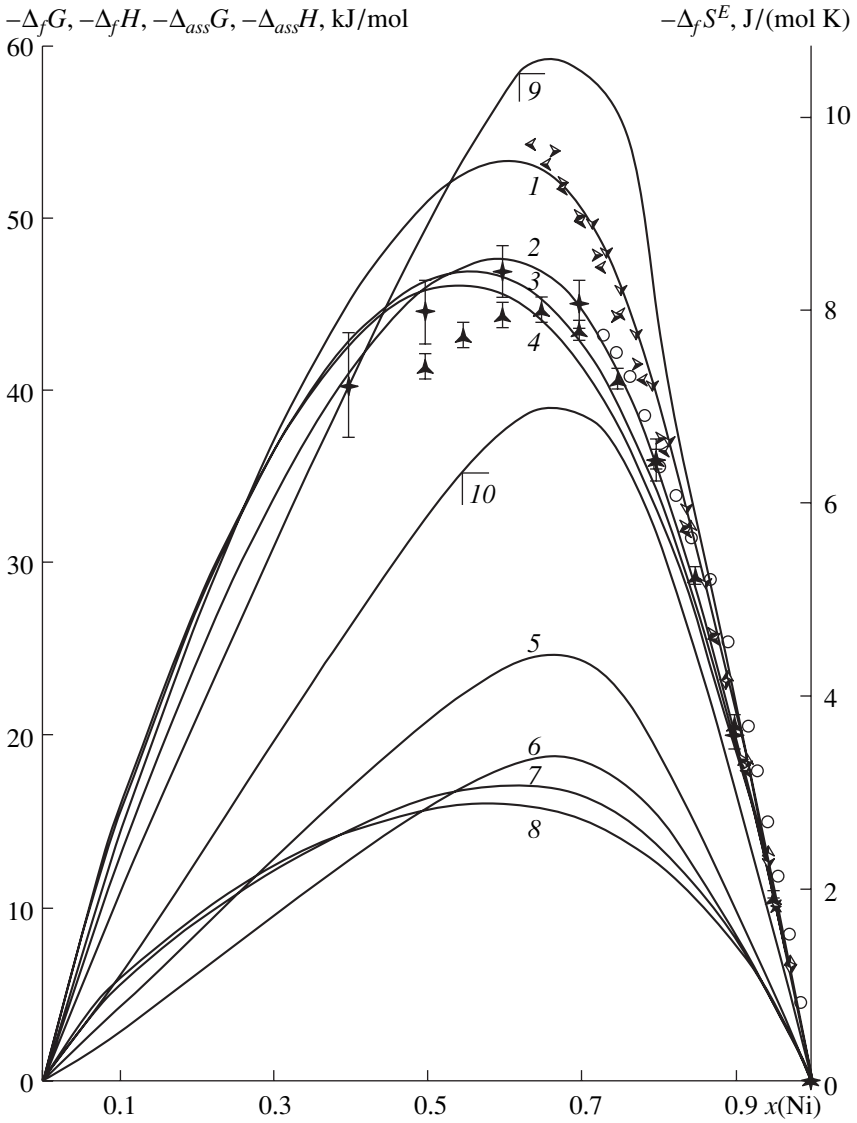

Fig. 1. Integral thermodynamic functions for the formation of the Ni–Zr melt from liquid components according to the results of this investigation: (*1*) $\Delta_f H$(1450 K), (*2*) $\Delta_f H$(1823 K), (*3*) $\Delta_f G$(1450 K), (*4*) $\Delta_f G$ (1823 K), (*9*) $\Delta_f S^E$(1823 K), (*10*) $\Delta_f S^E$(1450 K) and according to the data of other authors: (◇) [9], $\Delta_f H$(1823 K); (▲) [8], $\Delta_f H$(1963 K); (○), [4], the results obtained with a high-vacuum calorimeter, $\Delta_f H$(1838 K); and the data obtained with a SETARAM calorimeter: (◀) $\Delta_f H$(1740 K), (▶) $\Delta_f H$(1742 K), (▲) $\Delta_f H$(1743 K), and (▼) $\Delta_f H$(1741 K). The calculated contributions to the thermodynamic functions are related to the covalent (associative) interaction between components: (*5*) $\Delta_f H$(1450 K), (*6*) $\Delta_f H$1823 K), (*7*) $\Delta_f G$(1450 K), and (*8*) $\Delta_f G$(1823 K).

nickel–zirconium alloys was experimentally studied [4, 8, 9]. The results obtained (Fig. 1) are in good agreement with each other and, with allowance for a difference in the investigated temperature ranges, coincide with the data of the present study. Somewhat underestimated $\Delta_f H$ values were obtained only in [4], evidently owing to the partial oxidation of samples in the course of measurements carried out in ambient argon with a SETARAM calorimeter. This is corroborated by the fact that the discrepancy with results of other investigations and with the data of the same authors obtained by means of a high-vacuum calorimeter (Fig. 1) increases with zirconium content. In Fig. 1, in addition to the summary properties, we also display the values of change in the integral thermodynamic characteristics caused by the presence of the covalent constituent of the chemical bond, which leads to the association processes in the liquid. These values are calculated using Eqs. (1), (2), and parameters (3), and are shown in Fig. 1 for two temperatures: 1823 K, which is close to the upper limit of the measurement temperature range, and 1450 K, which is approximately a median temperature of the liquidus on the phase diagram for the Ni–Zr system [4]. As can be seen in Fig.1, the contribution associated with the metal constituent of the chemical bond prevails in the Gibbs energy and the enthalpy of

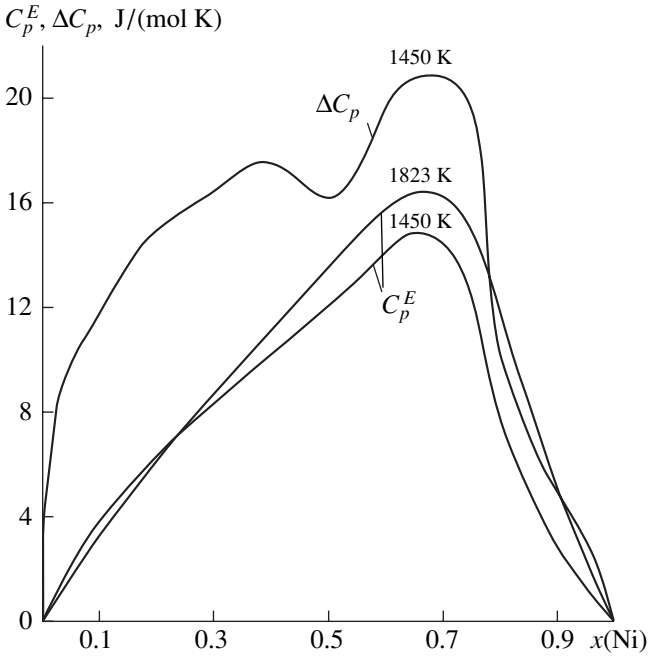

Fig. 2. Concentration dependences of the Ni–Zr-melt heat capacity C_p^E excessive with respect to the additive sum of characteristics of liquid components and the difference ΔC_p in the heat capacities of the liquid and crystals.

the Ni–Zr-melt formation. The strength of the covalent interaction is significantly lower; however, it increases rapidly with a decrease in temperature: while the covalent contribution to the enthalpy of the formation of the Ni–Zr liquid amounts only nearly one third of the total value at 1823 K, it exceeds one half at 1450 K. The total value of the excess enthalpy of the solution formation is related to the processes of association. It is negative within the entire concentration range and also rapidly increases in absolute value with a decrease in temperature (Fig. 1). On the other hand, the temperature effect on the metallic-type interaction is negligible.

According to conclusions following from the study [10], the kinetic and thermodynamic stimuli for the melt transformation into an amorphous state coincide and are reduced to the minimum values of the entropy $\Delta_m S$ of melting and to the maximum differences ΔC_p between the heat capacities of liquid and crystals. The last statement is equivalent to the requirement of minimum values for the excess entropy $\Delta_f S^E$ and maximum values of the heat capacity C_p^E of the melt, which are excessive with respect to an additive sum of characteristics of liquid components. The calculations performed (Fig. 2) showed that the quantity C_p^E, as well as the quantity $\Delta_f S^E$ for the Ni–Zr melt, is related exclusively to the association processes, i.e., to the covalent constituent of the chemical bond. The concentration dependence of C_p^E, as well as $\Delta_f S^E$, is strongly asymmetric and is even close to a triangular shape. The extremum is shifted towards nickel and lies in the region of the composition with the most strong associative group Ni_2Zr. As the temperature drops from 1823 to 1450 K, the value of C_p^E decreases slightly for the alloys with a high content of nickel and increases for the zirconium-based compositions. In Fig. 2, we also display the values of ΔC_p calculated for 1450 K with invoking the data on heat capacities of crystalline phases from [3, 11]. It can be seen that C_p^E constitutes the larger fraction of this characteristic, especially for the alloy compositions that pass most easily into an amorphous state. Thus, in spite of the lower energy contribution from the covalent constituent compared to the metal one of the chemical bond in the interaction between components, this is the covalent constituent that determines the predisposition of liquid alloys of nickel with zirconium to amorphization. This fact explains a number of specific features of the amorphization of metallic liquids, for example, the closeness in the glass-forming ability of alloys of zirconium with nickel and copper independently of a large difference in the intensity of the resulting interaction between components in the systems indicated.

ACKNOWLEDGMENTS

We are grateful to B.M. Mogutnov and Yu.S. Nechaev for valuable remarks in discussion of results of this study.

This work was supported by the Russian Foundation for Basic Research, project no. 01-02-16804.

REFERENCES

1. P. J. Desre, Mater. Res. Soc. Symp. Proc. **554**, 51 (1999).
2. A. I. Zaitsev, N. V. Korolyov, and B. M. Mogutnov, High Temp. Sci. **28**, 341 (1990).
3. A. T. Dinsdale, CALPHAD: Comput. Coupling Phase Diagrams Thermochem. **15** (4), 317 (1991).
4. I. Arpshofen, R. Luck, B. Predel, and J. E. Smith, J. Phase Equilib. **12** (2), 141 (1991).
5. A. I. Zaitsev and B. M. Mogutnov, High Temp. Mater. Sci. **34** (1/3), 155 (1995).
6. A. I. Zaitsev, A. D. Litvina, N. E. Shelkova, and B. M. Mogutnov, Thermochim. Acta **314**, 307 (1998).
7. A. S. Krylov and A. M. Katsnelson, Z. Metallkd. **84**, 641 (1993).
8. O. Yu. Sidorov, Yu. O. Esin, and P. V. Gel'd, Rasplavy **2** (3), 9 (1988).
9. A. A. Turchanin, M. A. Turchanin, and I. A. Tomilin, Mater. Sci. Forum **269**/**272**, 565 (1998).
10. A. I. Zaitsev and N. E. Shelkova, Z. Metallkd. **91**, 992 (2000).
11. J. F. Smith, Q. Jiang, R. Luck, and B. Predel, J. Phase Equilib. **12**, 538 (1991).

Translated by V. Bukhanov

Doklady Physics, Vol. 46, No. 10, 2001, pp. 715–717. Translated from Doklady Akademii Nauk, Vol. 380, No. 4, 2001, pp. 484–486.

TECHNICAL PHYSICS

On the Stability of the $Er_{0.45}Ho_{0.55}Fe_2$ Compound in the Fine-Grained State

Kh. Ya. Mulyukov*, I. Z. Sharipov*, and S. A. Nikitin**

Presented by Academician V. V. Osiko May 24, 2001

Received April 3, 2001

In studies of the magnetic properties of microcrystalline Fe–Nd–B alloys produced by the crystallization of quenched amorphous ribbons, the precipitation of pure iron in the course of specimen annealing was revealed [1, 2]. However, at that time, attention was not drawn to this fact. The phase instability in complex compounds was also observed in other studies. For example, the conversion of highest valence oxides to lowest valence oxides as well as the reduction of oxides to a pure metal in the course of the shear deformation under high pressure were demonstrated in [3, 4]. A phase layering in the course of alloy-powder processing in a ball mill is described in [5]. In these papers, the phase instability observed is attributed to an effect of the severe plastic deformation on the crystalline structure. It is unclear why the same phenomenon is observed in the course of annealing of a specimen with submicrocrystalline structure produced by crystallization of an amorphous alloy.

In our efforts to obtain additional insights into the phase instability of complex compounds, we studied the temperature dependence of the magnetization and phase composition of the $Er_{0.45}Ho_{0.55}Fe_2$ compound in the coarse-grained and fine-grained states. The choice of the matter for scientific enquiry is caused by the fact that this compound is ferrimagnetic and iron is its constituent. That is why, in this case, the temperature dependence of the magnetization can serve as a highly sensitive indicator of the change in the specimen phase composition.

A fragment of a cast alloy with a size of about 1mm was used as a specimen with the macrocrystalline structure. Because of the extraordinary brittleness of the chosen material, the fine crystalline state was obtained by grinding the material in an agate stamp. To prevent oxidation, the powder was crushed in the ambient ethanol. The powder with particle sizes on the order of 1 μm was obtained by the sedimentation method. The powder-particle size was determined using a JSM-840 scanning electron microscope. The temperature dependence of the specimen magnetization was recorded by the use of automatic vacuum scales [7] in the temperature range from 80 to 1080 K. The phase analysis of the specimens

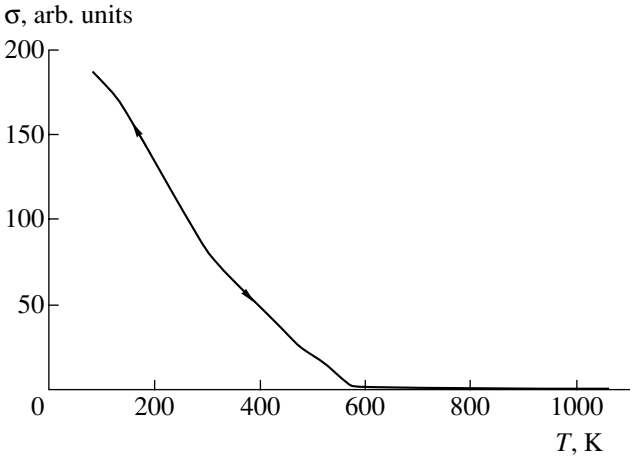

Fig. 1. Temperature dependence of the magnetization for the coarse-grained specimen.

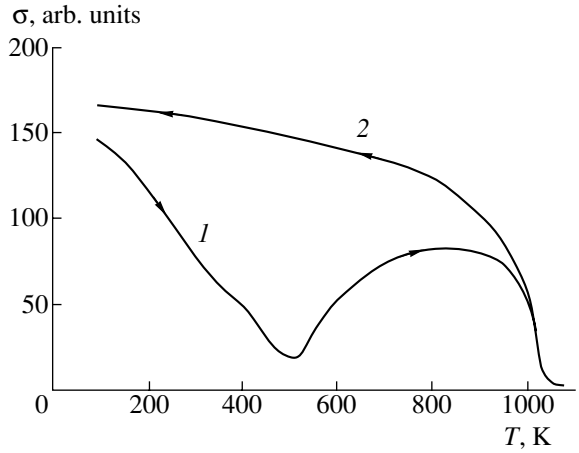

Fig. 2. Temperature dependence of the magnetization for the fine-grained powder.

* *Institute of Problems of Metal Superplasticity, Russian Academy of Sciences, ul. Khalturina 39, Ufa, 450001 Bashkortostan, Russia*

** *Moscow State University, Vorob'evy gory, Moscow, 119899 Russia*

1028-3358/01/4610-0715$21.00 © 2001 MAIK "Nauka/Interperiodica"

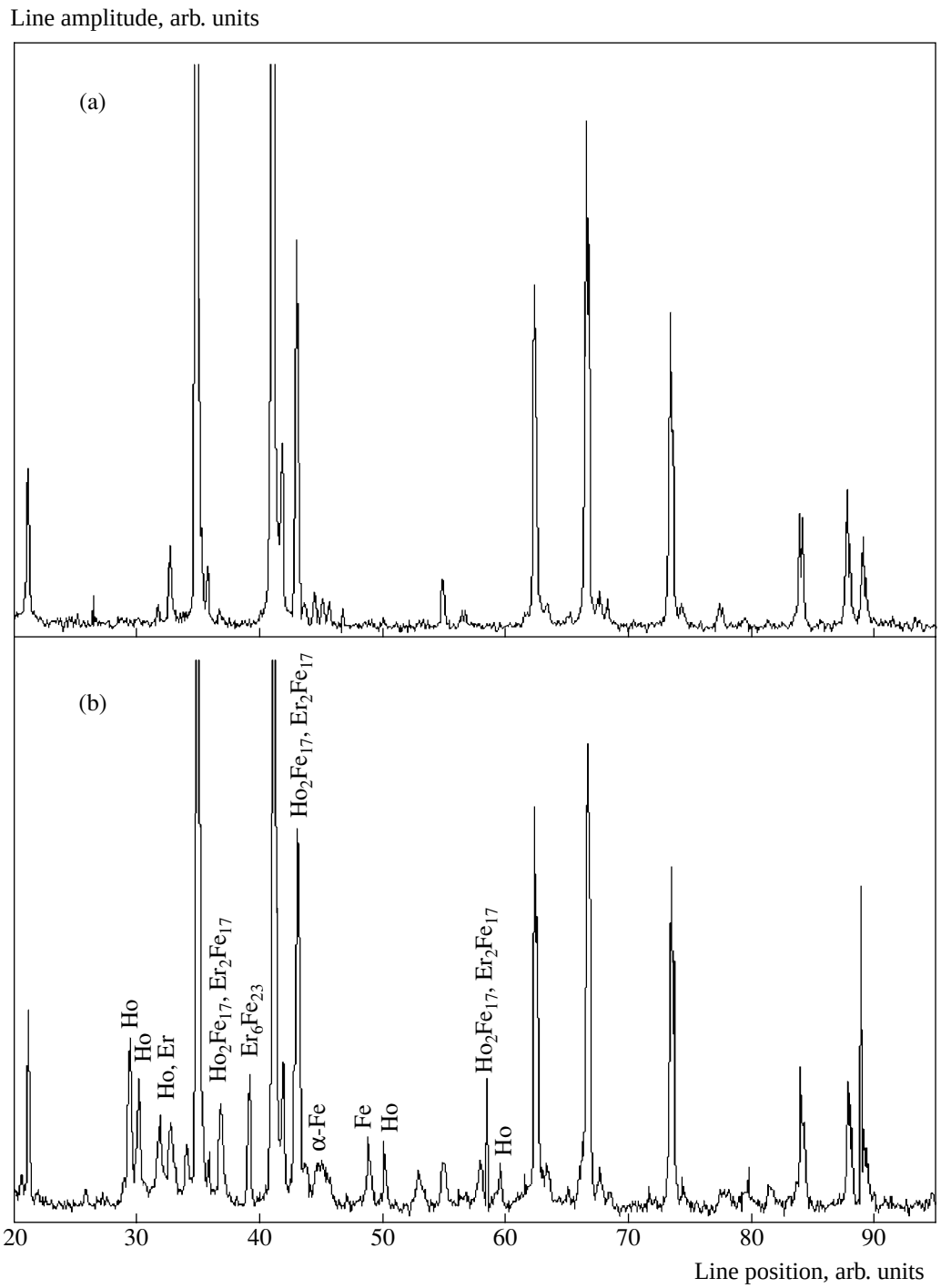

Fig. 3. X-ray diffraction pattern for the fine-grained powder (a) before and (b) after heating to 1080 K.

was carried out with an automated DRON-3M X-ray diffractometer.

The curve of the temperature dependence for the coarse-grained magnetization $\sigma(T)$ of the specimen is shown in Fig. 1. The specimen heating is seen to rapidly decrease the magnetization, which vanishes at 570 K. The distinctive feature of this curve is that the transition of the ferrimagnetic state into a paramagnetic one takes place abruptly. The curves recorded on the specimen heating and cooling essentially coincide. This confirms the phase-state stability of the coarse-grained specimen up to 1080 K.

The temperature dependence of the magnetization $\sigma(T)$ for the fine-grained specimen is shown in Fig. 2. The curve *1* obtained while heating the specimen significantly differs from the corresponding curve for the

coarse-grained specimen in Fig. 1. Initially, the specimen magnetization decreases as the temperature increases. However, above 500 K, the magnetization begins to increase from a nonzero value. The magnetization passes the maximum at 830 K and approaches zero only at 1033 K. Another feature of the dependence $\sigma(T)$ for the fine-grained specimen is the dissimilarity of the run of the curve *2* recorded while cooling the specimen from that obtained after its heating. In this case, curve *2* in Fig. 2 looks like the temperature dependence of the saturation magnetization for pure 3*d*-ferromagnets.

The unusual run of the curves $\sigma(T)$ for the fine-grained powder is presumably explained by a change of the specimen phase composition in the course of heating. The magnetization growth upon the specimen heating above 500 K should be related to the precipitation of a new phase with a large magnetic moment. The run of the curve $\sigma(T)$ corresponding to the precipitated phase implies that it is pure iron because the temperature of the disappearance of the specimen magnetization coincides with the Curie point for iron. It follows from this fact that the $Er_{0.45}Ho_{0.55}Fe_2$ compound decomposes with the precipitation of pure iron when fine particles of the compound are heated in vacuum. The same is evidenced by the fact that the contribution of the $Er_{0.45}Ho_{0.55}Fe_2$ compound into the magnetization is absent on the curve $\sigma(T)$ recorded while cooling the specimen.

To confirm the conclusion on the decomposition of fine particles of the $Er_{0.45}Ho_{0.55}Fe_2$ compound while heating in vacuum, which was based on the magnetic measurements, roentgenographic studies of the compound phase composition were carried out.

Figure 3a shows the X-ray diffraction pattern taken from the fine powder immediately after grinding. All peaks of the diffraction pattern correspond to the basic phase of the $Er_{0.45}Ho_{0.55}Fe_2$ compound. Consequently, in the course of grinding, the phase composition of the compound under study is unaffected.

In the diffraction pattern taken from the same fine powder but heated to 1080 K (see Fig. 3b), a number of additional peaks emerged. The phase identification carried out according to the angular position of the additional peaks shows that not only pure Fe but pure Ho, Er, and phases corresponding to the Ho_2Fe_{17}, Er_2Fe_{17}, and Er_6Fe_{23} compounds as well were formed in the course of heating of the fine powder of the compound under study. The notation for the corresponding phases is shown in Fig. 3b near the additional peaks.

There are also the basic-phase peaks in the diffraction pattern corresponding to the annealed powder. At the same time, there is no residual basic phase in the temperature-dependence curve for the magnetization obtained in the course of the fine-grained specimen cooling below 1080 K. The point is that a great deal of the material is required for carrying out the X-ray radiography. By this reason, the specimen was prepared from the ground powder not separated into fractions with different particle sizes. Because of this, when the specimen is heated, the compound decomposes in small-sized crystals of the powder, whereas the basic phase persists in large-sized ones. On the other hand, the availability of the basic-phase peaks in the diffraction pattern is convenient because, firstly, they are actually reference points, and secondly, it is clearly seen that the compound does not decompose in larger-sized particles.

It should be noted that whereas the magnetic measurements allowed the pure iron release to be basically recorded when heating the fine-grained specimen, the X-ray diffraction analysis also revealed the presence of two phases produced in the course of the decomposition.

Thus, the research performed discloses that the stability of the $Er_{0.45}Ho_{0.55}Fe_2$ compound depends on the crystallite size. Heating the compound crystals with a size of ~1 mm to 1080 K does not result in changing the phase composition. But when crystallites with a size of ~1 μm are heated, their decomposition into pure Fe, Er, Ho, and other compounds of these elements already begins at 500 K. Consequently, the phase instability of complex compounds can be observed not only under the action of high mechanical stresses but also at high temperatures.

ACKNOWLEDGMENTS

This work was supported by the Russian Foundation for Basic Research, project nos. 00-02-17723 and 00-15-99093 “Leading Scientific School.”

REFERENCES

1. T. Miyazaki, H. Takada, and M. Takahashi, Phys. Status Solidi A **99**, 611 (1987).
2. Kh. Ya. Mulyukov, R. Z. Valiev, G. F. Korznikova, and V. V. Stoljarov, Phys. Status Solidi A **112**, 137 (1989).
3. L. F. Vereshchagin, E. V. Zubova, K. P. Budrina, and G. L. Aparnikov, Dokl. Akad. Nauk SSSR **196**, 817 (1971) [Sov. Phys. Dokl. **16**, 127 (1971)].
4. S. S. Absalyamov and Kh. Ya. Mulyukov, Dokl. Akad. Nauk **375**, 469 (2000) [Dokl. Phys. **45**, 657 (2000)].
5. A. Ye. Yermakov, Mater. Sci. Forum **179**–**181**, 455 (1995).
6. C. E. Rodriquez Torres, F. N. Sanches, and L. A. Mendoza Zeilis, Phys. Rev. B **51**, 12142 (1995).
7. Kh. Ya. Mulyukov, I. Z. Sharipov, and S. S. Absalyamov, Prib. Tekh. Éksp., No. 3, 149 (1998).

Translated by V. Tsarev

Doklady Physics, Vol. 46, No. 10, 2001, pp. 718–721. Translated from Doklady Akademii Nauk, Vol. 380, No. 6, 2001, pp. 757–760.

TECHNICAL PHYSICS

A Regular Method of Searching for Discrete Symmetries in Models of Physical Processes

A. V. Kistovich and Yu. D. Chashechkin

Presented by Academician D. M. Klimov April 18, 2001

Received April 24, 2001

Many physical, chemical, and hydrodynamic systems with continuous distributions of parameters whose properties are described by nonlinear differential equations have an ordered structure with clearly identified elements. Striations in a gas discharge, regular structures formed by chemical reactions of the Belousov–Zhabotinsky type [1], regular cells of convective flows in a fluid layer between two planes [2], and periodic structures between differentially rotating coaxial cylinders [3] are objects of intense investigations. In certain cases, it is possible to choose characteristic symmetric functions that satisfactorily describe the regularity of the spatial structure of the phenomenon [1, 4, 5]. The existence of discrete symmetries of the same type in various physical systems indicates a possibility of constructing a regular method for their discovery.

In this paper, we propose an algorithm for searching for discrete symmetries of models of physical processes described by nonlinear differential equations based on combining immersion methods, the analysis of differential forms, and the calculation technique for continuous Lie groups.

We consider the system of differential equations of the general form

$$Eq_k(\{x_j\}, \{F_i\}, \{F_i'\}, \{F_i''\}, \ldots, \{F_i^{(l)}\}) = 0, \quad (1)$$

where $\{x_j\}$ is the set of differential variables, $\{F_i\}$ is the set of field variables, $\{F_i'\}$, $\{F_i''\}$, …, and $\{F_i^{(l)}\}$ are the sets of all partial derivatives of the first, second, and higher orders. In the case of the existence of discrete symmetries, the sets of variables $\{x_j\}$ and $\{F_i\}$ in Eqs. (1) pass to the sets of new variables $\{\tilde{x}_j\}$ and $\{\tilde{F}_i\}$ under the action of their operators:

$$(\{x_j\}, \{F_i\}) \mapsto (\{\tilde{x}_j(x_j, F_i)\}, \{\tilde{F}_i(x_j, F_i)\}). \quad (2)$$

In this case, the following differential equations are valid:

$$\tilde{E}q_k(\{\tilde{x}_j\}, \{\tilde{F}_i\}, \{\tilde{F}_i'\}, \{\tilde{F}_i''\}, \ldots, \{\tilde{F}_i^{(n)}\}) = 0. \quad (3)$$

These equations are derived from (1) by a formal replacement of the old variables by the new ones.

In the context of the formalism of differential forms [6], the set of Eqs. (1) is represented by the set of the 1-forms dx_1, dx_2, …, dx_n, dF_1, dF_2, …, dF_m and the forms of the type $dp^{(l)}_{q,ijk\ldots}$, where

$$p^{(l)}_{q,ijk\ldots} = \frac{\partial^{(l)} F_q}{\partial x_i \partial x_j \partial x_k \ldots} \quad (4)$$

denotes the derivative of the lth order for the qth field variable with respect to the differential variables x_i, x_j, …; the subscripts $i, j, \ldots$ must follow in a nondecreasing order. Correspondingly, for set (3), there is its own set of 1-forms $d\tilde{x}_1, d\tilde{x}_2, \ldots, d\tilde{x}_n, d\tilde{F}_1, d\tilde{F}_2, \ldots, d\tilde{F}_m$, and the forms $d\tilde{p}^{(l)}_{q,ijk\ldots}$.

The consideration is carried out in the extended space $dx_1, \ldots, d\tilde{x}_1, \ldots$, which is not the direct sum of its subspaces $dx_1, \ldots$, and $d\tilde{x}_1, \ldots$, because the basis forms $dx_1, \ldots, dF_m$, and $d\tilde{x}_1, \ldots, d\tilde{F}_m$ are connected by the automorphism relationships.

The automorphic transformations of the field and differential variables satisfy the relationships [7]

$$G_l = b_l^k \tilde{G}_k, \quad (5)$$

where G_l and $\tilde{G}_k$ are the Lie generators of sets (1) and (3), and b_l^k are the constant coefficients of a nondegenerate automorphism matrix, which, in terms of the differential forms, can be written as

$$\mathcal{L}_{\mathbf{v}_l}(\tilde{x}_j) = b_l^k \tilde{\mathcal{L}}_{\mathbf{v}_l}(\tilde{x}_j), \quad \mathcal{L}_{\mathbf{v}_l}(\tilde{F}_i) = b_l^k \tilde{\mathcal{L}}_{\mathbf{v}_l}(\tilde{F}_i). \quad (6)$$

Here, $\mathcal{L}_{\mathbf{v}}()$ and $\tilde{\mathcal{L}}_{\mathbf{v}}()$ denote the Lie derivatives with respect to the isovectors acting in the spaces of the old and new coordinates.

Institute of Problems of Mechanics,
Russian Academy of Sciences,
pr. Vernadskogo 101, Moscow, 117526 Russia

1028-3358/01/4610-0718$21.00

Because the operator of external differentiation commutes with the Lie derivative, the action on Eqs. (6) leads to the expressions

$$\mathcal{L}_{\mathbf{v}_l}(d\tilde{x}_j) = b_l^k \tilde{\mathcal{L}}_{\mathbf{v}_l}(d\tilde{x}_j), \quad \mathcal{L}_{\mathbf{v}_l}(d\tilde{F}_i) = b_l^k \tilde{\mathcal{L}}_{\mathbf{v}_l}(d\tilde{F}_i), \quad (7)$$

which show that the basis forms $dx_1, \ldots, dF_m$, and $d\tilde{x}_1, \ldots, d\tilde{F}_m$ are connected by the automorphism relationships.

The diffeomorphism between the derivatives of field functions in the old variables $p^{(l)}_{q,\,ijk\ldots}$ and in the new variables $\tilde{p}^{(l)}_{q,\,ijk\ldots}$ {induced by automorphism (7)} is represented as an overdetermined set of nonlinear algebraic equations.

The essence of the method proposed consists in the fact that two classes of 1-forms are singled out in extended co-tangential space: the class of basis (or identically annulled) forms and the class of forms annihilated at the solutions to sets (1), (3).

The identically annulled 1-forms can be written as

$$\omega_i^{(b)} = dF_i - \frac{\partial F_i}{\partial x_1}dx_1 - \frac{\partial F_i}{\partial x_2}dx_2 - \ldots - \frac{\partial F_i}{\partial x_n}dx_n, \quad (8)$$

where F_i is the field variable, and dF_i is its differential:

$$dF_i = \frac{\partial F_i}{\partial x_1}dx_1 + \frac{\partial F_i}{\partial x_2}dx_2 + \ldots + \frac{\partial F_i}{\partial x_n}dx_n. \quad (9)$$

In a similar way, the 1-forms $\tilde{\omega}_i^{(b)}$ defined on the new variables $\tilde{F}_i$ and $\tilde{x}_j$ are created. The differential forms annulled on the solutions to set (1) are sought as

$$\omega_i^{(s)} = \sum A^{q,\,ijk\ldots}_{(l)} dp^{(l)}_{q,\,ijk\ldots} + \sum B^j dx_j. \quad (10)$$

The functions $A^{q,\,ijk\ldots}_{(l)}$ and B^j [6] are chosen in such a way that equations (1) can be composed by means of the linear combinations of $\omega_i^{(s)}$ and using the external multiplying by the corresponding forms of differential variables $\{dx_j\}$. Differential forms annulled on solutions (3) have a similar appearance.

Let the symmetry transformations be given by the functions

$$\tilde{x}_k = \Phi_k(\{x_i\}, \{F_j\}), \quad \tilde{F}_l = \Psi_l(\{x_i\}, \{F_j\}). \quad (11)$$

Using the rules for differentiation of the composite functions and relationship (11), we can represent the basis forms in the new variables as

$$\tilde{\omega}_i^{(b)} = d\tilde{F}_i - \frac{\partial \tilde{F}_i}{\partial \tilde{x}_1}d\tilde{x}_1 - \frac{\partial \tilde{F}_i}{\partial \tilde{x}_2}d\tilde{x}_2 - \ldots - \frac{\partial \tilde{F}_i}{\partial \tilde{x}_n}d\tilde{x}_n$$

$$= \sum_k \left(\frac{\partial \Psi_i}{\partial x_k} - \tilde{p}^{(1)}_{i,1}\frac{\partial \Phi_1}{\partial x_k} - \tilde{p}^{(1)}_{i,2}\frac{\partial \Phi_2}{\partial x_k} - \ldots - \tilde{p}^{(1)}_{i,n}\frac{\partial \Phi_n}{\partial x_k}\right)dx_k$$

$$+ \sum_l \left(\frac{\partial \Psi_i}{\partial F_l} - \tilde{p}^{(1)}_{i,2}\frac{\partial \Phi_1}{\partial F_l} - \tilde{p}^{(1)}_{i,2}\frac{\partial \Phi_2}{\partial F_l} - \ldots - \tilde{p}^{(1)}_{i,n}\frac{\partial \Phi_n}{\partial F_l}\right)dF_l. \quad (12)$$

Automorphism (7) and the nondegeneracy condition for transformation (11) always provide the existence of the set of 0-forms a_i^j such that

$$\tilde{\omega}_i^{(b)} = a_i^k \omega_k^{(b)}, \quad i, k = 1, 2, \ldots, m, \quad (13)$$

where the summations are assumed over the repeated subscripts. Using (8), relationship (12) can be reduced to the form

$$\tilde{\omega}_i^{(b)} = \sum_k \left(\frac{\partial \Psi_i}{\partial x_k} - \tilde{p}^{(1)}_{i,1}\frac{\partial \Phi_1}{\partial x_k} - \tilde{p}^{(1)}_{i,2}\frac{\partial \Phi_2}{\partial x_k} - \ldots - \tilde{p}^{(1)}_{i,n}\frac{\partial \Phi_n}{\partial x_k}\right.$$

$$\left. + \sum_l p^{(1)}_{l,k}\left(\frac{\partial \Psi_i}{\partial F_l} - \tilde{p}^{(1)}_{i,2}\frac{\partial \Phi_1}{\partial F_l} - \tilde{p}^{(1)}_{i,2}\frac{\partial \Phi_2}{\partial F_l} - \ldots - \tilde{p}^{(1)}_{i,n}\frac{\partial \Phi_n}{\partial F_l}\right)\right)dx_k, \quad (14)$$

or

$$\tilde{\omega}_i^{(b)} = \sum_k \Omega_i^k dx_k,$$

where $\Omega_i^k = \langle \partial_{x_k} \rfloor \tilde{\omega}_i^{(b)} \rangle$. The expressions obtained represent the basis annulled forms as to the principle of its construction. At the same time, representation (14) makes it possible to interpret the annihilation of $\tilde{\omega}_i^{(b)}$ as a result of nulling all the Ω_i^k components. Thus, the set of equations arises that is defined in the extended tangential space $\{p^{(1)}_{i,j}, \tilde{p}^{(1)}_{i,j}\}$,

$$\Omega_i^k = 0, \quad i = 1, 2, \ldots, m, \quad k = 1, 2, \ldots, n. \quad (15)$$

The closure condition for basic annulled 1-forms (14) on the solutions to the extended set of equations creates the discrete symmetries of the original set (1). The analytical representation of the method of searching for symmetries followed from set (1) has the form

$$d\Omega_i^k = \lambda_i^{k,\,j}\omega_j^{(b)} + \mu_i^{k,\,p}\omega_p^{(s)} + \nu_i^{k,\,q}\tilde{\omega}_q^{(s)}, \quad i = 1, 2, \ldots, m, \quad k = 1, 2, \ldots, n, \quad (16)$$

where the summation is performed over the repeated subscripts. The existence of a relation between the basis forms in old and new variables (13) excludes the forms $\{\tilde{\omega}_i^{(b)}\}$ from the linear combination (16).

The features of the technique for application of the method are exhibited in analysis of the sin-Gordon equation, which is used in the description of dislocations, properties of ferromagnets, charge-density

waves, phase transitions, and surface epitaxial structures [8],

$$u''_{tt} - c^2 u''_{xx} + \omega^2 \sin u = 0. \quad (17)$$

In terms of differential forms, this equation can be written as

$$dq \wedge dx + c^2 dp \wedge dt - \omega^2 \sin u dx \wedge dt = 0, \quad p = u'_x, \quad q = u'_t. \quad (18)$$

The calculations are simplified in the case of symmetrization of the original equation by introducing the variables

$$y = \frac{x + ct}{2c}, \quad z = \frac{x - ct}{2c},$$

that transform (17) into

$$u''_{yz} - \omega^2 \sin u = 0. \quad (19)$$

The required 1-forms can be written as

$$\omega_P = dP - \omega^2 \sin u dz, \quad \omega_Q = dQ - \omega^2 \sin u dy, \quad P = u'_y, \quad Q = u'_z. \quad (20)$$

Taking into account the relationships

$$dP = \frac{2}{c}(dq + cdp), \quad dQ = \frac{2}{c}(-dq + cdp),$$

$$dy = \frac{1}{2}(dx + cdt), \quad dz = \frac{1}{2}(dx - cdt),$$

we obtain the 1-forms for Eq. (18):

$$\omega_p = dp - \frac{\omega^2}{2c^2} \sin u dx, \quad \omega_q = dq + \frac{\omega^2}{2} \sin u dx. \quad (21)$$

The sequential realization of procedure (9)–(16) leads to the following result for the admissible discrete symmetries:

$$\tilde{u} = \pm u + \pi n, \quad n \in Z, \quad \tilde{x} = \alpha x + \beta t, \quad \tilde{t} = \gamma x + \delta t, \quad (22)$$

where

$$\alpha = \pm 1, \quad \beta = \pm c \sqrt{1 - c^2 (-1)^n} \sqrt{\frac{(-1)^n}{1 - c^2 (-1)^n - c^4}},$$

$$\gamma = \pm \frac{1}{c} \sqrt{1 - c^2 (-1)^n}, \quad \delta = \pm c^2 \sqrt{\frac{(-1)^n}{1 - c^2 (-1)^n - c^4}}.$$

The signs for the values α, β, γ, and δ are chosen with allowance for the relationships

$$\alpha^2 - c^2 \gamma^2 = c^2 (-1)^n,$$

$$\alpha\beta - \gamma\delta = 0, \quad \beta^2 - c^2 \delta^2 = -c^2 (-1)^n.$$

The obtained sets include both the characteristics of the linearized equation (17) and more complicated types of symmetries. This is corroborated by the direct substitution of (22) into (17).

The equation describing the structure of a convective flow between the differentially rotating coaxial and spatially inhomogeneously heated cylinders is characterized by another type of discrete symmetries [4]:

$$A'_t = A''_{xx} + (1 + \varepsilon f(x))A - A^3 + \mu h(x), \quad f(x + L) = f(x), \quad h(x + M) = h(x). \quad (23)$$

Here, A is the order parameter that describes the direction and intensity of the fluid rotation, ε and μ are small perturbation parameters, and the functions $f(x)$ and $h(x)$ describe the local Rayleigh number and the spatial-heating distribution, respectively.

The set of 1-forms for Eq. (23) can be written as

$$\omega_A = dA - pdx - qdt,$$

$$\omega_p = dp - (q - (1 + \varepsilon f)A + A^3 - \mu h)dx - \omega_t dt, \quad (24)$$

$$\tilde{\omega}_p = d\tilde{p} - (\tilde{q} - (1 + \varepsilon \tilde{f})B + B^3 - \mu \tilde{h})d\xi - \tilde{\omega}_t d\tau,$$

where $\tilde{f} = f(\xi)$ and $\tilde{h} = h(\xi)$. In (24), we used the notation $p = A'_x$, $q = A'_t$, $\xi = \tilde{x}$, $\tau = \tilde{t}$, and $B = \tilde{A}$, while ω_t and $\tilde{\omega}_t$ are the unknown functions that arise in the context of the method of searching for discrete symmetries and must be determined.

In the degenerate case, when the Jacobian of transformation (2) vanishes and the condition

$$\frac{\partial^2 B}{\partial x \partial t} = 0 \quad (25)$$

is met for the coefficient B in (24), the partial solutions to (23) should be sought in the form $\varphi(x) + \psi(t)$. Thus, on the regular basis, we find the substitution that was previously used heuristically in constructing partial quasi-periodic or disordered nonasymptotic solutions [4, 5].

In the nondegenerate case with the supplementary condition $\varepsilon = \mu = 0$, transformation (2) in the form of

$$\xi = \pm x + x_0, \quad \tau = t + t_0, \quad B = \pm A, \quad x_0, t_0 = \text{const}, \quad (26)$$

describes the discrete reflection symmetry with respect to the origin of coordinates $x = 0$ and also the continuous shifts in space and in time. When the perturbation

parameters ε and μ vanish simultaneously, the symmetries yield three solutions in the degenerate case:

$$\xi = x, \quad \tau = t,$$
$$(1)\ B = 0,$$
$$(2)\ B = \pm 1, \tag{27}$$
$$(3)\ B = \pm\tanh\left(\frac{x}{\sqrt{2}} + x_0\right).$$

The first and the second solutions describe the equilibrium state and a uniform motion of fluid, respectively. The third solution known as the separatrix corresponds to fixed defects, for example, the domain walls between the regions with the opposite direction of the rotation of fluid during its separation in striations. This result agrees with [4].

Thus, the discrete-symmetry algorithm for nonlinear sets of partial differential equations in the degenerate case, when the Jacobian of transformation (2) vanishes, makes it possible to construct partial non-self-similar solutions.

ACKNOWLEDGMENTS

This work was supported by the Russian Foundation for Basic Research, project no. 99-05-64980, and by the Ministry of Education of the Russian Federation (The Federal Purposeful Program "Integratsiya," project no. 2.1-304).

REFERENCES

1. B. S. Kerner and V. V. Osipov, *Autosolitons: a New Approach to Problems of Self-Organization and Turbulence* (Nauka, Moscow, 1991; Kluwer, Dordrecht, 1994).
2. L. D. Landau and E. M. Lifshitz, *Course of Theoretical Physics*, Vol. 6: *Fluid Mechanics* (Nauka, Moscow, 1986; Pergamon, New York, 1987).
3. D. J. Tritton, *Physical Fluid Dynamics* (Clarendon, Oxford, 1988).
4. S. Aubry, Physica D (Amsterdam) **7**, 240 (1983).
5. P. Coulett, C. Elphick, and D. Repaux, Phys. Rev. Lett. **58**, 431 (1987).
6. B. K. Harrison and F. B. Estabrook, J. Math. Phys. **12**, 653 (1971).
7. P. E. Hydon, in *Modern Group Analysis VII. Developments in Theory, Computation and Application* (MARS, 1997), pp. 141–147.
8. *Solitons in Action*, Ed. by K. Lonngren and A. Scott (Academic, New York, 1978; Mir, Moscow, 1981).

Translated by V. Bukhanov

Doklady Physics, Vol. 46, No. 10, 2001, pp. 722–725. Translated from Doklady Akademii Nauk, Vol. 380, No. 4, 2001, pp. 487–490.

MECHANICS

Generalization of the Mindlin and Lord Kelvin Fundamental Solutions in the Classical Elasticity Theory

D. A. Pozharskiĭ

Presented by Academician I. I. Vorovich April 9, 2001

Received April 20, 2001

The Fredholm integral equations of the second kind obtained in [1] determine displacements and stresses in a three-dimensional elastic wedge when normal and tangential loads act on one face of the wedge, whereas various conditions exist on the other face. For the case when this face is stress-free, the Papkovich–Neuber functions are given in [2]. When an aperture angle of the wedge corresponds to a half-space, the formulas of [2] coincide with the well-known Boussinesq and Cerruti solutions. The solutions of [1, 2] use a Fourier–Kontorovich–Lebedev complex integral and the technique of reducing the three-dimensional problem of the elasticity theory to a generalized (in the sense of Vekua) Hilbert boundary value problem [3, 4]. In the present paper, by using this technique, generalizations of the two other fundamental solutions, i.e., those of Mindlin (1936) [5] and Lord Kelvin (Thomson, 1882) [6], are obtained in the framework of classical elasticity theory for the case of a three-dimensional wedge. The Papkovich–Neuber functions are given in the explicit form for three problems when a concentrated force acts in the bisector half-plane of the wedge, and for three variants of boundary conditions on the wedge faces.

Using cylindrical coordinates r, φ, z, we consider a three-dimensional elastic wedge ($0 \le r < \infty$, $|\varphi| \le \alpha$, $|z| < \infty$) with an aperture angle 2α and elastic characteristics G (shear modulus) and ν (Poisson's ratio). The z-axis is directed along the wedge edge so that the system of coordinates is right-handed (see the figure). Let the concentrated force P, perpendicular to the edge, act in the bisector half-plane $\varphi = 0$ of the wedge at the arbitrary point $r = x$, $z = y$. The faces $\varphi = \pm\alpha$ are either stress-free (problem $\mathcal{A}$), or are subjected to sliding support or fixed support (problems $\mathcal{B}$ and $\mathcal{C}$). Due to the symmetry of the problems with respect to the angle φ we consider the wedge region $-\alpha \le \varphi \le 0$, and write out the boundary conditions in the form

$$\mathcal{A}) \quad \varphi = -\alpha: \sigma_\varphi = \tau_{r\varphi} = \tau_{\varphi z} = 0, \tag{1}$$

$$\mathcal{B}) \quad \varphi = -\alpha: u_\varphi = \tau_{r\varphi} = \tau_{\varphi z} = 0, \tag{2}$$

$$\mathcal{C}) \quad \varphi = -\alpha: u_\varphi = u_r = u_z = 0, \tag{3}$$

$$\varphi = 0: \tau_{r\varphi} = \frac{1}{2}P\delta(r-x)\delta(z-y), \quad u_\varphi = \tau_{\varphi z} = 0. \tag{4}$$

We also suppose that stresses vanish at infinity.

We express the general solution of Navier equilibrium equations in cylindrical coordinates in terms of three Papkovich–Neuber harmonic functions $\Phi_n = \Phi_n(r, \varphi, z)$, $n = 0, 1, 2$, by the formulas

$$u_r = \frac{\partial\Phi_0}{\partial r} + \frac{1}{4(1-\nu)}\frac{\partial}{\partial r}(r\omega_1) - \omega_1, \qquad \omega_1 = \sin\varphi\Phi_1 - \cos\varphi\Phi_2, \tag{5}$$

$$u_\varphi = \frac{1}{r}\frac{\partial\Phi_0}{\partial\varphi} + \frac{1}{4(1-\nu)}\frac{\partial\omega_1}{\partial\varphi} - \omega_2, \qquad \omega_2 = \cos\varphi\Phi_1 + \sin\varphi\Phi_2, \tag{6}$$

$$u_z = \frac{\partial\Phi_0}{\partial z} + \frac{r}{4(1-\nu)}\frac{\partial\omega_1}{\partial z}. \tag{7}$$

The stresses can be determined from (5)–(7) using Hooke's law.

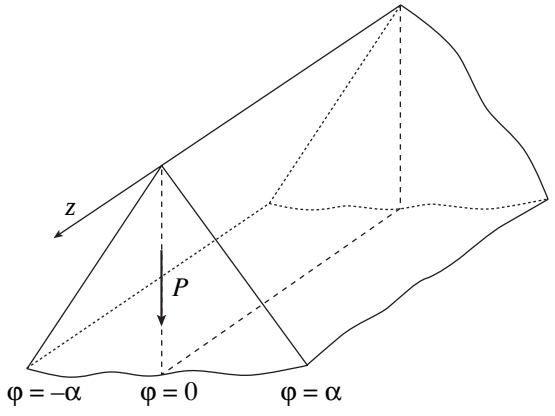

Concentrated force inside a three-dimensional wedge.

Institute of Mechanics and Applied Mathematics, Rostov State University, pr. Stachki 200/1, Rostov-on-Don, 344090 Russia

1028-3358/01/4610-0722$21.00

We present the solutions to boundary value problems (1)–(4) as a superposition of even and odd solutions with respect to z, considering collinear, equal or opposite forces at the points $r = x$, $z = \pm y$. We seek the harmonic functions Φ_n as a sin- or cos-Fourier integral with respect to z and a Kontorovich–Lebedev complex integral with respect to r [3, 4]. Using the well-known technique [3, 4], we obtain the solutions of the boundary value problems (1)–(4) in the form (5)–(7), where (we pass to real-valued Kontorovich–Lebedev integrals, $n = 0, 1, 2$)

$$\Phi_n(r, \varphi, z) = \frac{P}{2\pi^3 G}\int_0^\infty\int_0^\infty \sinh(\pi\tau)[A_n(\tau, \beta)\cosh(\varphi\tau) + B_n(\tau, \beta)\sinh(\varphi\tau)]\mathcal{K}_{i\tau}(\beta r)\cos(\beta[z-y])d\tau d\beta, \quad (8)$$

$$B_0(\tau, \beta) = \frac{x}{2(1-\nu)}\mathcal{K}_{i\tau}(\beta x), \qquad A_1(\tau, \beta) = 0, \quad B_2(\tau, \beta) = 2\mathcal{K}_{i\tau}(\beta x). \quad (9)$$

The functions (9) are the same for the three problems; $\mathcal{K}_{i\tau}(x)$ is the modified Bessel function. For problem $\mathcal{A}$ (1), (4) we have

$$A_0(\tau, \beta) = \frac{x\coth(\alpha\tau)}{2(1-\nu)}\mathcal{K}_{i\tau}(\beta x) - \frac{1-2\nu}{\beta\sinh(\alpha\tau)} \times \int_0^\infty \frac{W(t, \alpha)\Phi(t, \beta) + \cosh(\pi t/2)\Psi(t, \beta)}{\cosh(\pi t) + \cosh(\pi\tau)}\sinh\frac{\pi t}{2}dt, \quad (10)$$

$$B_1(\tau, \beta) = -\frac{2\sin(2\alpha)\mathcal{K}_{i\tau}(\beta x) + 4(1-\nu)\sinh(\alpha\tau)\cos\alpha\Psi(\tau, \beta)}{\cosh(2\alpha\tau) - \cos(2\alpha)} - \frac{4(1-\nu)\sinh(\alpha\tau)\cos\alpha\Phi(\tau, \beta)}{\cosh(\pi\tau/2)[\sinh(2\alpha\tau) + \tau\sin(2\alpha)]}, \quad (11)$$

$$A_2(\tau, \beta) = \frac{2\sinh(2\alpha\tau)\mathcal{K}_{i\tau}(\beta x) - 4(1-\nu)\cosh(\alpha\tau)\sin\alpha\Psi(\tau, \beta)}{\cosh(2\alpha\tau) - \cos(2\alpha)} - \frac{4(1-\nu)\cosh(\alpha\tau)\sin\alpha\Phi(\tau, \beta)}{\cosh(\pi\tau/2)[\sinh(2\alpha\tau) + \tau\sin(2\alpha)]}, \quad (12)$$

$$\Phi(t, \beta) = \Phi_*(t, \beta) + \cosh\frac{\pi t}{2}F(t, \beta), \qquad \mathcal{K}'_{it}(\beta x) = \frac{\partial}{\partial x}\mathcal{K}_{it}(\beta x), \quad (13)$$

$$F(t, \beta) = \frac{4\mathcal{K}_{it}(\beta x)}{\cosh(2\alpha t) - \cos(2\alpha)} \times \left(\frac{t\sinh(\alpha t)\cos\alpha}{2(1-\nu)} - \cosh(\alpha t)\sin\alpha\right) - \frac{2(1-\nu)\sinh(2\alpha t) + t\sin(2\alpha)}{\cosh(2\alpha t) - \cos(2\alpha)}\Psi(t, \beta) + (1-\nu)^{-1}[t\sinh(\alpha t)\cos\alpha\mathcal{K}_{it}(\beta x) + x\cosh(\alpha t)\sin\alpha\mathcal{K}'_{it}(\beta x)] + \frac{1-2\nu}{1-\nu} \times \int_0^\infty \frac{2\sinh(\alpha u)\cos\alpha\mathcal{K}_{iu}(\beta x) - (1-\nu)\sin(2\alpha)\Psi(u, \beta)}{[\cosh(2\alpha u) - \cos(2\alpha)][\cosh(\pi u) - \cosh(\pi t)]} \times \sinh(\pi u)du, \quad (14)$$

$$\Psi(t, \beta) = \frac{t\cosh(\alpha t)\cos\alpha\mathcal{K}_{it}(\beta x) + x\sinh(\alpha t)\sin\alpha\mathcal{K}'_{it}(\beta x)}{(1-\nu)(1-2\nu)}. \quad (15)$$

The function $\Phi_*(t, \beta)$ for a fixed β satisfies the Fredholm integral equation of the second kind ($0 \le t < \infty$)

$$\Phi_*(t, \beta) = (1-2\nu)\int_0^\infty L(t, u) \times \left[\Phi_*(u, \beta) + \cosh\frac{\pi u}{2}\left(F(u, \beta) + \frac{\Psi(u, \beta)}{W(u, \alpha)}\right)\right]du - \frac{\beta x}{1-\nu}\cosh\frac{\pi t}{2}\int_0^\infty \frac{\sinh(\pi\tau)\cosh(\alpha\tau)g(\tau, \alpha)\mathcal{K}_{i\tau}(\beta x)}{\cosh(\pi\tau) + \cosh(\pi t)}d\tau, \quad (16)$$

$$L(t, u) = 2\cosh\frac{\pi t}{2}\sinh\frac{\pi u}{2}W(u, \alpha) \times \int_0^\infty \frac{\sinh(\pi\tau)g(\tau, \alpha)d\tau}{[\cosh(\pi\tau) + \cosh(\pi t)][\cosh(\pi\tau) + \cosh(\pi u)]}, \quad (17)$$

$$W(t, \alpha) = \frac{\cosh(2\alpha t) - \cos(2\alpha)}{\sinh(2\alpha t) + t\sin(2\alpha)}, \qquad g(t, \alpha) = \frac{\coth(\alpha t)\sin^2(2\alpha)}{\cosh(2\alpha t) - \cos(4\alpha)}. \quad (18)$$

For problem $\mathcal{B}$ (2), (4) we have

$$A_0(\tau, \beta) = \frac{x\coth(\alpha\tau)}{2(1-\nu)}\mathcal{K}_{i\tau}(\beta x), \qquad B_1(\tau, \beta) = -\frac{2\sin(2\alpha)\mathcal{K}_{i\tau}(\beta x)}{\cosh(2\alpha\tau) - \cos(2\alpha)}, \quad (19)$$

$$A_2(\tau, \beta) = \frac{2\sinh(2\alpha\tau)\mathcal{K}_{i\tau}(\beta x)}{\cosh(2\alpha\tau) - \cos(2\alpha)}. \quad (20)$$

For problem $\mathcal{C}$ (3), (4)

$$A_0(\tau, \beta) = \frac{x\tanh(\alpha\tau)}{2(1-\nu)}\mathcal{K}_{i\tau}(\beta x), \quad \kappa = 3 - 4\nu, \quad (21)$$

$$B_1(\tau, \beta) = -\frac{2\sin(2\alpha)[\tau\sin(2\alpha)\mathcal{K}_{i\tau}(\beta x) - x\sinh(2\alpha\tau)\mathcal{K}'_{i\tau}(\beta x)]}{[\cosh(2\alpha\tau) + \cos(2\alpha)][\kappa\sinh(2\alpha\tau) - \tau\sin(2\alpha)]}, \quad (22)$$

$$A_2(\tau, \beta) = -\frac{2[\cosh(2\alpha\tau) - 1]}{[\cosh(2\alpha\tau) + \cos(2\alpha)][\kappa\sinh(2\alpha\tau) - \tau\sin(2\alpha)]} \times [(\tau\coth(\alpha\tau)\sin(2\alpha) - \kappa\cosh(2\alpha\tau) - \kappa\cos(2\alpha)) \times \mathcal{K}_{i\tau}(\beta x) - 2x\sin^2\alpha\mathcal{K}'_{i\tau}(\beta x)]. \quad (23)$$

Integrals (8) converge for functions (9)–(23) for all $\varphi \in [-\alpha, 0]$.

The solution to problem $\mathcal{A}$ in the form (8)–(18) for $\alpha = \pi/2$ coincides with the Mindlin solution for a half-space. For this case we have $\Phi_*(t, \beta) = B_1(\tau, \beta) = 0$, and using the integral

$$\int_0^\infty \frac{\cosh(\pi t/2)\mathcal{K}_{it}(\beta x)}{\cosh(\pi t) + \cosh(\pi\tau)}dt = \frac{\beta}{2\cosh(\pi\tau/2)}\int_x^\infty \mathcal{K}_{i\tau}(\beta x)dx,$$

we obtain

$$A_0(\tau, \beta) = \frac{x[\cosh(\pi\tau) + \kappa]}{2(1-\nu)\sinh(\pi\tau)}\mathcal{K}_{i\tau}(\beta x) + \frac{2(1-2\nu)}{\sinh(\pi\tau)}\int_x^\infty \mathcal{K}_{i\tau}(\beta x)dx,$$

$$A_2(\tau, \beta) = \frac{2[\cosh(\pi\tau) + \kappa]\mathcal{K}_{i\tau}(\beta x) - 4x\mathcal{K}'_{i\tau}(\beta x)}{\sinh(\pi\tau)}.$$

We show the coincidence for the displacement $u_r(r, 0, z)$. Calculating integrals [7], we obtain

$$\Phi_0(r, 0, z) = \frac{P}{8\pi G} \times \left(\frac{x}{2(1-\nu)R_-} + \frac{\kappa x}{2(1-\nu)R_+} + 2(1-2\nu)\int_x^\infty \frac{dx}{R_+}\right),$$

$$\Phi_2(r, 0, z) = \frac{P}{4\pi G}\left(\frac{1}{R_-} + \frac{\kappa}{R_+} - 2x\frac{\partial}{\partial x}\frac{1}{R_+}\right),$$

$$R_\pm = \sqrt{(r \pm x)^2 + (z-y)^2},$$

and, using the first formula of (5), we determine

$$u_r(r, 0, z) = \frac{P}{16\pi(1-\nu)G}\left(\frac{\kappa}{R_-} + \frac{5 - 12\nu + 8\nu^2}{R_+} + \frac{(r-x)^2}{R_-^3} + \frac{\kappa(r+x)^2 - 2rx}{R_+^3} + \frac{6rx(r+x)^2}{R_+^5}\right).$$

This agrees exactly with the second expression of formula (9.25) in [8] (the displacement u_z in Cartesian coordinates corresponds to the displacement u_r in cylindrical coordinates).

The solution to problem $\mathcal{B}$ in the form (8), (9), (19), (20) for $\alpha = \pi$ coincides with the fundamental Lord Kelvin solution for an elastic space. For this case, we have

$$A_0(\tau, \beta) = \frac{x\coth(\pi\tau)}{2(1-\nu)}\mathcal{K}_{i\tau}(\beta x),$$

$$B_1(\tau, \beta) = 0, \quad A_2(\tau, \beta) = 2\coth(\pi\tau)\mathcal{K}_{i\tau}(\beta x),$$

and, for instance, for the displacement $u_r(r, 0, z)$, we similarly arrive at the formulas

$$\Phi_0(r, 0, z) = \frac{Px}{16\pi(1-\nu)GR_-}, \quad \Phi_2(r, 0, z) = \frac{P}{4\pi GR_-},$$

$$u_r(r, 0, z) = \frac{P}{16\pi(1-\nu)G}\left(\frac{\kappa}{R_-} + \frac{(r-x)^2}{R_-^3}\right).$$

This result is in agreement with formulas (9.2) and (9.4) for u_z in [8].

We now explain why the solutions to problems $\mathcal{B}$ and $\mathcal{C}$ are simpler than that for problem $\mathcal{A}$. As is known [1, 4], the problem on the action of concentrated forces on one face of a three-dimensional wedge whose other face is stress-free can be reduced to two Fredholm integral equations of the second kind. When, however, the other face has a sliding support or is fixed, the corresponding problem is reduced to only one Fredholm equation. For the wedge with a stress-free face, we can then express displacements as a combination of two Neumann series that serve as the solutions to the two Fredholm equations. At the same time, for the other two cases, displacements can be represented as a single Neumann series. The boundary conditions (1)–(4) correspond to the inverse problems, because in relation (4), the displacement u_φ is given instead of the stress σ_φ. Therefore, the solutions to problems (1)–(4) must contain the inversions of the indicated Neumann series. One Neumann operator series for problems $\mathcal{B}$ and $\mathcal{C}$ has a simple inverse operator in the form (see formula (1.6) in [9])

$$\left[\sum_{n=0}^\infty (1-2\nu)^n\mathcal{T}^n\right]^{-1} = I - (1-2\nu)\mathcal{T},$$

where $\mathcal{T}$ is a known operator and I is the identity operator. For problem $\mathcal{A}$, the inversion of the combination of two Neumann series has a complicated form (see theorem in [4, p. 160]). This inversion contains the solution of the Fredholm integral equation whose kernel has the form (17), (18). Fredholm integral equations with the same kernel occur in the problem on a cut

(crack) in a three-dimensional wedge with stress-free faces [9, 10] and in the problem on the action of concentrated forces on one wedge face when the other face has a sliding support [1, 4] (in these problems), the same components of the stress tensor and of the displacement vector are given). As is proved in [1, 4], the solution of such Fredholm integral equations and, therefore, of integral equation (16), for any angle α and at least for $\nu > 0.053$, can be represented by a Neumann series which converges uniformly in the Banach space $C_M(0, \infty)$ of functions that are continuous and bounded on the semiaxis. In other words, the solution to problem $\mathcal{A}$ for $\nu > 0.053$ can be written as a functional series in powers of $1–2\nu$.

The formulas obtained can be applied, for example, to problems on a thin rigid inclusion in a three-dimensional wedge; similar problems for a space and a layer were considered in [11].

ACKNOWLEDGMENTS

The work was supported by the Russian Foundation for Basic Research (project no. 99-15-96012) and by the Humboldt Foundation (Germany).

REFERENCES

1. I. A. Lubyagin, D. A. Pozharskiĭ, and M. I. Chebakov, Dokl. Akad. Nauk SSSR **321**, 58 (1991) [Sov. Phys. Dokl. **36**, 797 (1991)].
2. D. A. Pozharskiĭ, Dokl. Akad. Nauk **372**, 333 (2000) [Dokl. Phys. **45**, 236 (2000)].
3. A. F. Ulitko, *Method of Vector Eigenfunctions in Spatial Problems of Theory of Elasticity* (Naukova Dumka, Kiev, 1979).
4. V. M. Aleksandrov and D. A. Pozharskiĭ, *Nonclassical Spatial Problems in Mechanics of Contact Interactions of Elastic Bodies* (Faktorial, Moscow, 1998).
5. R. D. Mindlin, Physics **7**, 195 (1936).
6. W. Thomson, *Mathematical and Physical Papers* (Cambridge Univ. Press, Cambridge, 1882), Vol. 1, p. 97.
7. I. S. Gradshteĭn and I. M. Ryzhik, *Table of Integrals, Series, and Products* (Nauka, Moscow, 1971; Academic, New York, 1980).
8. H. G. Hahn, *Elastizitätstheorie* (Teubner, Stuttgart, 1985).
9. D. A. Pozharskiĭ, Izv. Akad. Nauk, Mekh. Tverd. Tela **28** (6), 105 (1993).
10. D. A. Pozharskiĭ, Prikl. Mat. Mekh. **58**, 148 (1994).
11. V. M. Aleksandrov, B. I. Smetanin, and B. V. Sobol', *Thin Stress Concentrators in Elastic Bodies* (Nauka, Moscow, 1993).

Translated by D. Pozharskiĭ

Doklady Physics, Vol. 46, No. 10, 2001, pp. 726–731. Translated from Doklady Akademii Nauk, Vol. 380, No. 4, 2001, pp. 491–496.

MECHANICS

Exact Solutions to the Navier–Stokes Equations with Generalized Separation of Variables

A. D. Polyanin

Presented by Academician F. L. Chernous'ko May 10, 2001

Received May 14, 2001

In this paper, we find new multiparameter families of exact solutions (among them, periodic solutions) to the steady-state and unsteady Navier–Stokes equations. We also construct more general solutions depending on one or several arbitrary functions. Various modifications of the method of generalized separation of variables are employed for finding the exact solutions.

Self-similar and invariant solutions to the Navier–Stokes equations were considered in [1–6]. A number of exact solutions to nonlinear heat-conduction equations and other nonlinear equations of the second order with the generalized separation of variables were given in [5, 7–10].

1. EQUATION FOR THE STREAM FUNCTION

The two-dimensional nonstationary equations for a viscous incompressible fluid,

$$\frac{\partial u_1}{\partial t} + u_1\frac{\partial u_1}{\partial x} + u_2\frac{\partial u_1}{\partial y} = -\frac{1}{\rho}\frac{\partial p}{\partial x} + \nu\Delta u_1,$$

$$\frac{\partial u_2}{\partial t} + u_1\frac{\partial u_2}{\partial x} + u_2\frac{\partial u_2}{\partial y} = -\frac{1}{\rho}\frac{\partial p}{\partial y} + \nu\Delta u_2,$$

$$\frac{\partial u_1}{\partial x} + \frac{\partial u_2}{\partial y} = 0,$$

can be reduced to a nonlinear equation of the fourth order for the stream function w introduced by the formulas $u_1 = \dfrac{\partial w}{\partial y}$ and $u_2 = -\dfrac{\partial w}{\partial x}$ (with the subsequent elimination of the pressure from the first two equations by cross differentiation):

$$\frac{\partial}{\partial t}(\Delta w) + \frac{\partial w}{\partial y}\frac{\partial}{\partial x}(\Delta w) - \frac{\partial w}{\partial x}\frac{\partial}{\partial y}(\Delta w) = \nu\Delta\Delta w,$$
$$\Delta w = \frac{\partial^2 w}{\partial x^2} + \frac{\partial^2 w}{\partial y^2}. \qquad (1)$$

Institute of Problems in Mechanics,
Russian Academy of Sciences,
pr. Vernadskogo 101, Moscow, 117526 Russia

2. EXACT SOLUTIONS WITH THE GENERALIZED SEPARATION OF VARIABLES

New exact solutions to Eq. (1) with the generalized (incomplete) separation of its variables are described below. These solutions are sought in the form of finite sums,

$$w(x, y, t) = \sum_{k=1}^{n} f_k(x)g_k(y, t)$$

or

$$w(x, y, t) = \sum_{k=1}^{n} f_k(x, t)g_k(y),$$

where the functions $f_k(x)$ and $g_k(y, t)$ [or $f_k(x, t)$ and $g_k(y)$] should be chosen to satisfy the equation under consideration. For nonlinear equations, in contrast to linear ones, the functions $g_k(y, t)$ with different subscripts k are related to each other and to the functions $f_m(x)$.

We now consider the simplest case when a set of the functions depending on the coordinate [for example, $f_k(x)$] is described by linear differential equations with constant coefficients. In this paper, we use the most widespread solutions to such equations,

$$f_k(x) = x^k, \quad f_k(x) = e^{\lambda_k x},$$

$$f_k(x) = \sin(\alpha_k x), \quad f_k(x) = \cos(\beta_k x),$$

and their linear superpositions in order to find exact solutions to Eq. (1) (here, λ_k, α_k, and β_k are free parameters). Another set of the functions, $g_k(y, t)$, is determined by solving the corresponding nonlinear equations.

Remark. Solutions with another generalized separation of variables is given in Sections 3 (2°) and 4 (2° and 9°).

1028-3358/01/4610-0726$21.00

3. STEADY-STATE SOLUTIONS IN THE CARTESIAN AND POLAR COORDINATE SYSTEMS

1°. There are the exact solutions with the generalized separation of variables:

$$w(x, y) = 6\nu x(y+\lambda)^{-1} + A(y+\lambda)^3 + B(y+\lambda)^{-1} + C(y+\lambda)^{-2} + D \quad (\nu \neq 0),$$

$$w(x, y) = (Ax + B)e^{-\lambda y} + \nu\lambda x + C,$$

$$w(x, y) = A\exp(-\lambda x) + B\exp(-\lambda y) + \nu\lambda(x - y) + C,$$

$$w(x, y) = A\exp(\lambda x) + B\exp(-\lambda y) + \nu\lambda(x + y) + C,$$

$$w(x, y) = [A\sinh(\beta x) + B\cosh(\beta x)]e^{-\lambda y} + \frac{\nu}{\lambda}(\beta^2 + \lambda^2)x + C,$$

$$w(x, y) = [A\sin(\beta x) + B\cos(\beta x)]e^{-\lambda y} + \frac{\nu}{\lambda}(\lambda^2 - \beta^2)x + C,$$

$$w(x, y) = Ae^{\lambda y + \beta x} + Be^{\gamma x} + \nu\gamma y + \frac{\nu}{\lambda}\gamma(\beta - \gamma)x + C,$$

$$\gamma = \pm\sqrt{\lambda^2 + \beta^2},$$

where A, B, C, D, β, and λ are arbitrary constants.

Taking in the second solution $A = -\nu\lambda$, $B = C = 0$, and $\lambda = \sqrt{\frac{k}{\nu}}$, we obtain

$$w = \sqrt{k\nu}x\left[1 - \exp\left(-\sqrt{\frac{k}{\nu}}y\right)\right].$$

This solution describes a steady-state fluid flow caused by the motion of the surface points $y = 0$ with the velocity $u_1|_{y=0} = kx$.

2°. There exists the more general exact solution with incomplete separation of its variables:

$$w(x, y) = F(z)x + G(z), \quad z = y + kx.$$

Here, the functions $F = F(z)$ and $G = G(z)$ are described by the system of ordinary differential equations of the fourth order,

$$F_z'F_z'' - FF_{zzz}''' = \nu(k^2 + 1)F_{zzzz}'''', \tag{2}$$

$$G_z'F_{zz}'' - FG_{zzz}''' = \nu(k^2 + 1)G_{zzzz}'''' + 4k\nu F_{zzz}''' + \frac{2k}{(k^2 + 1)}FF_{zz}''. \tag{3}$$

Integrating these equations, we obtain the new system of equations of the third order,

$$(F_z')^2 - FF_{zz}'' = \nu(k^2 + 1)F_{zzz}''' + A, \tag{4}$$

$$G_z'F_z' - FG_{zz}'' = \nu(k^2 + 1)G_{zzz}''' + \psi(z) + B, \tag{5}$$

where A and B are arbitrary constants and the function $\psi(z)$ is determined by the formula

$$\psi(z) = 4k\nu F_{zz}'' + \frac{2k}{k^2 + 1}\int FF_{zz}''dz.$$

The order of autonomous equation (4) can be lowered by unity.

Equation (2) has the following particular solutions:

$$F(z) = az + b, \quad z = y + kx,$$

$$F(z) = 6\nu(k^2 + 1)(z + a)^{-1},$$

$$F(z) = ae^{-\lambda z} + \lambda\nu(k^2 + 1),$$

where a, b, and λ are arbitrary constants.

In general, the substitution $U = G_z'$ reduces Eq. (5) to a linear inhomogeneous equation of the second order, which has a nontrivial particular solution in the case of $\psi = B = 0$ (i.e., in the homogeneous case):

$$U = \begin{cases} F_{zz}'', & \text{if } F_{zz}'' \neq 0 \\ F, & \text{if } F_{zz}'' = 0. \end{cases}$$

Hence, its general solution can be expressed in terms of quadratures [11, 12].

3°. There is a solution with the generalized separation of variables in the polar coordinate system:

$$w(r, \theta) = f(r)\theta + g(r).$$

Here, $x = r\cos\theta$, $y = r\sin\theta$, and the functions $f = f(r)$ and $g = g(r)$ satisfy the system of ordinary differential equations

$$-f_r'\mathbf{L}(f) + f[\mathbf{L}(f)]_r' = \nu r\mathbf{L}^2(f), \tag{6}$$

$$-g_r'\mathbf{L}(f) + f[\mathbf{L}(g)]_r' = \nu r\mathbf{L}^2(g), \tag{7}$$

where $\mathbf{L}(f) = r^{-1}(rf_r')_r'$.

The exact solution to Eqs. (6) and (7) takes the form

$$f(r) = C_1\ln r + C_2, \quad g(r) = C_3r^2 + C_4\ln r + C_5\int\left[\int rQ(r)dr\right]\frac{dr}{r} + C_6,$$

$$Q(r) = \int r^{(C_2/\nu)-1}\exp\left(\frac{C_1}{2\nu}\ln^2 r\right)dr,$$

where C_1, C_2, C_3, C_4, C_5, and C_6 are arbitrary constants.

4. UNSTEADY SOLUTIONS IN THE CARTESIAN AND POLAR COORDINATE SYSTEMS

1°. There is an exact solution with an incomplete separation of variables:

$$w(x, y, t) = F(y, t)x + G(y, t). \tag{8}$$

Here, the functions $F = F(y, t)$ and $G = G(y, t)$ are determined by the system of one-dimensional equations of the fourth order:

$$\frac{\partial^3 F}{\partial t \partial y^2} + \frac{\partial F}{\partial y}\frac{\partial^2 F}{\partial y^2} - F\frac{\partial^3 F}{\partial y^3} = \nu\frac{\partial^4 F}{\partial y^4}, \tag{9}$$

$$\frac{\partial^3 G}{\partial t \partial y^2} + \frac{\partial G}{\partial y}\frac{\partial^2 F}{\partial y^2} - F\frac{\partial^3 G}{\partial y^3} = \nu\frac{\partial^4 G}{\partial y^4}. \tag{10}$$

Equation (9) is solved independently of Eq. (10). Integrating Eqs. (9) and (10) over y yields

$$\frac{\partial^2 F}{\partial t \partial y} + \left(\frac{\partial F}{\partial y}\right)^2 - F\frac{\partial^2 F}{\partial y^2} = \nu\frac{\partial^3 F}{\partial y^3} + f_1(t), \tag{11}$$

$$\frac{\partial^2 G}{\partial t \partial y} + \frac{\partial F}{\partial y}\frac{\partial G}{\partial y} - F\frac{\partial^2 G}{\partial y^2} = \nu\frac{\partial^3 G}{\partial y^3} + f_2(t). \tag{12}$$

Here, $f_1(t)$ and $f_2(t)$ are arbitrary functions. Equation (12) is linear in the function G. After performing the substitution

$$\begin{gathered} G = \int U dy - hF + h_t' y, \\ U = U(y, t), \quad F = F(y, t), \end{gathered} \tag{13}$$

with the function $h = h(t)$ satisfying the linear ordinary differential equation

$$h_{tt}'' - f_1(t)h = f_2(t), \tag{14}$$

equation (12) is reduced to the linear homogeneous equation of the second order,

$$\frac{\partial U}{\partial t} = \nu\frac{\partial^2 U}{\partial y^2} + F\frac{\partial U}{\partial y} - \frac{\partial F}{\partial y}U. \tag{15}$$

Thus if a particular solution to Eq. (9) or Eq. (11) is known, the determination of the function G is reduced to solving linear equations (14) and (15) with the subsequent integration in formula (13).

The exact solutions to Eq. (9) are listed in Table 1. The ordinary differential equations presented in the two last lines of Table 1 have the traveling-wave solution and the self-similar solution. These equations are autonomous; hence, their order can be lowered.

The general solution to the inhomogeneous equation (14) is found with the help of a fundamental set of solutions to the corresponding homogeneous equation (with $f_2 \equiv 0$). Necessary formulas and the fundamental solutions to homogeneous equation (14), which correspond to all exact solutions listed in Table 1, can be found in handbooks [11, 12].

For arbitrary function $F = F(y, t)$, Eq. (15) has a trivial solution. The expressions in Table 1 and formula (13) with $U = 0$ describe certain exact solutions of the form (8). A wider class of exact solutions can be obtained if nontrivial solutions to Eq. (15) are considered.

In Table 2, we present transformations that simplify Eq. (15) for some of the solutions to Eq. (9) [or (11)] listed in Table 1. It is seen that in the first two cases the solutions to Eq. (15) are expressed in terms of solutions to the conventional heat-conduction equation with constant coefficients. In the other three cases, Eq. (15) is reduced to an equation in separable variables.

2°. There is a more general exact solution with incomplete separation of variables:

$$w(x, y, t) = F(\xi, t)x + G(\xi, t), \quad \xi = y + kx.$$

Here, the functions $F(\xi, t)$ and $G = G(\xi, t)$ are determined from the system of one-dimensional equations of the fourth order:

$$\frac{\partial^3 F}{\partial t \partial \xi^2} + \frac{\partial F}{\partial \xi}\frac{\partial^2 F}{\partial \xi^2} - F\frac{\partial^3 F}{\partial \xi^3} = \nu(k^2 + 1)\frac{\partial^4 F}{\partial \xi^4}, \tag{16}$$

$$\begin{aligned} \frac{\partial^3 G}{\partial t \partial \xi^2} + \frac{\partial G}{\partial \xi}\frac{\partial^2 F}{\partial \xi^2} - F\frac{\partial^3 G}{\partial \xi^3} &= \nu(k^2 + 1)\frac{\partial^4 G}{\partial \xi^4} \\ &+ 4\nu k\frac{\partial^3 F}{\partial \xi^3} + \frac{2k}{k^2 + 1}\left(F\frac{\partial^2 F}{\partial \xi^2} - \frac{\partial^2 F}{\partial t \partial \xi}\right). \end{aligned} \tag{17}$$

Integrating Eqs. (16) and (17) over ξ, we arrive at

$$\frac{\partial^2 F}{\partial t \partial \xi} + \left(\frac{\partial F}{\partial \xi}\right)^2 - F\frac{\partial^2 F}{\partial \xi^2} = \nu(k^2 + 1)\frac{\partial^3 F}{\partial \xi^3} + f_1(t), \tag{18}$$

$$\frac{\partial^2 G}{\partial t \partial \xi} + \frac{\partial F}{\partial \xi}\frac{\partial G}{\partial \xi} - F\frac{\partial^2 G}{\partial \xi^2} = \nu(k^2 + 1)\frac{\partial^3 G}{\partial \xi^3} + Q(\xi, t), \tag{19}$$

where $f_1(t)$ is an arbitrary function and $Q(\xi, t)$ is determined by the formula

$$\begin{aligned} Q(\xi, t) &= 4\nu k\frac{\partial^2 F}{\partial \xi^2} - \frac{2k}{k^2 + 1}\frac{\partial F}{\partial t} \\ &+ \frac{2k}{k^2 + 1}\int F\frac{\partial^2 F}{\partial \xi^2} d\xi + f_2(t), \end{aligned}$$

with $f_2(t)$ being an arbitrary function.

Equation (19) is linear in the function G. The substitution $U = \dfrac{\partial G}{\partial \xi}$ reduces this equation to the linear equation of the second order

$$\frac{\partial U}{\partial t} = \nu(k^2 + 1)\frac{\partial^2 U}{\partial \xi^2} + F\frac{\partial U}{\partial \xi} - \frac{\partial F}{\partial \xi}U + Q(\xi, t). \tag{20}$$

Thus when a particular solution to Eq. (16) or (18) is known, the function G is determined by the linear equation (20) of the second order. With the help of the scaling of the independent variables, $\xi = (k^2 + 1)\zeta$ and

Table 1. Exact solutions to Eqs. (9) and (11). Here, $\varphi(t)$ and $\psi(t)$ are arbitrary functions, while A and λ are arbitrary constants

No.	Function $F = F(y, t)$ (the general form of solution)	Function $f_1(t)$ in Eq. (11)	Defining coefficients (or defining equation)
1	$F = \varphi(t)y + \psi(t)$	$f_1(t) = \varphi_t' + \varphi^2$	–
2	$F = \dfrac{6\nu}{y + \psi(t)} + \psi_t'(t)$	$f_1(t) = 0$	–
3	$F = A\exp[-\lambda y - \lambda\psi(t)] + \psi_t'(t) + \nu\lambda$	$f_1(t) = 0$	–
4	$F = Ae^{-\beta t}\sin[\lambda y + \lambda\psi(t)] + \psi_t'(t)$	$f_1(t) = Be^{-2\beta t}$	$\beta = \nu\lambda^2$, $B = A^2\lambda^2 > 0$
5	$F = Ae^{-\beta t}\cos[\lambda y + \lambda\psi(t)] + \psi_t'(t)$	$f_1(t) = Be^{-2\beta t}$	$\beta = \nu\lambda^2$, $B = A^2\lambda^2 > 0$
6	$F = Ae^{\beta t}\sinh[\lambda y + \lambda\psi(t)] + \psi_t'(t)$	$f_1(t) = Be^{2\beta t}$	$\beta = \nu\lambda^2$, $B = A^2\lambda^2 > 0$
7	$F = Ae^{\beta t}\cosh[\lambda y + \lambda\psi(t)] + \psi_t'(t)$	$f_1(t) = Be^{2\beta t}$	$\beta = \nu\lambda^2$, $B = -A^2\lambda^2 < 0$
8	$F = F(\xi)$, $\xi = y + \lambda t$	$f_1(t) = A$	$-A + \lambda F_{\xi\xi}'' + (F_\xi')^2 - FF_{\xi\xi}'' = \nu F_{\xi\xi\xi\xi}'''$
9	$F = t^{-1/2}[H(\xi) - \dfrac{1}{2}\xi]$, $\xi = yt^{-1/2}$	$f_1(t) = At^{-2}$	$\dfrac{3}{4} - A - 2H_\xi' + (H_\xi')^2 - HH_{\xi\xi}'' = \nu H_{\xi\xi\xi}'''$

Table 2. Transformations of Eq. (15) for corresponding exact solutions to Eq. (11). The numbers in the first column correspond to the numbers of the exact solutions $F = F(y, t)$ in Table 1

No.	Transformation of Eq. (15)	The equation obtained
1	$U = \dfrac{1}{\Phi(t)}u(z, \tau)$, $\tau = \int\Phi^2(t)dt$, $z = y\Phi(t) + \int\psi(t)\Phi(t)dt$, $\Phi(t) = \exp[\int\varphi(t)dt]$	$\dfrac{\partial u}{\partial\tau} = \nu\dfrac{\partial^2 u}{\partial z^2}$
2	$U = \zeta^{-3}u(\zeta, t)$, $\zeta = y + \psi(t)$	$\dfrac{\partial u}{\partial t} = \nu\dfrac{\partial^2 u}{\partial\zeta^2}$
3	$U = e^\eta Z(\eta, t)$, $\eta = -\lambda y - \lambda\psi(t)$	$\dfrac{\partial Z}{\partial t} = \nu\lambda^2\dfrac{\partial^2 Z}{\partial\eta^2} + (\nu\lambda^2 - A\lambda e^\eta)\dfrac{\partial Z}{\partial\eta}$
8	$U = u(\xi, t)$, $\xi = y + \lambda t$	$\dfrac{\partial u}{\partial t} = \nu\dfrac{\partial^2 u}{\partial\xi^2} + [F(\xi) - \lambda]\dfrac{\partial u}{\partial\xi} - F_\xi'(\xi)u$
9	$U = t^{-1/2}u(\xi, \tau)$, $\xi = yt^{-1/2}$, $\tau = \ln t$	$\dfrac{\partial u}{\partial\tau} = \nu\dfrac{\partial^2 u}{\partial\xi^2} + H(\xi)\dfrac{\partial u}{\partial\xi} + [1 - H_\xi'(\xi)]u$

$t = (k^2 + 1)\tau$, Eq. (16) is reduced to Eq. (9), in which ζ and τ should be substituted for y and t (exact solutions to Eq. (9) are described in Table 1).

3°. There is an exact solution [a particular case of solutions taking form (8)]

$$w(x, y, t) = e^{-\lambda y}[f(t)x + g(t)] + \varphi(t)x + \psi(t)y + \chi(t),$$

$$f(t) = C_1E(t), \quad E(t) = \exp[\nu\lambda^2 t - \lambda\int\varphi(t)dt],$$

$$g(t) = C_2E(t) - C_1E(t)\int\psi(t)dt.$$

Here, $\varphi(t)$, $\psi(t)$, and $\chi(t)$ are arbitrary functions, and C_1, C_2, and λ are arbitrary parameters.

4°. There is an exact solution

$$w(x, y, t) = e^{-\lambda y}[A(t)e^{\beta x} + B(t)e^{-\beta x}] + \varphi(t)x + \psi(t)y + \chi(t),$$

$$A(t) = C_1\exp[\nu(\lambda^2 + \beta^2)t - \beta\int\psi(t)dt - \lambda\int\varphi(t)dt],$$

$$B(t) = C_2\exp[\nu(\lambda^2 + \beta^2)t + \beta\int\psi(t)dt - \lambda\int\varphi(t)dt],$$

in which $\varphi(t)$, $\psi(t)$, and $\chi(t)$ are arbitrary functions and C_1, C_2, λ, and β are arbitrary parameters.

5°. There is an exact solution

$$w(x, y, t) = e^{-\lambda y}[A(t)\sin(\beta x) + B(t)\cos(\beta x)] + \varphi(t)x + \psi(t)y + \chi(t).$$

Here, $\varphi(t)$, $\psi(t)$, and $\chi(t)$ are arbitrary functions, λ and β are arbitrary parameters, and the functions $A(t)$ and $B(t)$ satisfy the linear nonautonomous system of ordinary differential equations

$$\begin{aligned} A_t' &= [\nu(\lambda^2 - \beta^2) - \lambda\varphi(t)]A + \beta\psi(t)B, \\ B_t' &= [\nu(\lambda^2 - \beta^2) - \lambda\varphi(t)]B - \beta\psi(t)A. \end{aligned} \tag{21}$$

The general solution to system (21) takes the form

$$A(t) = \exp[\nu(\lambda^2 - \beta^2)t - \lambda\int\varphi dt] \times [C_1\sin(\beta\int\psi dt) + C_2\cos(\beta\int\psi dt)],$$

$$B(t) = \exp[\nu(\lambda^2 - \beta^2)t - \lambda\int\varphi dt] \times [C_1\cos(\beta\int\psi dt) - C_2\sin(\beta\int\psi dt)],$$

where $\varphi = \varphi(t)$, $\psi = \psi(t)$, and C_1 and C_2 are arbitrary constants. In particular, if $\varphi = \frac{\nu}{\lambda}(\lambda^2 - \beta^2)$ and $\psi = a$, we obtain the periodic solution

$$A(t) = C_1\sin(a\beta t) + C_2\cos(a\beta t),$$

$$B(t) = C_1\cos(a\beta t) - C_2\sin(a\beta t).$$

6°. There are exact solutions

$$w(x, y, t) = A(t)\exp(k_1x + \lambda_1y) + B(t)\exp(k_2x + \lambda_2y) + \varphi(t)x + \psi(t)y + \chi(t),$$

in which $\varphi(t)$, $\psi(t)$, and $\chi(t)$ are arbitrary functions; k_1, λ_1, k_2, and λ_2 are arbitrary parameters related by one of the two equations

$k_1^2 + \lambda_1^2 = k_2^2 + \lambda_2^2$ (the first family of the solutions),

$k_1\lambda_2 = k_2\lambda_1$ (the second family of the solutions),

and the functions $A(t)$ and $B(t)$ satisfy the linear ordinary differential equations

$$A_t' = [\nu(k_1^2 + \lambda_1^2) + \lambda_1\varphi(t) - k_1\psi(t)]A,$$

$$B_t' = [\nu(k_2^2 + \lambda_2^2) + \lambda_2\varphi(t) - k_2\psi(t)]B.$$

These equations are easily solved:

$$A(t) = C_1\exp[\nu(k_1^2 + \lambda_1^2)t + \lambda_1\int\varphi(t)dt - k_1\int\psi(t)dt],$$

$$B(t) = C_2\exp[\nu(k_2^2 + \lambda_2^2)t + \lambda_2\int\varphi(t)dt - k_2\int\psi(t)dt].$$

7°. There is an exact solution

$$w(x, y, t) = [C_1\sin(\lambda x) + C_2\cos(\lambda x)] \times [A(t)\sin(\beta y) + B(t)\cos(\beta y)] + \varphi(t)x + \chi(t).$$

Here, $\varphi(t)$ and $\chi(t)$ are arbitrary functions, C_1, C_2, λ, and β are arbitrary parameters, and the functions $A(t)$ and $B(t)$ satisfy the linear non-autonomous system of ordinary differential equations

$$\begin{aligned} A_t' &= -\nu(\lambda^2 + \beta^2)A - \beta\varphi(t)B, \\ B_t' &= -\nu(\lambda^2 + \beta^2)B + \beta\varphi(t)A. \end{aligned} \tag{22}$$

The general solution to system (22) takes the form

$$A(t) = \exp[-\nu(\lambda^2 + \beta^2)t] \times [C_3\sin(\beta\int\varphi dt) + C_4\cos(\beta\int\varphi dt)], \quad \varphi = \varphi(t),$$

$$B(t) = \exp[-\nu(\lambda^2 + \beta^2)t] \times [-C_3\cos(\beta\int\varphi dt) + C_4\sin(\beta\int\varphi dt)],$$

where C_3 and C_4 are arbitrary constants.

8°. There is an exact solution

$$w(x, y, t) = [C_1\sinh(\lambda x) + C_2\cosh(\lambda x)] \times [A(t)\sin(\beta y) + B(t)\cos(\beta y)] + \varphi(t)x + \chi(t),$$

in which $\varphi(t)$ and $\chi(t)$ are arbitrary functions, C_1, C_2, λ, and β are arbitrary parameters, and the functions $A(t)$ and $B(t)$ satisfy the linear non-autonomous system of ordinary differential equations

$$\begin{aligned} A_t' &= \nu(\lambda^2 - \beta^2)A - \beta\varphi(t)B, \\ B_t' &= \nu(\lambda^2 - \beta^2)B + \beta\varphi(t)A. \end{aligned} \tag{23}$$

The general solution to system (23) takes the form

$$A(t) = \exp[\nu(\lambda^2 - \beta^2)t] \times [C_3\sin(\beta\int\varphi dt) + C_4\cos(\beta\int\varphi dt)], \quad \varphi = \varphi(t),$$

$$B(t) = \exp[\nu(\lambda^2 - \beta^2)t] \times [-C_3\cos(\beta\int\varphi dt) + C_4\sin(\beta\int\varphi dt)],$$

where C_3 and C_4 are arbitrary constants.

9°. There is an exact solution

$$w(x, y, t) = u(z, t) + \varphi(t)x + \psi(t)y, \quad z = kx + \lambda y.$$

Here $\varphi(t)$ and $\psi(t)$ are arbitrary functions, k and λ are arbitrary parameters, and the function $u(z, t)$ satisfies the linear differential equation of the fourth order:

$$\frac{\partial^3 u}{\partial t\partial z^2} + [k\psi(t) - \lambda\varphi(t)]\frac{\partial^3 u}{\partial z^3} = \nu(k^2 + \lambda^2)\frac{\partial^4 u}{\partial z^4}.$$

The transformation

$$U(\xi, t) = \frac{\partial^2 u}{\partial z^2}, \quad \xi = z - \int [k\psi(t) - \lambda\varphi(t)]dt$$

reduces this equation to the conventional heat-conduction equation

$$\frac{\partial U}{\partial t} = \nu(k^2 + \lambda^2)\frac{\partial^2 U}{\partial \xi^2}.$$

10°. There is a solution with the generalized separation of variables in the polar coordinate system:

$$w(r, \theta, t) = f(r, t)\theta + g(r, t).$$

Here, $x = r\cos\theta$ and $y = r\sin\theta$, the functions $f = f(r, t)$ and $g = g(r, t)$ satisfy the system of equations

$$\mathbf{L}(f_t) - r^{-1} f_r \mathbf{L}(f) + r^{-1} f[\mathbf{L}(f)]_r = \nu \mathbf{L}^2(f), \quad (24)$$

$$\mathbf{L}(g_t) - r^{-1} g_r \mathbf{L}(f) + r^{-1} f[\mathbf{L}(g)]_r = \nu \mathbf{L}^2(g), \quad (25)$$

the subscripts r and t imply the corresponding partial derivatives, and

$$\mathbf{L}(f) = r^{-1}(r f_r)_r, \quad \mathbf{L}^2(f) = \mathbf{L}\mathbf{L}(f).$$

For the particular solution $f = \varphi(t)\ln r + \psi(t)$ to Eq. (24) (φ and ψ are arbitrary functions), Eq. (25) is reduced to a linear equation of the second order by the substitution $U = \mathbf{L}(g)$.

ACKNOWLEDGMENTS

The work was performed under financial support of the Russian Foundation for Basic Research, projects nos. 00-02-18033 and 00-03-32055.

REFERENCES

1. L. G. Loĭtsyanskiĭ, *Mechanics of Liquids and Gases* (Nauka, Moscow, 1973).
2. H. Schlichting, *Boundary Layer Theory* (McGraw-Hill, New York, 1968; Nauka, Moscow, 1974).
3. V. V. Pukhnachev, Zh. Prikl. Mekh. Tekh. Fiz., No. 1, 83 (1960).
4. L. V. Ovsyannikov, *Group Analysis of Differential Equations* (Nauka, Moscow, 1978; Academic, New York, 1982).
5. V. K. Andreev, O. V. Kaptsov, V. V. Pukhnachev, and A. A. Rodionov, *Application of Group-Theoretic Methods in Hydrodynamics* (Nauka, Novosibirsk, 1994).
6. *CRC Handbook of Lie Group to Differential Equations*, Ed. by N. H. Ibragimov (CRC, Boca Raton, 1995), Vol. 2.
7. V. A. Galaktionov and S. A. Posashkov, Zh. Vychisl. Mat. Mat. Fiz. **29**, 497 (1989).
8. V. A. Galaktionov, S. A. Posashkov, and S. R. Svirshchevskiĭ, Diff. Urav. **31**, 253 (1995).
9. V. F. Zaĭtsev and A. D. Polyanin, *Handbook of Differential Equations with Partial Derivatives: Exact Solutions* (Mezhd. Progr. Obraz., Moscow, 1996).
10. A. D. Polyanin, A. I. Zhurov, and A. V. Vyazmin, J. Non-equilib. Thermodyn. **25** (3/4), 251 (2000).
11. E. Kamke, *Differentialgleichungen*, Bd. 1: *Gewöhnliche Differentialgleichungen* (Geest and Portig, Leipzig, 1964; Nauka, Moscow, 1971).
12. V. F. Zaĭtsev and A. D. Polyanin, *Handbook of Ordinary Differential Equations* (Fizmatlit, Moscow, 2001).

Translated by V. Chechin

Doklady Physics, Vol. 46, No. 10, 2001, pp. 732–735. Translated from Doklady Akademii Nauk, Vol. 380, No. 5, 2001, pp. 619–622.

MECHANICS

On the Solution to a Class of the Mixed Problems for a Layered Half-Space

Academician V. A. Babeshko*, T. I. Belyankova, and V. V. Kalinchuk****

Received June 20, 2001

A number of dynamic mixed problems in the theory of elasticity, electroelasticity, and mathematical physics for semibounded bodies of the layered half-space type leads to the equation

$$\mathbf{k}q = \int_{-a}^{a} k(x_1 - \xi)q(\xi)d\xi = f(x_1), \quad |x_1| \le a, \quad (1)$$

with the oscillating kernel whose symbol has branch points on the real axis:

$$k(s) = \frac{1}{2\pi}\int_{\Gamma} K(\alpha)e^{i\alpha s}d\alpha. \quad (2)$$

In this paper, we present the theorem which establishes the form of the solution to equation (1). Owing to the use of direct numerical procedures, this theorem is an extension of the solution to the equation of type (1) that was obtained, in particular, in [1–3] under the assumption that K in (2) is meromorphic. The application of numerical methods enables us to use an exact representation of the symbols of the integrated-operator kernels omitting a traditional approximation stage. As a result, we retain all the specific features of the equation, including branch points of the kernel symbol. This permits us to consider at greater length the dynamic properties of the problem and to improve the accuracy of the solution obtained.

1. We assume that: (i) $K(\alpha)$ is an even function having a finite number of branch points on the real axis; this number depends on the problem type and the properties of the medium material; (ii) $K(\alpha)$ is meromorphic in the complex plane with cuts that do not pass to one another, are located in the quadrants I and III, and connect the branch points with the infinitely distant point; (iii) $K(\alpha)$ has on the real axis a finite number of zeros γ_k ($k = 1, 2, \ldots, n_2$) and poles z_k ($k = 1, 2, \ldots, n_1$), as well as a countable set of complex zeros and poles with the points of condensation in certain sectors containing the imaginary axis; and (iv) $K(\alpha)$ takes the form

$$K(\alpha) = c|\alpha|^{-1}[1 + O(\alpha^{-1})]$$

at infinity. The position of the contour Γ corresponds to the emission conditions, and equation (1) is uniquely resolvable for any twice continuously differentiable function $f(x_1)$ [4]. We introduce the functions

$$\Pi(\alpha) = \prod_{k=1}^{M}(\alpha^2 - \gamma_k^2)(\alpha^2 - z_k^2)^{-1} \quad (3)$$

and

$$K_0(\alpha) = \Pi^{-1}(\alpha)K(\alpha),$$

where z_k ($k = 1, 2, \ldots, n_1$) and γ_k ($k = 1, 2, \ldots, n_2$) are real, and the remaining z_k ($k = n_1 + 1, \ldots, M$) and γ_k ($k = n_2 + 1, \ldots, M$), $M \ge \max\{n_1, n_2\}$ are the complex poles and zeros of $K(\alpha)$ that lie in the band $|\mathrm{Im}\,\alpha| \le E_0$. It follows from (3) that K_0 retains in itself all unaccounted in Π singularities of K, above all, the branch points on the real axis.

Theorem. *The Fourier transform of the solution to Eq.* (1) *is given by the formula*

$$Q(\alpha) = T(\alpha)\Pi^{-1}(\alpha) + \sum_{k=1}^{2M} C_k R_k(\alpha), \quad (4)$$

$$T(\alpha) = T_0(\alpha) + \sum_{k=1}^{2M} C_k T_k(\alpha),$$
$$T_k(\alpha) = \sum_{p=1}^{N} \beta_k^p \Phi_p(\alpha), \quad k = 0, 1, \ldots, 2M. \quad (5)$$

Here, $R_k(\alpha)$ is the function that satisfies the condition $Q(\alpha) = R_k(\alpha)$, $\alpha = \pm z_k$, $k = 1, 2, \ldots, M$ [1–3]; β_k^p are the components of the vectors $\mathbf{B}_k = \{\beta_k^p\}_{p=1}^N$, which satisfy the systems

$$\mathbf{A}\mathbf{B}_k = \mathbf{F}_k, \quad \mathbf{A} = \|A_{pl}\|_{p,l=1}^N, \quad \mathbf{F}_k = \{f_k^l\}_{l=1}^N,$$

* *Kuban State University, ul. Karla Libknekhta 9, Krasnodar, 350640 Russia*

** *Research Institute of Mechanics and Applied Mathematics, Rostov State University, Rostov-on-Don, Russia*

1028-3358/01/4610-0732$21.00

$$A_{pl} = \int_\Gamma K_0(\alpha)\Phi_p(\alpha)\Phi_l^*(\alpha)d\alpha,$$
$$f_0^l = \int_{-a}^{a} f(x_1)\varphi_l(x_1)dx_1, \quad f_k^l = \int_\Gamma K(\alpha)\Phi_l(\alpha)e^{-i\alpha x_1^k}d\alpha; \tag{6}$$

()* *implies a complex conjugate quantity*;

$$\Phi_p(\alpha) = -i\alpha^{-1}[e^{i\alpha a_p} - e^{i\alpha a_{p-1}}] \tag{7}$$

is the Fourier transform of the coordinate function

$$\varphi_p(x_1) = \begin{cases} 1, & x_1 \in [a_{p-1}, a_p] \\ 0, & x_1 \notin [a_{p-1}, a_p], \end{cases} \quad p = 1, 2, \ldots, N, \tag{8}$$

in which a_p, $p = 1, 2, \ldots, N-1$ *are the points that divide the segment* $[-a, a]$ *into equal parts,* $a_0 = -a$, $a_N = a$; *and the constants* C_k *appearing in* (4) *and* (5) *are found from the constraints*

$$T(\pm\gamma_n) = 0, \quad n = 1, 2, \ldots, M. \tag{9}$$

2. The proof is based on the method of regularization of an integral operator developed in [1–3], which represents a solution in the form

$$q(x_1) = q_0(x_1) + r(x_1) \tag{10}$$

provided that

$$\mathbf{V}(\alpha)q = \mathbf{V}(\alpha)r, \quad \mathbf{V}(\alpha)q_0 = 0, \quad \alpha = \pm z_k, \quad k = 1, 2, \ldots, M \tag{11}$$

[$\mathbf{V}(\alpha)$ and $\mathbf{V}^{-1}(x_1)$ are, respectively, the operators of the direct and inverse Fourier transforms]. Without loss of generality and on account of the arbitrariness in (11), we can choose r in the form

$$r(x_1) = \sum_{k=1}^{2M} C_k r_k(x_1). \tag{12}$$

Upon substituting (10), with (12) taken into account, and passing to the new unknown quantity

$$t(x_1) = \mathbf{V}^{-1}(x_1)T, \quad T(\alpha) = \Pi(\alpha)Q_0(\alpha), \tag{13}$$

equation (1) converts to the form

$$\mathbf{k}_0 t = \sum_{k=1}^{2M} C_k f_k(x_1) + f_0(x_1), \quad |x_1| \le a. \tag{14}$$

The validity of the theorem statement is achieved by introducing the set of the coordinate functions (8), by representing the solution in the form

$$t(x_1) = t_0(x_1) + \sum_{k=1}^{2M} C_k t_k(x_1),$$
$$t_k(x_1) = \sum_{p=1}^{N} \beta_k^p \varphi_p(x_1), \quad k = 0, 1, \ldots, 2M, \tag{15}$$

and by substituting it into Eq. (14) with subsequent application of Galerkin's scheme. Condition (9) follows from the lemma given in [5], which establishes the equivalency of transformations.

When exploring the dynamics of massive bodies, mechanical or electromechanical systems interacting with an elastic or electroelastic medium, the main problem is to calculate the integral characteristics of the problem (the response of the medium on the die action, charge, etc.). The necessity of calculating the density of these characteristics (contact stresses, charge distribution density, etc.) drops out. In this case, it is possible to restrict consideration by the Fourier transform of the problem solution. In other words, the class of r-functions in (12) can be substantially expanded by taking, for example,

$$r_k(x_1) = \delta(x_1 - x_1^k), \tag{16}$$

as the components, where x_1^k are the coordinates of the points that divide the segment $[-a, a]$ into equal parts. In this case,

$$R_k(\alpha) = e^{i\alpha x_1^k}, \tag{17}$$

which considerably simplifies formula (4). To calculate the integral characteristics of the problem, it is sufficient to put $\alpha = 0$ in (4).

3. Let $\mathbf{A}$ and $\mathbf{A}^{-1}$ be constructed. Then, the solutions to systems (6) take the form

$$\mathbf{B}_k = \mathbf{A}^{-1}\mathbf{F}_k. \tag{18}$$

It follows from (18) that the solution of $2M + 1$ systems of algebraic equations (9) is concentrated on the calculation of the matrices $\mathbf{A}$ and $\mathbf{A}^{-1}$, a procedure that is sufficient to perform once. Next, we should calculate all the vectors $\mathbf{B}_k$, whose components are β_k^p, $p = 1, \ldots, N$, $k = 0, 1, 2, \ldots, 2M$.

Remark 1. We assumed above that z_k and γ_k are single-valued. The extension to the case of multiple zeros and poles is, in principle, not difficult. However, in this case, representation (3) and the form of relationships (9) change [1].

Remark 2. When the function $q(x_1)$, as the solution to the original equation (1), must be calculated, we should use formula (4) and choose $r(x_1)$ from the class $\mathbf{L}_p$, $p > 1$, or, when r is used in form (16), introduce $t(x_1)$

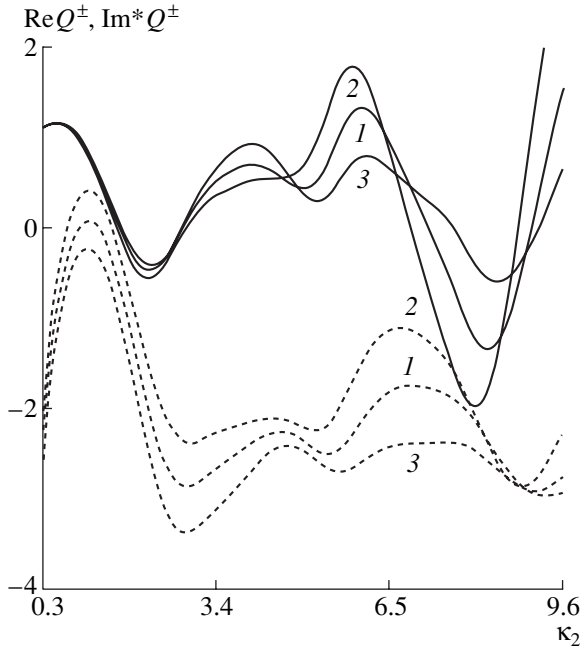

Fig. 1. Effect of localization of prestresses on the dynamic stiffness of the medium as illustrated by the graphs $\mathrm{Re}\,Q^{\pm}$ and $\mathrm{Im}^*Q^{\pm} = \kappa_2^{-1}\,\mathrm{Im}\,Q^{\pm} + 6$. See details in the text.

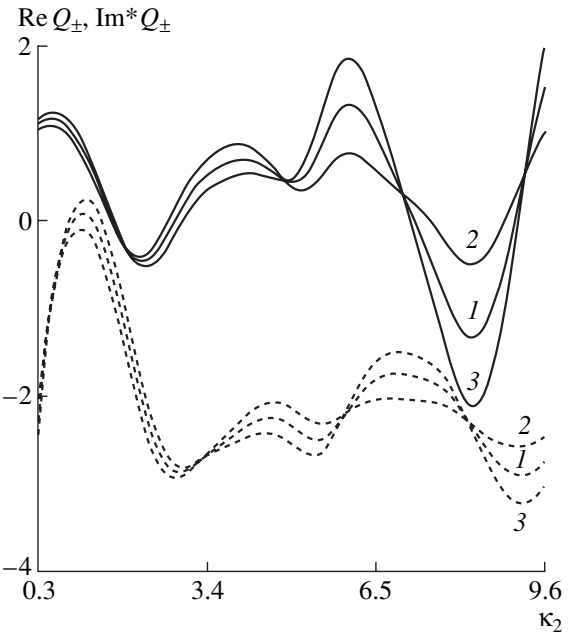

Fig. 2. Effect of localization of prestresses on the dynamic stiffness of the medium as illustrated by the graphs $\mathrm{Re}\,Q_{\pm}$ and $\mathrm{Im}^*Q_{\pm} = \kappa_2^{-1}\,\mathrm{Im}\,Q_{\pm} + 6$. See details in the text.

such that $r(x_1)$ is present in the final expression only under the integration sign [1].

Remark 3. The method is extended without difficulty to the class of three-dimensional axisymmetric problems of the elasticity theory. In this case, α is replaced by a new variable $u = \sqrt{\alpha_1^2 + \alpha_2^2}$. The proposed approach, providing a high accuracy in considering dynamic properties, makes it possible to study subtle problems of contact interaction, in particular, the effect of initial stresses on the dynamic stiffness of the medium.

4. We now consider Eq. (1), which arises in the study of the interaction of a die with a two-layered prestressed half-space, when

$$K(\alpha) = \sum_{k=1}^{2} [\Delta_{k3}\cosh\sigma_k^{(1)}h + \Delta_{k+2,3}\sinh\sigma_k^{(1)}h],$$

$$\Delta_{lp} = \frac{\Delta_{lp}^0}{\Delta^0}, \quad l, p = 1, 2, \ldots, 6, \quad \Delta^0 = \det\|T_{lp}\|_{l,p=1}^6,$$

$$T_{1k} = l_{1k}^{(1)}\cosh\sigma_k^{(1)}h, \quad T_{1,k+2} = l_{1k}^{(1)}\sinh\sigma_k^{(1)}h, \quad T_{1,k+4} = 0,$$

$$T_{2k} = l_{3k}^{(1)}\sinh\sigma_k^{(1)}h, \quad T_{2,k+2} = l_{3k}^{(1)}\cosh\sigma_k^{(1)}h, \quad T_{2,k+4} = 0,$$

$$T_{3k} = 0, \quad T_{3,k+2} = f_k^{(1)}, \quad T_{3,k+4} = -f_k^{(2)},$$

$$T_{4k} = 1, \quad T_{4,k+2} = 0, \quad T_{4,k+4} = -1,$$

$$T_{5k} = l_{1k}^{(1)}, \quad T_{5,k+2} = 0, \quad T_{5,k+4} = -l_{1k}^{(2)},$$

$$T_{6k} = 0, \quad T_{6,k+2} = l_{3k}^{(1)}, \quad T_{6,k+4} = -l_{3k}^{(2)},$$

where $f_k^{(n)} = -i\alpha S_{3k}^{(n)}(\sigma_k^{(n)}S_{1k}^{(n)})^{-1}$ $(n, k = 1, 2)$; Δ_{lp}^0 are the cofactors of T_{lp}; and the superscript indicates that the given quantity belongs to layer (1) or half-space (2):

$$l_{1k}^{(n)} = \chi_{3113}^{(n)}\sigma_k^{(n)}f_k^{(n)} - i\alpha\chi_{1313}^{(n)},$$

$$S_{1k}^{(n)} = B_{32}^{(n)}H_{1k}^{(n)} + \alpha^2 B_{13}^{(n)}B_{23}^{(n)},$$

$$l_{3k}^{(n)} = \chi_{3333}^{(n)}\sigma_k^{(n)} - i\alpha\chi_{3311}^{(n)}f_k^{(n)},$$

$$S_{3k}^{(n)} = B_{12}^{(n)}H_{3k}^{(n)} - \sigma_k^{(n)^2}B_{13}^{(n)}B_{23}^{(n)},$$

$$H_{mk}^{(n)} = \chi_{3mm3}^{(n)}\sigma_k^{(n)^2} - (\chi_{kmmk}^{(n)}\alpha^2 - \rho^{(n)}\omega^2),$$

$$B_{mk}^{(n)} = \chi_{mmkk}^{(n)} + \chi_{mkmk}^{(n)},$$

$$\chi_{lmsp} = \delta_{ls}\delta_{mp}s_{lm}^{1n} + \delta_{ms}\delta_{lp}\nu_l^2 s_{lm}^{2n} + \delta_{lm}\delta_{sp}s_{ls}^{3n},$$

$$s_{lm}^{1n} = 2J_n^{-1}[-\psi_{0n} + \psi_{2n}\nu_{nl}^2\nu_{nm}^2],$$

$$s_{lm}^{2n} = 2J_n^{-1}[\psi_{1n} + \psi_{2n}(\nu_{nl}^2 + \nu_{nm}^2)],$$

$$s_{lm}^{3n} = 4J_n^{-1}\sum_{M=0}^{2}\sum_{N=0}^{2} V_{MN}^{(n)}\nu_{nl}^{2M}\nu_{nm}^{2N}.$$

Here, δ_{mp} is Kronecker's symbol, $\rho^{(n)}$ is the density, and ν_{nm} is the relative elongation of filaments of the layer ($n = 1$) or the half-space ($n = 2$) along the x_m-axis. The coefficients ψ_{nl} and $V_{lm}^{(n)}$, $l, m = 0, 1, 2$, depend on the form of the elastic potential and on the initial deformed state (IDS). Their appearance for some particular cases is given in [5–9]; $\sigma_k^{(n)}$ are derived from the characteristic equation

$$H_{1k}^{(n)}H_{3k}^{(n)} + \alpha^2\sigma_k^{(n)^2}B_{13}^{(n)^2} = 0.$$

5. Numerical analysis was performed for a medium that represents a layer (bronze) arranged on the half-space (steel 35KhGSA) [6]). The IDS was set by the conditions: $\nu_{nl} = \nu_{n2} = \nu_{n3} = 1 \pm \zeta$ ($n = 1$ stands for the layer, $n = 2$ for the half-space) and $\zeta = 0.005$.

The effect of localization of prestresses on the dynamic stiffness of the medium is illustrated in Figs. 1 and 2, in which we plotted the graphs $\mathrm{Re}\,Q^{\pm}$, $\mathrm{Im}^*Q^{\pm} = \kappa_2^{-1}\,\mathrm{Im}\,Q^{\pm} + 6$ (Fig. 1) and $\mathrm{Re}\,Q_{\pm}$, $\mathrm{Im}^*Q_{\pm} = \kappa_2^{-1}\,\mathrm{Im}\,Q_{\pm} + 6$ (Fig. 2). The functions $Q^{\pm}$ and $Q_{\pm}$ are calculated using formula (4) [$f(x_1) = 1$] for the cases of the preliminary compression (–) or tension (+) of the layer (superscript) or the half-space (subscript). Curves *1* correspond to the natural state, curves *2* correspond to tension, and curves *3* to compression of the corresponding domain of the composite medium. From these graphs, it follows that in the absence of initial stresses the quantities $\mathrm{Re}\,Q_0$ and Im^*Q_0 exhibit oscillations that are due to the heterogeneity of the medium. The appearance of these oscillations substantially depends on the IDS localization. The compression of the layer (curve *3* in Fig. 1), as well as the tension of the half-space (curve *2* in Fig. 2), decrease the heterogeneity of the layered structure. Conversely, the tension of the layer, as does the compression of the half-space, enhances the medium heterogeneity. This confirms the previously indicated [7–9] specific character of the action of the IDS on the dynamic stiffness of the medium, namely, the increase of the dynamic stiffness under compression of the layer or the homogeneous half-space and, conversely, its decrease under tension.

ACKNOWLEDGMENTS

This study was supported by the Russian Foundation for Basic Research.

REFERENCES

1. V. A. Babeshko and O. D. Pryakhina, Prikl. Mat. Mekh. **44** (3), 477 (1980).
2. V. A. Babeshko, *Generalized Factorization Method in Tree-Dimensional Dynamical Mixed Problems of Theory of Elasticity* (Nauka, Moscow, 1984).
3. I. I. Vorovich, V. A. Babeshko, and O. D. Pryakhina, *Dynamics of Massive Bodies and Resonance Effects in Deformable Media* (Nauchnyĭ Mir, Moscow, 1999).
4. I. I. Vorovich and V. A. Babeshko, *Dynamical Mixed Problems of Theory of Elasticity for Non-classical Areas* (Nauka, Moscow, 1979).
5. V. A. Babeshko, Dokl. Akad. Nauk SSSR **242** (1), 62 (1978) [Sov. Phys. Dokl. **23**, 685 (1978)].
6. A. I. Lur'e, *Nonlinear Theory of Elasticity* (Nauka, Moscow, 1980).
7. T. I. Belyankova and V. V. Kalinchuk, Prikl. Mat. Mekh. **57** (4), 123 (1993).
8. T. I. Belyankova and V. V. Kalinchuk, Izv. Akad. Nauk, Mekh. Tverd. Tela, No. 6, 83 (1994).
9. T. I. Belyankova and V. V. Kalinchuk, Izv. Akad. Nauk, Mekh. Tverd. Tela, No. 2, 89 (1998).

Translated by A. Kozlenkov

Doklady Physics, Vol. 46, No. 10, 2001, pp. 736–739. Translated from Doklady Akademii Nauk, Vol. 380, No. 5, 2001, pp. 623–626.

MECHANICS

The Asymptotic Stability of a Steady Flow of an Ideal Incompressible Fluid through a Permeable Domain

A. B. Morgulis and V. I. Yudovich

Presented by Academician I. I. Vorovich April 3, 2001

Received April 25, 2001

We consider dynamics of an ideal homogeneous incompressible fluid passing through a given domain $D \subset \mathbb{R}^2$. Euler equations of motion of the fluid are written as

$$\partial_t \mathbf{v} + \boldsymbol{\omega} \wedge \mathbf{v} = -\nabla H, \quad \operatorname{div}\mathbf{v} = 0, \tag{1}$$

where $\mathbf{v}$ is the fluid velocity, $\boldsymbol{\omega} = \operatorname{rot}\mathbf{v}$, $H = P + \frac{v^2}{2}$, and P is the pressure. We assume that, at any time $t \geq 0$, the following conditions

$$\begin{aligned} (\mathbf{v} \cdot \mathbf{n})(x, t) &= \gamma(x, t), \quad x \in S, \\ \omega(x, t) &= \omega^+(x, t), \quad x \in S_t^+ \subset S \end{aligned} \tag{2}$$

are set at the boundary S of domain D. Here, $\mathbf{n}$ is the unit vector of the outward normal to $S = \partial D$, γ and ω^+ are the given functions ($\int_S \gamma ds = 0$ for all $t \geq 0$), and the *inlet* S_t^+ and the *outlet* S_t^- are the parts of the boundary S through which the fluid inflows into domain D and, respectively, outflows from it at the time moment $t \geq 0$. Therefore, by definition,

$$S_t^+ = \{x \in S: \gamma(x, t) < 0\}$$

and

$$S_t^- = \{x \in S: \gamma(x, t) > 0\}.$$

It will be recalled that Kochin was the first, who has analyzed the general problem of unsteady fluid flow [1]. In his study, the boundary conditions (2) were proposed. Yudovich [2] established that a two-dimensional problem defined by Eq. (1) and boundary conditions (2) is globally solvable. In what follows, we consider only this two-dimensional problem and refer it to as the problem Y.

Rostov State University, Rostov-on-Don, Russia

In the general case, problem (1), (2) is overdetermined [3]. At the same time, the correctness (but only local in time) was proved for some other boundary value problems in the case of two- and three-dimensional Euler equations [4, 5].

The permeation of fluid through the boundary of the flow domain involves a complicated dissipation–pumping mechanism: while penetrating into this domain, fluid particles bring in (or bring out, when leaving it) energy, enstrophy, kinetic momentum, and other material quantities. For example, a strong pumping effect arises when the flow inlet contains a closed curve c. In this case, the equality

$$\frac{d}{dt}\oint_c \mathbf{v} \cdot \mathbf{dx} = -\int_c \omega^+ \gamma ds \tag{3}$$

follows from the equations of motion and from the boundary conditions (2). If the functions ω^+ and γ are independent of time t and the integral in the right-hand side of equality (3) does not vanish, the velocity circulation around the contour c increases linearly with time. Thus, the *generation of the accelerating rotation occurs by blowing*. In this case, there are no steady-state regimes, and all solutions of the unsteady problem are unbounded.

At the same time, the enstrophy of the flow declines when its vortex is identically equal to zero at the inlet. In this case, dissipation concentrates at the outlet and may seem weak, but actually it may result in the asymptotic (exponential or even nilpotent) stability of the steady-state regime. Here we are dealing with such a stability.

Let problem Y have a steady-state solution with the velocity field $\mathbf{v}$ and the vortex ω. We make the following assumptions:

(H1) the flow domain is bounded, simply connected, and piecewise smooth;

(H2) the normal velocity γ is given in such a manner that the inlet S^+ and the outlet S^- are the connected smooth arcs without common end points; the set of angular points of domain D coincides with the set

1028-3358/01/4610-0736$21.00

$\partial S^+ \cup \partial S^-$ of points where the inlet, outlet, and rigid wall join;

(H3) the complete efflux condition is fulfilled; i.e., $\inf\{|\mathbf{v}(x)|, x \in D\} > 0$, so that the flow has no stagnation points both inside the flow region and on the rigid wall;

(H4) the boundary arcs of the flow region intersect each other at the right angles, and the steady-state solution is regular to such an extent that $\mathbf{v} \in C^\infty(D) \cap C(\bar{D})$ and $\omega \in C^1(\bar{D})$.

The flow (or its velocity field $\mathbf{v}$) that satisfies condition (H3) will be termed a *through* flow.

The condition of regularity (H4) has a minor character and can be weakened. The condition of single connectedness is essential, as follows from the above example.

The condition of full permeation (H3), i.e., the absence of stagnation zones in the flow, is of fundamental importance for all the results we consider below. Moreover, this condition justifies, to a certain extent, the assumptions on the smoothness of the principal solution [6]. The point is that the vortex of the flow with stagnation points can undergo discontinuities along the separatrix streamlines. At the same time, a large number of explicitly smooth solutions (both through and non-through) to the steady-state problem Y are known. The simplest among them are shear flows with rectilinear or circular streamlines parallel to the rigid walls of the channel.

The problem with initial and boundary value conditions, which arises as a result of the linearization of problem Y, will be named the LY problem. In the single connected domain D, problem LY has the form

$$\begin{aligned} &\partial_t\sigma + (\mathbf{v}, \nabla)\sigma + K\sigma = 0, \\ &\sigma|_{S^+} = 0, \quad \sigma|_{t=0} = \xi. \end{aligned} \tag{4}$$

Here, $S^+ = S_t^+$ is the mainstream inlet; σ is the vortex disturbance; and $K\sigma = \nabla\omega \wedge \nabla G\sigma$, where G is the Green operator of the problem; i.e., $-\Delta\varphi = \sigma$, $\varphi|_S = 0$.

When $\omega \equiv \text{const}$, we eliminate from Eq. (4) the term $K\sigma$, which reduces problem LY to a problem on the passive transport of the scalar σ by the known velocity field $\mathbf{v}$, so that

$$\partial_t\sigma + (\mathbf{v}, \nabla)\sigma = 0, \quad \sigma|_{S^+} = 0, \quad \sigma|_{t=0} = \xi. \tag{5}$$

Transport problem (5) for an arbitrary smooth field $\mathbf{v}$ is integrable in Lagrange coordinates, which are the time $\tau(x, t)$ and the point $a(x, t)$ where a fluid particle that occupies position x at the time instant t originally appeared in domain D.

According to the full-efflux condition, the quantity $t - \tau(x, t)$ (*the age of the fluid particle*) is uniformly bounded in the half-cylinder $D \times \{t > 0\}$. The maximal age of the particle (*the full efflux time*) is denoted by t_* so that

$$t_* = \sup\{t - \tau(x, t), x \in D, t > 0\}.$$

Proposition 1. *For any through vector field* $\mathbf{v}$, *the solution* σ_0 *to the transport problem* (5) *with the arbitrary initial function* ξ *is identically equal to zero in the half-cylinder* $D \times \{t > t_*\}$. *In particular, the through flow with a constant vortex is nilpotently stable.*

In general, we consider problem LY as a disturbed transport problem (5). Clearly, the disturbing operator K: $L_2(D) \longrightarrow L_2(D)$ is completely continuous.

Proposition 2. *Under the full-efflux condition, the spectrum of problem LY is discrete in the sense that the corresponding resolvent* $R(\lambda)$: $L_2(D) \longrightarrow L_2(D)$ *is a meromorphic function of the complex variable* λ. *In this case the real parts of eigenvalues are bounded from above.*

We represent the solution σ of problem LY as a perturbation-theory series so that

$$\sigma(t) = \sigma_0(t) + \ldots + \sigma_k(t) + \ldots,$$

where σ_0 is the solution to the transport problem (5), and the functions σ_k ($k = 1, 2, \ldots, \infty$) are defined by the recurrence relationships

$$\sigma_k(x, t) = -\int_{\tau(x, t)}^{t} (K\sigma_{k-1})(X(s, x, t), s)ds. \tag{6}$$

Here $X(s, x, t) \in D$ is the position that was occupied at the moment $s \in (\tau(x, t), t)$ by the fluid particle, which is located at the time instant $t > 0$ at the point $x \in D$. Note that the length of the integration segment in integral (6) does not exceed the time of the full efflux t_* and, therefore, the disturbances σ_k are different from zero only when $t < (k + 1)t_*$.

Theorem 1. *Let the mainstream be through. Then, for all* $t > t_*$, *the evolutionary operator* $U(t) : \xi \mapsto \sigma(t)$ *of problem LY is compact in* $L_2(D)$.

Let D' *be the fixed subdomain of domain* D *bounded by both a pair of the internal streamlines and the arcs* S^+ *and* S^-. *Then, for any positive integer* m *and for the instant* $t > mt_*$, *the following estimates of the derivatives with respect to the space norm* $L_2(D')$ *take place*:

$$\left\|(\partial_{t,x}^m\sigma)(t)\right\|_{2,D'} \le c\sup\{\|\sigma(s)\|_{2,D}, s \in (t - mt_*, t)\}, \quad t > mt_*. \tag{7}$$

Here, the constant c *depends, in general, on subdomain* D', *but does not depend on the initial disturbance and on the time* t. *Moreover, for all* $t > t_*$, *the derivatives* $(\partial_t\sigma)(t)$ *and* $(\mathbf{v}, \nabla)\sigma(t)$ *satisfy inequality* (7), *where* $m = 1$ *and* $D' = D$.

Having compared Theorem 1 with the known examples of loss of the smoothness of disturbances [7, 8, 9, 13, 14], we can suggest that the flow smoothness improves in the part of the flow where rapid drift of disturbances occurs and worsens in places where disturbances drift slowly. The simplest condition for asymptotic stability is related to the dimensionless quantity $q_v = t_* \lambda_1^{-1/2}(D) \max_D |\nabla \omega|$, where $\lambda_1(D)$ is the minimum eigenvalue of the first boundary value problem for the operator $-\Delta$ in domain D. The flow (or its velocity field $\mathbf{v}$) that satisfies the condition $q_v < 1$ is hereafter referred to as fast one.

Theorem 2. *The fast flow is exponentially asymptotically stable within the linear approximation in the enstrophy metric* (*i.e., in the metric* $L_2(D)$ *for vortex disturbances*). *In this case, for an arbitrary* $n = 0,1, \ldots$ *and for the instant* $t > nt_*$, *the following inequality holds*

$$\|\sigma(t)\|_{2,D} \le \max(1, e^{\mu t_*})[r(-\mu)]^n (1 - r(\mu))^{-1} \|\sigma(0)\|_{2,D}, \quad t > nt_*, \tag{8}$$

where $r(\mu) = q_v(\exp(\mu t_*) - 1)(\mu t_*)^{-1}$ *and the number* μ *is arbitrary solution to the inequality* $\max[r(\mu), r(-\mu)] < 1$. *Moreover, the higher norms of the disturbance whose estimates are given in Theorem 1 are exponentially damped as* $t \longrightarrow +\infty$.

In particular, any shear flow turns into a fast flow when a sufficiently large constant V_0 is added to its profile V. It is important that the fast flow remains fast after a small smooth deformation (caused, e.g., by the disturbance of the boundary data in problem Y) and in cases when disturbances of the vortex are C^1 small. For example, any steady flow that is close to the through Couette flow is fast.

More precise stability conditions are obtained by the second Lyapunov's method using Lyapunov functions introduced by Arnol'd [12]. This approach appears especially attractive if we note that the dependence of the vortex ω of the through flow on its stream function ψ is single valued and allows explicit expression in terms of the boundary data ω^+ and γ of the steady problem Y. Thus, the through steady flow is arranged in a substantially simpler form than the arbitrary flow in which the functional dependence of the vortex and the stream function is not necessarily single valued. Although the single-valuedness takes place when the flow maximizes its energy [10, 11], even in this case the function $\omega(\psi)$ is arranged in a complicated way, and its explicit expression is unknown.

Arnold's theorem [12] is extended onto problem Y in the following way. Let the stream function ψ of the basic flow be expressed in terms of its vortex ω by the equality $\psi = \Psi(\omega)$. Here, the function Ψ is determined on the entire axis $\mathbb{R}$, and its derivative Ψ' is uniformly bounded. We introduce the function Φ_ω assuming that $\Phi_\omega(\sigma) = f(\omega + \sigma) - f(\omega) - \Psi(\omega)\sigma$, where f is the primitive function of the function Ψ. By virtue of the nonlinear equation of disturbances, we define the functional W and its derivative $\dot{W}$ by the equalities

$$W(\sigma) = \int_D \left[\frac{(\nabla G\sigma)^2}{2} - \Phi_\omega(\sigma)\right] dz, \qquad \dot{W}(\sigma) = \int_{S^-} \gamma \Phi_\omega(\sigma) ds. \tag{9}$$

Theorem 3. *Let the condition* $\operatorname{ess\,inf}|\Psi'| > 0$ *be fulfilled. If in this case the function* Ψ *increases, we assume, in addition, that the functional* $-W$ *is positive definite so that* $\inf\{-W(\sigma)\|\sigma\|_{2,D}^{-2} : \sigma \in L_2(D)\} > 0$. *Then, an arbitrary solution* $\sigma(t)$ *to the nonlinear equation of disturbances admits a priori estimate* $\|\sigma(t)\|_{2,D}^2 \le c\|\sigma(0)\|_{2,D}^2$, *where the constant* c *is independent of time* t *and of vortex* $\sigma(0)$ *of the initial disturbance.*

As an example, we consider a shear flow with rectilinear streamlines in the channel of length l. (Here, l is the projection of the channel length onto the x-axis parallel to the streamlines.) Let the profile of the shear flow V have the form $V(y) = \sin \mu y$, $y \in (0, 1)$, $\mu > 0$. This flow is non-through. At the same time, Theorem 3 yields the estimate of the enstrophy for the flow finite disturbances, at least until $\mu < \pi(1 + l^{-2})^{1/2}$. For comparison, in the case of a channel of infinite length and disturbances being periodic along the channel, the Arnol'd theorem gives a result only under the condition $\mu < \pi$.

Now, let the flow profile have the form $V(y) = e^{-\mu y}$, $y \in (0, 1)$, $\mu > 0$. When the channel length is finite, this through flow satisfies the conditions of Theorem 3 for all μ, but the condition $q_v < 1$ is fulfilled only for $\mu \ll 1$. Hereafter, it will be shown, however, that the through flow is asymptotically stable within the linear approximation under the *linearized* conditions of Theorem 3.

We now introduce the function κ by the equality $\kappa(x) = \left(\frac{\nabla\psi}{\nabla\omega}\right)(x)$, $x \in D$. We linearize Theorem 3, assuming that $\Psi(h) = \kappa h$ and $\Phi_\omega(h) = \frac{\kappa h^2}{2}$ in (9).

Theorem 4. *Let the function* $\kappa = \frac{\nabla\psi}{\nabla\omega}$ *be bounded and definite in sign in the sense that* $\operatorname{ess\,inf}|\kappa| > 0$. If, *in this case, function* κ *is positive, we assume, in addition, that the functional* $-W$ $\left(\text{where } \Phi_\omega(\sigma) = \frac{\kappa\sigma^2}{2}\right)$ *is positively defined on* $L_2(D)$. *Then the system LY is stable according to Lyapunov in the enstrophy metric.*

Note that Theorems 3 and 4 do not use the condition of complete efflux. If, however, the latter is satisfied, then, according to Theorem 1, the bounded trajectories of the system LY are compact in $L_2(D)$, allowing us to establish the asymptotic stability of through flows in line with the Barbashin–Krasovskiĭ theorem. Following this sample, we find from formula (9) that ω-limiting set M of an arbitrary trajectory of system LY consists of smooth functions equal to zero in both the inlet S^+ and the outlet S^-. Therefore, the restriction of system LY on M is reversible: motions are invariant with respect to the change of the field $\mathbf{v}$ to the field $-\mathbf{v}$ with a simultaneous time inversion.

Theorem 5. *Let the through flow* $\mathbf{v}$ *satisfy the conditions of Theorem 4. Then, all the motions of system LY tend to the finite-dimensional subspace* $\mathbb{X}_0$ *spanned by the system of eigenvectors of the neutral spectrum of problem LY.*

The question on the existence of the neutral spectrum for the individual flow is difficult to solve. A simple general answer can, however, be given for analytic flow families.

Theorem 6. *Let a family of through flows* $\mathbf{v}_\mu$ *analytically depend on the parameter* μ, *and allow that for any* μ *the field* $\mathbf{v}_\mu$ *satisfies the conditions of Theorem 4. Then, the dimension of the neutral subspace* $\mathbb{X}_0$ *is constant within the family. If, in this case, the family contains a fast flow, then all its elements are asymptotically stable in the enstrophy metric within the linear approximation. Moreover, as* $t \longrightarrow +\infty$, *the higher norms of disturbances, whose estimates are given in Theorem 1, are damped.*

Theorem 6 entails, e.g., an asymptotic stability of shear flows with profiles $V(y) = \exp(-\mu y)$ for an arbitrary $\mu > 0$.

In conclusion, we consider one of the possible mechanisms for the onset of instability.

Theorem 7. *Assume that the family* $\mathbf{v}_\mu$ *of through flows is defined and analytic in the neighborhood of point* 0. *Let, in addition, the following conditions be fulfilled for* $\mu = 0$: (*a*) *the functions* $\kappa_0 = \dfrac{\nabla\psi_0}{\nabla\omega_0}$ *and* $\nu_0 = \kappa_0^{-1}$ *are limited and positive,* (*b*) *the minimal eigenvalue* α *of the problem* $(-\Delta\varphi = (\alpha + \nu_0)\varphi$ *in domain* D, $\varphi = 0$ *on* S) *is equal to zero, and* (*c*) *the function* $\partial_\mu\kappa_\mu$ *in domain D is nonpositive and is not identically equal to zero. Then there exists a vicinity* I_0 *of the point* $\mu = 0$, *such that in this vicinity the analytic branch* λ_μ *of simple real eigenvalues of problem LY is determined and this branch transversally intersects the imaginary axis for* $\mu = 0$. *Then the flow* $\mathbf{v}_\mu$ *is unstable for all positive values* $\mu \in I_0$ and stable for all negative values $\mu \in I_0$.

It should be noted that the instability of the flow with rectilinear streamlines cannot arise according to the scenario of Theorem 7. At the same time, this scenario is realized for certain flows with circular streamlines in the annual sector with an angular opening exceeding π.

ACKNOWLEDGMENTS

The research described in this paper was supported in part by Award #RM1-2084 of the US Civil Research & Development Foundation (CRDF) for the Independent States of the Former Soviet Union (CRDF).

REFERENCES

1. M. E. Kochin, Prikl. Mat. Mekh. **20** (10), 5 (1956).
2. V. I. Yudovich, Mat. Sb. **64**, 562 (1964).
3. A. V. Kazhikhov, Prikl. Mat. Mekh. **44**, 947 (1980).
4. S. N. Antontsev, A. V. Kazhikhov, and V. N. Monakhov, *Boundary-Value Problems of Mechanics of Inhomogeneous Liquids* (Nauka, Novosibirsk, 1983).
5. V. M. Solopenko, Dokl. Akad. Nauk SSSR **305**, 567 (1989) [Sov. Phys. Dokl. **34**, 204 (1989)].
6. G. V. Alekseev, Din. Sploshnoĭ Sredy, No. 10, 5 (1972); No. 15, 7 (1973).
7. V. I. Yudovich, Din. Sploshnoĭ Sredy, No. 16, 71 (1974).
8. V. I. Arnol'd, Prikl. Mat. Mekh. **36**, 255 (1972).
9. A. N. Kraĭko, Prikl. Mat. Mekh. **46**, 972 (1982).
10. A. I. Shnirelman, Russ. J. Math. Phys. **1** (1), 105 (1993).
11. G. R. Burton, Math. Ann. **276**, 225 (1987).
12. V. I. Arnol'd, Izv. Vyssh. Uchebn. Zaved., Mat., No. 5, 3 (1966).
13. V. I. Yudovich, Dokl. Akad. Nauk **370**, 760 (2000) [Dokl. Phys. **45**, 88 (2000)].
14. V. I. Yudovich, Chaos **10** (3), 105 (2000).

Translated by A. Kozlenkov

Doklady Physics, Vol. 46, No. 10, 2001, pp. 740–741. Translated from Doklady Akademii Nauk, Vol. 380, No. 5, 2001, pp. 627–629.

MECHANICS

Geometric Model of Internal Self-Balanced Stresses in Solids

Academician V. P. Myasnikov and M. A. Guzev

Received July 13, 2001

As is well known, conditions of mechanical equilibrium of a solid have the following form:

$$\int_{\partial V} X_i dS = \int_{\partial V} \sigma_{ij} n_j dS = 0, \quad i, j = 1, 2, 3,$$
$$\int_{\partial V} (\sigma_{il} x_k - \sigma_{kl} x_i) n_l dS + \int_V (\sigma_{ki} - \sigma_{ik}) dV = 0, \tag{1}$$

where V is the volume occupied by the solid under consideration and ∂V is its surface. In the absence of mass forces inside the volume V of the body, the Cauchy equations of equilibrium are valid:

$$\frac{\partial \sigma_{ij}}{\partial x_j} = 0. \tag{2}$$

In the classical theory of elasticity, the condition $\sigma_{ij} = 0$ is assumed to be met at equilibrium both in the bulk and on the surface of the solid. However, it is well known that under equilibrium conditions (1) and (2), stresses inside the solid are nonzero. Welds can serve as an example. Experimental study [1] shows that stresses in welds are comparable with those arising under external actions.

In engineering, various technological procedures are used making it possible to reduce the level of internal stresses or, on the contrary, to elevate it. As such procedures, we can indicate various types of thermal treatments: annealing, quenching, etc. As a rule, the explanation of results of the action of such technological procedures on a material is associated with a redistribution or disappearance of defects in its internal structure.

The physical theories of strength and plasticity considered various models of defects in the crystal structure of materials resulting in nonzero stresses under equilibrium conditions (see, for example, [2, Section IV]). As early as the 1950s, the analysis of these physical models led Kondo [3] and Bilby [4] to the conclusion of the necessity to use non-Euclidean geometric objects in their description, which were forbidden in the classical theory of elasticity.

Institute of Automatics and Control Processes, Far East Division, Russian Academy of Sciences, ul. Radio 5, Vladivostok, 690041 Russia

Thus, the experimental investigations explicitly indicate the existence of nonzero internal self-balanced stresses. To describe them on the basis of physical models of defects in the internal structure of a material, it is necessary to use mathematical objects inconsistent with the Euclidean geometric description of deformation properties for elastic continuum. However, the contradiction that arises can be overcome on the basis of solutions to problem (1), (2).

In fact, nonzero solutions to Eqs. (2) are well known in the classical theory of elasticity [2] and are related to the introduction of stress functions. The general solution to (2) can be represented in the following form:

$$\sigma_{ij} = (\mathrm{rot}\boldsymbol{\Omega}_i)_j, \quad i, j = 1, 2, 3, \tag{3}$$

where $\boldsymbol{\Omega}_i$ are three arbitrary vector functions. It should be noted that σ_{ij} has the gauge invariance [5] with respect to the transformation $\boldsymbol{\Omega}_i' = \boldsymbol{\Omega}_i + \nabla\Phi_i$. Thus only the vortex component of fields $\boldsymbol{\Omega}_i$ contributes to the stresses. From the total set of solutions (3), we choose the solutions that can be represented in the form:

$$\sigma_{ij} = \varepsilon_{ipq}\varepsilon_{jmn}\left(\frac{\partial \Gamma_{qm,p}}{\partial x_n} - \frac{\partial \Gamma_{qn,p}}{\partial x_m}\right)\sigma_0 l^2, \tag{4}$$

where ε_{ipq} is the Levi–Civita symbol and $\Gamma_{qm,p}$ are considered as a certain set of stress functions. The constants σ_0 and l have the dimension of stress and length.

Taking into account the necessity of introducing non-Euclidean objects for describing the defects, we interpret $\Gamma_{qm,p}$ as the objects of connectedness on the manifold generated by the internal defect structure of a material. For general affine connectednesses, the following relationship [5] takes place:

$$\frac{\partial \Gamma_{qm,p}}{\partial x_n} - \frac{\partial \Gamma_{qn,p}}{\partial x_m} = R_{pqmn}$$
$$- g^{ls}(\Gamma_{qn,s}\Gamma_{pm,l} - \Gamma_{qm,s}\Gamma_{pn,l} + \Gamma_{qn,s}K_{mlp} - \Gamma_{qm,s}K_{npl}), \tag{5}$$

where

$$K_{npl} = \frac{\partial g_{pl}}{\partial x_n} - \Gamma_{pn,l} - \Gamma_{ln,p}. \tag{6}$$

Here R_{pqmn} is the tensor of connected curvature, K_{npl} is the nonmetric tensor, and g_{ij} is the metric of manifold generated by defects.

1028-3358/01/4610-0740$21.00 © 2001 MAIK "Nauka/Interperiodica"

The geometric objects involved in (5) and (6) were used in [6–9] to analyze the general relationships of nonequilibrium thermodynamics in models of continuum with an internal structure. From the physical point of view, these geometric objects are compared to various defect structures [10].

In the general case, the stress tensor given by formula (4) is asymmetric. The set of functions determining (4) by means of (5) and (6) is reasonably large: these are 27 objects of connectedness and 6 metric-tensor components. A decrease in the number of functions used in the theory is associated with the hypothesis on the geometric structure of the manifold under consideration. In particular, if the manifold is Riemannian, $\Gamma_{qn,s}$ are expressed through the metric according to the Christoffel formulas, and the nonmetric tensor $K_{pql} = 0$. In this case, the internal stresses are completely determined by the manifold metric and are equal to

$$\sigma_{ij} = 2\sigma_0 l^2 \varepsilon_{ipq}\varepsilon_{jmn}\frac{\partial^2 g_{pm}}{\partial x_n \partial x_q}. \quad (7)$$

Expressions (4) identically satisfy Eqs. (2). It is possible to directly verify the validity of integral equilibrium conditions (1). Now it should be noted that the pointwise equilibrium conditions used in the theory of elasticity are invalid for stress field (4):

$$\sigma_{ij} n_j|_{\partial V} \neq 0.$$

By virtue of the linearity of equilibrium conditions, it is always possible to introduce the elastic-stress field τ_{ij} so that

$$\frac{\partial \tau_{ij}}{\partial x_j} = 0, \quad \tau_{ij} n_j|_{\partial V} = -\sigma_{ij} n_j|_{\partial V},$$
$$\tau_{ij} = \rho(\delta_{ik} - 2A_{ik})\frac{\partial U}{\partial A_{kj}}, \quad (8)$$

where U is the internal energy of an elastic solid, and A_{ij} is the Almansi tensor. The combined action of the fields provides the validity of all the equilibrium conditions:

$$\frac{\partial(\tau_{ij} + \sigma_{ij})}{\partial x_j} = 0, \quad (\tau_{ij} n_j + \sigma_{ij} n_j)|_{\partial V} = 0.$$

Somewhat more cumbersome calculations show that the moment conditions in (1) are also met if we consider the relationships of the moment theory of elasticity.

We now turn to discussing the results obtained. The stress field

$$T_{ij} = \tau_{ij} + \sigma_{ij}$$

satisfies equilibrium equations (2) and satisfies pointwise the conditions of the absence of external forces on the solid surface:

$$\frac{\partial T_{ij}}{\partial x_j} = 0, \quad T_{ij} n_j|_{\partial V} = 0.$$

Thus formulas (7) and (8) represent the set of possible distributions for the nonzero internal stresses in a continuum. It should be emphasized that the fields τ_{ij} and σ_{ij} interact only through the boundary-value condition in (8). This fact indicates the important role of the solid surface in studying deformation characteristics of a solid. This feature of the free surface of deformable solids was emphasized in [11].

As a result, the structure of an internal-stress field is formed from both the field of stresses generated by defects and the elastic-stress field that compensates for the surface nonequilibrity of the defects. The joint action of these stresses enables the sample to hold the given shape, and their variation leads automatically to a change in the shape of the solid when the defects emerge from the bulk of the solid body to its surface. The last statement follows directly from the invariance of distribution (7) with respect to motions of continuum generated by the infinitesimal diffeomorphic maps.

The question on a particular type of the metric g_{ij} depends on the prehistory of formation of defects and requires an analysis of dissipative processes in the material on the basis of the models considered previously in [6–9].

ACKNOWLEDGMENTS

This work was supported by the Russian Foundation for Basic Research, project nos. 99-01-00636 and 01-01-96904.

REFERENCES

1. G. N. Chernyshev, A. L. Popov, V. M. Kozintsev, and I. I. Ponomarev, *Residual Stresses in Deformed Solids* (Nauka, Moscow, 1996).
2. L. D. Landau and E. M. Lifshitz, *Course of Theoretical Physics*, Vol. 7: *Theory of Elasticity* (Pergamon, New York, 1986; Nauka, Moscow, 1987).
3. K. Kondo, in *Proceedings of the 2nd Japanese National Congress on Applied Mechanics, Tokyo, 1953*, p. 41.
4. B. A. Bilby, R. Bullough, and E. Smith, Proc. R. Soc. London, Ser. A **231**, 263 (1955).
5. B. A. Dubrovin, S. P. Novikov, and A. T. Fomenko, *Modern Geometry: Methods and Applications* (Springer, New York, 1984; Nauka, Moscow, 1986).
6. M. A. Guzev and V. P. Myasnikov, Izv. Akad. Nauk, Mekh. Tverd. Tela, No. 4, 156 (1998).
7. V. P. Myasnikov and M. A. Guzev, Tr. Mat. Inst. im. V. A. Steklova, Ross. Akad. Nauk **223**, 30 (1998).
8. V. P. Myasnikov and M. A. Guzev, Prikl. Mekh. Tekh. Fiz. **40** (2), 163 (1999).
9. V. P. Myasnikov and M. A. Guzev, Fiz. Mezomekh. **3** (1), 5 (2000).
10. A. V. Grachev, A. I. Nesterov, and S. G. Ovchinikov, Phys. Status Solidi B **156**, 403 (1989).
11. V. E. Panin, Yu. V. Grinyaev, V. I. Danilov, *et al.*, *Structural Levels of Plastic Deformation and Fracture* (Nauka, Novosibirsk, 1990).

Translated by V. Bukhanov

Doklady Physics, Vol. 46, No. 10, 2001, pp. 742–746. Translated from Doklady Akademii Nauk, Vol. 380, No. 5, 2001, pp. 630–634.

MECHANICS

Hamiltonian Description of Motion in a Perfect Stratified Fluid

N. N. Romanova and I. G. Yakushkin

Presented by Academician G.S. Golitsyn April 20, 2001

Received April 25, 2001

In this paper, a method for describing the two-dimensional motion of a perfect stratified fluid is proposed. The method is based on Hamiltonian equations written out in natural semi-Lagrangian coordinates in terms of two physical variables, namely, vorticity and density. It is shown that the equations obtained, which make the most use of the conservation laws, are convenient for studying both the wave motion in a stratified fluid and the hydrodynamic stability of shear flows. On the basis of the approach derived, the problem is solved for waves in a flow exhibiting a continuous vorticity distribution in a layer of finite thickness. The dynamics of developing perturbances is determined by the parameter a that characterizes the vorticity gradient in the layer and by the parameter ϵ proportional to the ratio of the layer thickness to the wavelength. If the gradients of the unperturbed vorticity are sufficiently high, then the frequency of the discrete-spectrum mode obtained differs from the mode frequency corresponding to the vorticity jump by the value on the order of ϵ. With decreasing the parameter a, i.e., decreasing the vorticity gradient in the layer, a wave packet appears corresponding to the continuous spectrum, which determines the perturbation dynamics. The results obtained make it possible, in particular, to estimate the limits of applicability of the finite-layer approximation for certain flow types.

Investigating two-dimensional motions of ideal fluid is a necessary stage in solving numerous particular problems of hydrodynamics and geophysics, including the description of wave motion and the analysis of the hydrodynamic stability of shear flows. As was recently shown, the most efficient method for solving these problems in linear and nonlinear formulation is the Hamiltonian formalism [1–3].

This method is actively used for studying discrete models of flows with in-layer constant density and vorticity [4–6]. In this case, it remains unclear to what extent the results obtained are suitable for describing flows with a continuous stratification and what is the difference between continuous and discrete models [7].

Obukhov Institute of Atmospheric Physics, Russian Academy of Sciences, Pyzhevskiĭ per. 3, Moscow, 109017 Russia

In this paper, equations usually applied for describing wave motion in continuous models for flows of ideal incompressible fluids (in the linear approximation, these are Rayleigh equations and Taylor–Goldstein equations) are presented in a certain integro-differential form. This form is more convenient for comparison with discrete models. The optimal formulation of the model should take into account conservation laws valid for the problem under consideration and, therefore, includes three stages. First, the relevant equations are written out in terms of quantities being conserved in the given setting, namely, of the density and vorticity. In this setting, the plasma-hydrodynamic analogy is manifested especially clearly, because the spatial vorticity distribution is naturally compared with the electron-velocity distribution function [8, 9].

The second stage is the passage to the semi-Lagrangian coordinates that are also directly associated with conservation laws. Retaining the Eulerian x-coordinate, we use, instead of the vertical coordinate, the Lagrangian variable h numbering the surface on which the motion of fluid particles occurs. These coordinates present the possibility of uniformly analyzing continuous and discrete stratified fluid flows. In essence, such an approach may be called a generalization of the contour-dynamics method. In this case, we may consider an arbitrary surface corresponding to a constant value of the Lagrangian variable as a boundary of the domain. This Lagrangian–Eulerian representation is discussed, e.g., in [10] when describing two-dimensional flows in a continuously stratified fluid.

The third stage involves the reduction of the obtained equations to the Hamiltonian form most suitable for developing approximate methods and constructing the perturbation theory. The Hamiltonian formalism for waves on a fluid surface was proposed in [11] and developed in [2, 4–6] for multilayer models with constant values of the layer density and vorticity. For analyzing perturbations in continuous models in the framework of the Lagrangian–Eulerian description, the Hamiltonian structure was introduced into kinetic equations for collisionless plasma and into the Benney equation for nonpotential waves in shallow water [3].

In the present paper, we propose two methods for representing equations of the two-dimensional dynamics of the incompressible stratified ideal fluid in the

1028-3358/01/4610-0742$21.00

Boussinesq approximation in the form of a Hamiltonian system in the Lagrangian–Eulerian (i.e., semi-Lagrangian) coordinate system.

The two-dimensional dynamics of the incompressible ideal fluid in the Boussinesq approximation can be represented by the equations

$$\partial_t \rho + u\partial_x \rho + w\partial_z \rho = 0, \quad (1)$$

$$\partial_t \Omega + u\partial_x \Omega + w\partial_z \Omega - \frac{g\partial_x \rho}{\rho} = 0, \quad (2)$$

where ρ is the density, Ω is the component of the vorticity vector rot **V** orthogonal to the (x, z)-plane, **V** is the velocity vector, and g is the gravitational acceleration.

The horizontal and vertical components of the velocity vector are written out as $u = -\partial_z \Psi$ and $w = \partial_x \Psi$, where the stream function Ψ satisfies the Poisson equation $\Delta\Psi = -\Omega$ and is expressed in terms of the vorticity Ω in the form

$$\Psi = -\int \Omega(x', z')G(x - x', z - z')dx'dz',$$

where

$$G(x - x', z - z') = \frac{1}{4\pi}\ln((x - x')^2 + (z - z')^2)$$

is the Green function for the Laplace operator. Henceforth, the integral symbol implies the double integration over the entire (x, z)-plane. In the state of rest, the medium is described by the density distribution and vorticity distribution, each depending only on the vertical coordinate. It is easy to show that the system of integro-differential equations (1), (2) is adequate to both continuous and stratified media [12]. In the latter case, it is equivalent to the system afforded by the boundary conditions and leads to solutions containing generalized functions. It is worth noting that, for such a formulation of the problem and for a medium with a constant density, the plasma-hydrodynamic analogy is manifested especially clearly [8, 9, 13]. In this case, it is natural to compare the spatial vorticity distribution $\Omega(x, z, t)$ and the velocity hydrodynamic field with the distribution $n(x, v, t)$ of the electric charge in the phase plane and with the electric field, respectively. This comparison is justified because both distributions are obtained as the solutions of the Poisson equation. In both cases, the z-coordinate evidently corresponds to the velocity v-coordinate in the phase plane. The only difference lies in the fact that in the plasma case the electric field does not depend on the charge velocity.

We now pass to the formulation of the problem in the semi-Lagrangian coordinate system. We determine the Lagrangian coordinate h with the help of the equation of a surface in which either the density or vorticity are invariant:

$$\partial_t h + u\partial_x h + w\partial_z h = 0.$$

We represent the dependence of the vertical z-coordinate on h in the form

$$z = s(x, t, h) = h + \eta(x, h, t).$$

In the coordinates x and h, system (1), (2) is written out as

$$\frac{\partial s}{\partial t} + u\frac{\partial s}{\partial x} = w, \quad (3)$$

$$\left(\frac{\partial \Omega}{\partial t} + u\frac{\partial \Omega}{\partial x}\right)\frac{\partial s}{\partial h} - N^2\frac{\partial s}{\partial x} = 0, \quad (4)$$

where the Brunt–Väisälä frequency squared, N^2, is determined by the expression

$$N^2 = -\frac{g}{\rho}\frac{d\rho}{dh}.$$

Since the quantity $s' = \dfrac{\partial s}{\partial h}$ satisfies the equation

$$\frac{\partial s'}{\partial t} + \frac{\partial (us')}{\partial x} = 0,$$

we have for the vorticity density, expressed in semi-Lagrangian coordinates as

$$\tilde{\Omega}(x, h, t) = \Omega(x, s, t)s' = \Omega(x, s, t)\left(1 + \frac{\partial \eta}{\partial h}\right),$$

the equation

$$\frac{\partial \tilde{\Omega}}{\partial t} + \frac{\partial (u\tilde{\Omega})}{\partial x} - N^2\frac{\partial s}{\partial x} = 0. \quad (5)$$

The system of equations (3), (5) is, in fact, a system of equations of the contour dynamics, which is written out for the continuous model of a stratified flow. We represent the Hamiltonian (i.e., the energy normalized to the averaged density) in the form

$$H = \int\left(\frac{1}{2}\Psi(x, z, t)\Omega(x, z, t) + \frac{gz\rho}{\rho_0}\right)dx\,dz$$

$$= -\frac{1}{2}\iint \Omega(x, z)\Omega(x', z')G(x - x', z - z')dx\,dz\,dx'dz'$$

$$+ \int\frac{gz\rho}{\rho_0}dx\,dz = -\frac{1}{2}\iint \tilde{\Omega}(x, h)\tilde{\Omega}(x', h')G(x - x', s(x, h)$$

$$- s(x', h'))dx\,dh\,dx'dh' + \int\frac{gs\rho}{\rho_0}\frac{\partial s}{\partial h}dx\,dh.$$

We now calculate the variational derivatives

$$\frac{\delta H}{\delta \tilde{\Omega}(x, h)} = -\int \tilde{\Omega}(x', h')G(x - x', h + \eta$$

$$- h' - \eta')dx'dh' = \Psi(x, h + \eta(x, h)),$$

$$\frac{\delta H}{\delta \eta(x, h)} = -\int \tilde{\Omega}(x', h')\tilde{\Omega}(x, h)$$

$$\times \frac{\partial}{\partial \eta} G(x - x', h + \eta - h' - \eta') dx' dh'$$

$$+ N^2(h)\eta(x, h) = -u(x, h)\tilde{\Omega}(x, h) + N^2(h)\eta(x, h).$$

Clearly, equations of motion (3), (5) can be represented in the Hamiltonian form

$$\frac{\partial \eta(x, h, t)}{\partial t} = \frac{\partial}{\partial x}\left(\frac{\delta H}{\delta \tilde{\Omega}(x, h, t)}\right),$$

$$\partial \tilde{\Omega}(x, h, t)\partial t = \frac{\partial}{\partial x}\left(\frac{\delta H}{\delta \eta(x, h, t)}\right).$$

In order to pass to the canonical form, it is sufficient to replace the variable $\tilde{\Omega} = -\frac{\partial \Phi}{\partial x}$, whereupon the equations written out in terms of the function Φ acquire the standard form

$$\frac{\partial \eta(x, h, t)}{\partial t} = \frac{\delta H}{\delta \Phi(x, h, t)},$$
$$\frac{\partial \Phi(x, h, t)}{\partial t} = -\frac{\delta H}{\delta \eta(x, h, t)}. \quad (6)$$

Here, we may consider the quantities η and Φ as the generalized coordinate and the generalized momentum, respectively.

The equations obtained are convenient for considering the interaction of waves with flows and vortices. If we are interested in the development of disturbances against the background of a given flow, then we should use the expansion of the Green function entering into the expression for the Hamiltonian in terms of a small nonlinearity parameter. In this case, it is convenient to pass to another Hamiltonian structure expressed in terms of variables that describe perturbances.

Following [4], in which similar variables were introduced for the description of the wave motion for in-layer constant-vorticity flows, we determine the variable ϕ according to the formula:

$$\tilde{\Omega}(x, h, t) = \nu(h) + \frac{\partial(\nu\eta)}{\partial h} - \frac{\partial \phi}{\partial x}.$$

Here, $\nu(h)$ is the vorticity of the unperturbed flow. The variable of the type of the η-coordinate remains the same. For in-layer stratified fluid models, the function ϕ corresponds to the difference of hydrodynamic potentials on each side of the interface [11, 4].

The variational derivatives of the Hamiltonian H with respect to η and ϕ are

$$\frac{\delta H}{\delta \phi(x, h, t)} = w(x, h, t) - u(x, h, t)\frac{\partial \eta(x, t, h)}{\partial x}, \quad (7)$$

$$\frac{\delta H}{\delta \eta(x, h, t)} = -u(x, h, t)\left(\frac{\partial \phi(x, h, t)}{\partial x} - \nu_h(h)\eta(x, h, t)\right) + N^2(h)\eta(x, h, t). \quad (8)$$

It follows from Eqs. (7), (8) that the equations of motion (3) and (5) are representable in the following Hamiltonian form:

$$\frac{\partial}{\partial x}\dot{\phi}(x, t, h) = -\frac{\partial}{\partial x}\frac{\delta H}{\delta \eta(x, t, h)} + \nu_h \frac{\delta H}{\delta \phi(x, t, h)}, \quad (9)$$

$$\dot{\eta}(x, t, h) = \frac{\delta H}{\delta \phi(x, t, h)}, \quad (10)$$

where the dot denotes the differentiation with respect to time.

Here, the variables turn out to be noncanonical. However, as a rule, solving particular problems is based on the subsequent representation of the system in terms of normal canonical variables. In these variables, the quadratic term of the expression for the perturbance energy has the simplest form [5, 6].

The linearized equations are derived from the system of equations (9), (10) when we retain the basic quadratic term in the expansion of the Hamiltonian H in powers of the variables ϕ and η. This term has the form

$$H_2 = \frac{1}{2}\int (\phi S[\phi] + 2\nu(h)\eta\phi_x + (N^2 + \nu(h)\nu_h(h))\eta^2) dx\, dh,$$

where

$$S[\phi(x, h)] = \int \tilde{S}(x - x', h - h')\phi(x', h') dx' dh'$$

and

$$\tilde{S}(x - x', h - h') = \frac{1}{4\pi}\int |k| \exp(ik(x - x')) \exp(-|k||h - h'|) dk.$$

The system of equations (9), (10), like system (6), can be employed to describe the perturbance dynamics of both continuously stratified flows and flows with in-layer stratification. Substituting into Eqs. (9), (10) expressions for the Brunt–Väisälä frequency and for the derivative of the unperturbed vorticity with respect to h, which is represented in the form

$$N(h) = \sum_{j=1}^{n} N_j \delta(h - h_j),$$
$$\nu_h(h) = \sum_{j=1}^{n} \Delta\nu_j \delta(h - h_j), \quad (11)$$

we arrive at the equations for perturbances in the in-layer stratified flows, which were found previously in [4].

In order to study flows with more or less arbitrary stratification, we may use the generalizing model (11) describing the Brunt–Väisälä frequency and the deriva-

tive of the vorticity as a sum of functions concentrated near the levels h_j:

$$N(h) = \sum_{j=1}^{n} N_j(h-h_j), \quad \nu_h(h) = \sum_{j=1}^{n} \nu_{hj}(h-h_j). \quad (12)$$

If the parameters of an unperturbed flow are given in the form of (11) or (12), then the Hamiltonian can be represented in the form $H = H_0 + H_{\text{int}}$, where the first term is the sum of Hamiltonians for elementary interacting layers, while the second describes the interlayer interaction. In the case of a proper choice of a partition adequate to a particular problem, we are able to study first the perturbance development in individual layers and, furthermore, to take into account the interlayer interaction.

On the basis of this method, we can study linear waves being developed against the background of a homogeneous (in density) flow. Although the approach being used for solving this problem is equivalent to the method based on the solution to the Rayleigh equation, this approach turns out to be more convenient for analysis and makes it possible to clarify certain points open to questions until now.

We next assume that the derivative ν_h of the mainstream vorticity differs from zero only in the narrow layer with the thickness Δh in the vicinity of the layer h_0 and that this thickness is small compared to the characteristic wavelength in the horizontal direction. We also assume that $\nu_h = \frac{\Delta\nu}{\Delta h}\mu(\xi)$, where $\xi = \frac{h-h_0}{\Delta h}$. Thus $\mu(\xi)$ differs from zero only for $|\xi| < 1$. Let also $\int\mu(\xi)d\xi = 1$. We take the velocity profile in the form $V(h) = V(h_0) + \nu\Delta h V(\xi)$, where $V(\xi) = \xi + a\lambda(\xi)$, $\mu(\xi) = \lambda''(\xi)$. We additionally introduce the parameter $a = \frac{\Delta\nu}{\nu}$. If $\mu(\xi) = \delta(\xi)$, then we are dealing with a flow model that exhibits a vorticity jump. We assume the initial perturbance to be concentrated in this layer as well. Substituting quadratic Hamiltonian H_2 into Eqs. (9), (10) and assuming N to be zero, we arrive at the system of linear equations with respect to ϕ and η. In terms of the Fourier transform over x, the equation for ϕ has the form

$$\frac{\partial\phi}{\partial\tau} + iq\left(V_0 + \epsilon\xi + \frac{\epsilon a\xi^2}{2}\right)\phi = ia\,\mathrm{sgn}\,q\int\exp(-\epsilon|q||\xi-\xi'|)\phi(\xi')d\xi', \quad (13)$$

where $\tau = \nu t$ is the dimensionless time, $q = \frac{k}{k_0}$ is the dimensionless wave number, and $V_0 = k_0\nu V(h_0)$. As is seen, the properties of Eq. (13) are governed by the dimensionless parameters $\epsilon = k_0\Delta h$ and $a = \frac{\Delta\nu}{\nu}$.

Equation (13) is very similar to that describing waves in plasma free of magnetic field. In this case, the quantity ϕ plays the role of an electron distribution function. By virtue of this fact, it is reasonable to apply methods developed in plasma theory. These methods were used by various authors while studying waves in hydrodynamic flows [13]. Nevertheless, in our approach, parallels with plasma theory are especially obvious. We initially assume that the parameter a is on the order of unity and consider the hydrodynamic approach. We search for the solution in the form $\phi = e^{-i\omega\tau}\Phi$. Using the smallness of the parameter ϵ and preserving in Eq. (13) basic terms, we obtain

$$\left(\omega - q\left(V_0 + \epsilon\xi + \frac{\epsilon a\xi^2}{2}\right)\right)\Phi + \frac{a}{2}\int\Phi(\,\mathrm{sgn}\,q - \epsilon q|\xi-\xi'|)d\xi' = 0. \quad (14)$$

We also assume $\mu(\xi) = \frac{1}{2}[\theta(\xi+1) - \theta(\xi-1)]$. Integrating (14) over ξ and introducing the notation $\Omega = \omega - qV_0$, we arrive at

$$\left(\Omega + a\,\mathrm{sgn}\,q - \frac{\epsilon aq}{2}\right)A_0 - \epsilon qA_1 - \frac{3\epsilon aq}{2}A_2 = 0,$$

where

$$A_0 = \int\Phi d\xi, \quad A_1 = \int\xi\Phi d\xi, \quad A_2 = \int\xi^2\Phi d\xi.$$

We obtain two subsequent equations multiplying (14) sequentially by ξ and ξ^2, integrating, and preserving only basic terms in ϵ:

$$\Omega A_1 = 0, \quad \Omega A_2 + \frac{\mathrm{sgn}\,qA_0}{6} = 0.$$

As a result, the dispersion equation acquires the form

$$D(\Omega) = \left[\Omega + \frac{a}{2}(\,\mathrm{sgn}\,q - \epsilon q)\right]\Omega + \frac{\epsilon|q|a^2}{8} = 0.$$

The discrete-mode frequency is determined (to within the terms on the first order of smallness in ϵ) by the expression

$$\Omega = -a\,\mathrm{sgn}\frac{q}{2} + \frac{3\epsilon aq}{4}. \quad (15)$$

For $\epsilon = 0$, we have a case of a vorticity jump. Within the limits of the accuracy used by us, the mode determined by the second root is not reliable. In order to analyze the low-frequency region, we should use a method that, in analogy with plasma theory, may be called the kinetic approach. We now consider the parameter a to be small (on the order of ϵ). Retaining only basic terms in Eq. (14), we have

$$(\Omega - \epsilon q\xi)\Phi + \frac{a}{2}\,\mathrm{sgn}\,q\int\Phi d\xi' = 0,$$

from which it follows

$$\Phi + \frac{a\,\mathrm{sgn}\,q}{2(\Omega - \epsilon q\xi)}\int \Phi d\xi' = 0.$$

Upon integration, we arrive at the dispersion equation in the form

$$D(\Omega) = 1 + \frac{a}{2}\mathrm{sgn}\,q[\ln(\Omega + \epsilon q) - \ln(\Omega - \epsilon q)] = 0.$$

The position of the pole associated with the discrete mode is determined by the expression

$$\Omega = -\epsilon q \coth\left(\frac{\epsilon|q|}{a}\right).$$

As is seen, the pole tends to q or $-q$ as $a \longrightarrow 0$, depending on the sign of a. If $a \gg \epsilon$, we have an expression that coincides with Eq. (15) in the principal order. In addition to the pole, the dispersion equation determines branching points associated with the wave packet that corresponds to the continuous spectrum [14, 15]. At small values of the parameter a, the discrete-mode frequency is very close to this packet and, for finite times, cannot be considered separately from it. In this case, the behavior of the summary wave depends greatly on the sign of the vorticity derivative [7]. Moreover, the discrete-spectrum mode can either transform into a wave packet of the continuous spectrum or become unstable as a result of interaction with another layer. Thus we can conclude that the approximation of the continuously stratified flow by the finite-layer model is possible when parameters characterizing the flow at high vorticity-gradient levels satisfy the condition $\frac{\Delta\nu}{\nu} \sim 1, k_0\Delta h \ll 1$. This condition, in fact, coincides with the condition of applicability of the hydrodynamic approach.

ACKNOWLEDGMENTS

This work was supported by the Russian Foundation for Basic Research, project nos. 01-05-64466 and 01-05-64042, and by the INTAS grant no. 97-575.

REFERENCES

1. V. E. Zakharov, Izv. Vyssh. Uchebn. Zaved., Radiofiz. **17**, 431 (1974).
2. V. P. Goncharov and V. I. Pavlov, *Problems of Hydrodynamics in Hamiltonian Description* (Mosk. Gos. Univ., Moscow, 1993).
3. V. E. Zakharov and E. A. Kuznetsov, Usp. Fiz. Nauk **167**, 1137 (1997) [Phys. Usp. **40**, 1087 (1997)].
4. V. P. Goncharov, Izv. Akad. Nauk SSSR, Fiz. Atmos. Okeana **22**, 468 (1986).
5. N. N. Romanova, Nonlinear Processes in Geophysics **1**, 234 (1994).
6. N. N. Romanova, Nonlinear Processes in Geophysics **5**, 241 (1999).
7. M. Kelbert and I. Sazonov, *Pulses and Other Wave Processes in Fluids: An Asymptotic Approach to Initial Problems* (Kluwer, Boston, 1996).
8. B. B. Kadomtsev, *Collective Phenomena in Plasmas* (Nauka, Moscow, 1988).
9. A. A. Galeev and R. Z. Sagdeev, in *Reviews of Plasma Physics*, Ed. by M. A. Leontovich (Atomizdat, Moscow, 1973; Consultants Bureau, New York, 1979), Vol. 7.
10. M. A. Virasoro, Phys. Rev. Lett. **47**, 1181 (1981).
11. V. E. Zakharov, Prikl. Mekh. Teor. Fiz. **2**, 86 (1966).
12. I. A. Sazonov and I. G. Yakushkin, Izv. Akad. Nauk, Fiz. Atmos. Okeana **35**, 472 (1999).
13. Yu. A. Stepanyants and A. L. Fabrikant, *Wave Propagation in Shear Flows* (Nauka, Moscow, 1996).
14. K. M. Case, Phys. Fluid **3**, 143 (1960).
15. L. A. Dikiĭ, *Hydrodynamic Stability and Atmosphere Dynamics* (Gidrometeoizdat, Leningrad, 1976).

Translated by G. Merzon

Doklady Physics, Vol. 46, No. 10, 2001, pp. 747–750. Translated from Doklady Akademii Nauk, Vol. 380, No. 6, 2001, pp. 761–764.

MECHANICS

Numerical Simulation of a Far Vortex Wake for an Aircraft in the Takeoff and Landing Regimes

Al. S. Belotserkovskiĭ and A. S. Ginevskiĭ

Presented by Academician O.M. Belotserkovskiĭ April 8, 2001

Received May 18, 2001

Studies of tendencies in the development of airplane vortex wakes became rather urgent in recent years. This is associated with the fact that a flying aircraft produces a long-lived and extended (up to 10 to 12 km) vortex wake in the atmosphere, which may constitute a threat for other aircrafts. At the present time, methods of mathematical simulation of airplane vortex wakes that take into account effects of atmospheric parameters, namely, atmosphere stratification, turbulence, side wind, etc. [1–3] are developed.

The problem of the interaction of the airplane vortex wake with the Earth's surface in takeoff and landing regimes acquired great importance due to continuously rising airport loading, which results in reduced time intervals between subsequent operations of airplanes. In this light, studies of the behavior of the airplane vortex system in the vicinity of airport surfaces are not only of scientific but also practical importance.

In theoretical investigations of the interaction of a pair of oppositely rotating vortex bundles with a screen, the two-dimensional unsteady problem is solved in a plane perpendicular to the vortex-bundle direction. The initial vortex system (including the diameter of vortex bundles, the distance between the bundles, their altitude with respect to the screen surface, and the distribution of tangential velocities in the vortex bundle) is either given arbitrarily or is borrowed from experiments. The clearest data are obtained in the course of numerically solving Reynolds equations closed with the help of a certain differential turbulence model. The results of numerically simulating the two-dimensional problem on the interaction of a vortex pair with a screen [4, 5] make it possible to describe basic features of this interaction. We imply the flow separation from the screen, the interaction of the primary and secondary vorticity, and the creation of the loop-shaped trajectory for the motion of primary vortices.

At high Reynolds numbers, the method of discrete vortices combined with the methods of boundary-layer theory can be successfully applied for solving the problem on the interaction of the airplane vortex wake with the Earth's surface. In particular, this is stipulated by the fact that in such a case the flow contains domains of both the concentrated vorticity and the potential flow. Even the first experimental studies of the wing vortex system in a wind tunnel demonstrated that, near the screen, not only the drop of trailing vortices but also an increase in the distance between them occurs (as follows from the theory of an inviscid fluid). In addition, a lift of both vortices (their jump upward) to a certain level appears with a subsequent motion along a loop-shaped trajectory. It was shown that the appearance of this trajectory is caused by the separation of the boundary layer that arises on the screen in the case of a transverse (wingspan) flow induced near the screen surface by the wing vortex system. While separating the boundary layer, secondary vortices coming down into the flow interact with the primary vortices, and as a result of this interaction there arises a loop-shaped trajectory in their motion.

We consider the quasi-three-dimensional schematization of the flow. In other words, we analyze the behavior of the vortex system in a number of cross sections corresponding to different time moments. We list characteristic features of this method used for numerically simulating the airplane vortex system near the Earth.

1. The initial airplane vortex system is determined in the framework of the linear theory of the discrete-vortex method. This method allows us to simulate the wake near the airplane, including the vortex wake of the horizontal tail and the process of the convolution of this wake into two centered vortex bundles for an airplane with a given geometry, given angles of attack for the wing and for the tail, and given the flap inclination angle. In the case of the existence of a weak side wind, the vortex system of the vertical tail should be taken into account, which is calculated in the linear approximation. In these cases, a plate-shaped schematization of the fuselage, wings, and the empennage is used [2]. Here the circulation and shape of the vortex bundles and the velocity distribution inside and outside of them, as well as the position of these bundles along the stream

State Scientific Research Center TsAGI, ul. Radio 17, Moscow, 107005 Russia

1028-3358/01/4610-0747$21.00

at various distances from the Earth's surface, are determined.

2. The wing spanwise flow (induced by the vortex bundles, i.e., by the primary vortices) near the Earth's surface is used below for calculating parameters of the boundary layer and its separation in the cases of both the absence and the existence of a weak side wind. Using the values of the velocity at the outer surface of the boundary layer in the separation cross section $u_{z\delta}$, we can find the circulation of the secondary vortices coming off into the flow:

$$\Gamma = \left(\frac{d\Gamma}{dt}\right)\Delta t = \frac{1}{2}u_{z\delta}^2\Delta t .$$

Allowing for the roughness of the runway surface and a large extension of the boundary-layer development domain that attains several tens of meters, the boundary layer on this runway may be assumed with a high degree of confidence to be completely turbulent.

3. Furthermore, in the framework of the discrete-vortex method, the unsteady problem on the interaction of primary and secondary vortices is solved with their dissipation taken into account. Strictly speaking, the boundary layer in the problem under consideration is unsteady. However, in the framework of the approximations used, we may restrict our analysis by the quasi-steady approximation.

4. In the absence of a side wind, the distribution of the velocity induced by the vortex bundles on the Earth's surface is symmetric with respect to the symmetry plane $z = 0$. In the presence of the side wind, the pattern becomes asymmetric, and the calculation of the boundary layer is performed on either side from the critical point on the Earth's surface. In this case, the wind velocity is assumed to be constant along the vertical coordinate, and its effect is reduced to the windward shift of the vortex system.

5. In order to obey the impenetrability condition on the Earth's surface, fictitious mirror-reflected vortices are added into both the basic vortex system and the system of secondary vortices. With the help of the vortex-bundle circulation determined by the above method, we can find the distribution of the transverse (wingspan) velocities induced by these vortex bundles. This approach makes it possible to calculate parameters of the turbulent boundary layer, the position of its separation point, and the velocity on the outer edge of the boundary layer in the separation cross sections and to find the value of the secondary-vortex circulation at each time instant.

We now consider the approximate method for the determination of the circulation dissipation in the primary and secondary vortices and allow for the effect of the atmospheric turbulence on the circulation of these vortices. For the primary vortices, we have the expression

$$\frac{\Gamma_1(t)}{\Gamma_0} = \left[1 - \exp\left(-\frac{r^2}{4\nu_{t1}t}\right)\right]\exp\left(-c\frac{qt}{b_1}\right). \qquad (1)$$

Here Γ_1 and Γ_0 are current and initial values of the primary-vortex circulation, respectively; t is time; q is the root-mean-square velocity pulsation in the atmosphere; $b_1(t)$ is the distance between the centers of the primary vortices; $r = [(z - z_i)^2 + (y - y_i)^2]^{1/2}$ is the radius-vector modulus for a point with the coordinates z and y with respect to the vortex with coordinates z_i, y_i; ν_{t1} is the coefficient of the turbulent viscosity; and c is the empirical multiplier. The first multiplier in the right-hand side of expression (1) takes into account the circulation dissipation caused by the action of the viscosity of the medium and of the turbulence inside the vortex bundle. The second multiplier in expression (1) allows for the circulation variation with time, which is caused by the effect of the atmospheric turbulence. According to the calculations and to results of processing the experimental data [9], the average value of ν_{t1} for the vortex bundle reaches approximately 0.25 m^2/s. This value is obtained as a result of replacing the kinematic viscosity ν of the medium by the corresponding coefficient of the turbulent viscosity ν_{t1} in the well-known approximate formula for a rectilinear vortex fiber [7].

We assume that an expression with a structure similar to formula (1) can also be presented for secondary vortices in the separation cross section of a turbulent boundary layer. However, one difference exists: this expression involves the value of the characteristic turbulent viscosity in the trailing point of the vorticity center ν_{t2} at a distance $y = \delta_*$ from the Earth's surface (δ_* is the thickness of the boundary layer in its separation cross section):

$$\Gamma_2(t) = \frac{1}{2}(u_{z\delta}^2)_{\text{sep}}K(t)\exp\left(-c\frac{qt}{b_2}\right)\Delta t ,$$

$$K(t) = 1 - \exp\left[-\frac{y^2+(z-z_{\text{sep}})^2}{4\nu_{t2}t}\right]. \qquad (2)$$

Here, $b_2(t)$ is the distance (along the horizontal z-axis) between secondary vortices. The difference between formulas (1) and (2) consists in the fact that the circulation $\Gamma_1(t)$ decreases with time, whereas the circulation $\Gamma_2(t)$ for the boundary layer initially increases (due to the summation over Δt) and then decreases due to dropping $K(t)$.

In order to determine parameters of the turbulent boundary layer and the position of its separation point, we exploit one of the well-known integral one-parametric calculation methods [9].

In accordance with the procedure described, the far vortex wake of a Boeing-727 airplane was calculated

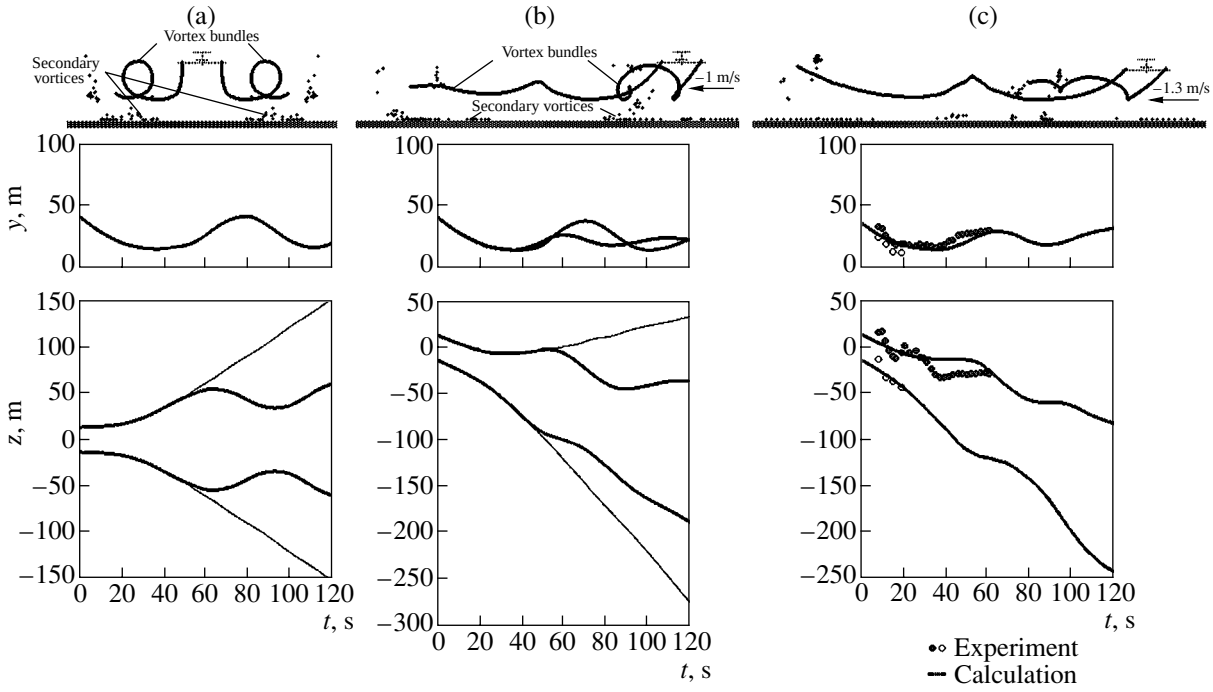

Fig. 1.

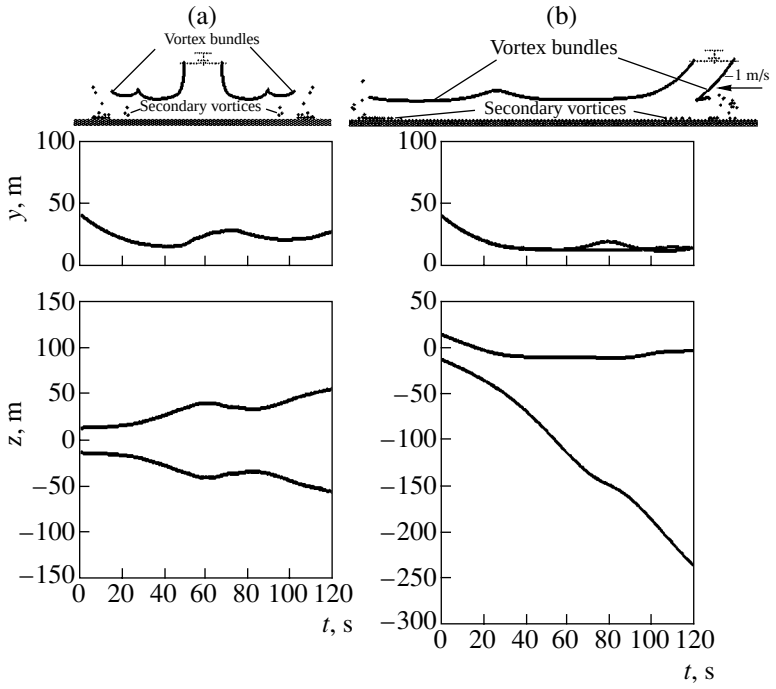

Fig. 2.

for the first time with the Earth's boundary layer taken into consideration. The code operation time was 15 to 20 s, depending on the initial conditions, using an IBM PC with a Pentium III-550 processor. Figure 1a (above) shows the positions of the far vortex wake and of secondary vortices at the instant of time corresponding to the 120th s (the back view) at a flight altitude of 40 m. The flight velocity was V_∞ = 72 m/s, a side wind was absent, the wing angle of attack reached $\alpha = 8.1°$, and the flap inclination angle was 25°. These calculations were performed for the value $\nu_{t1} = 0.25$ m^2/s. The results obtained illustrate the development of the loop-shaped

trajectory for the motion of primary vortices. Analysis of the calculated data corresponding to different flight altitudes shows that allowance for the effect of the boundary layer significantly changes the position of primary vortices, this effect being enhanced with a decrease in the flight altitude. Figure 1a (below) demonstrates the altitude y and the coordinate z of the primary vortices as a function of time. Figure 1b presents the calculated data corresponding to the same flight conditions as in the case of the existence of a side wind with the velocity $u_w = -1$ m/s. Thin lines in Figs. 1a and 1b correspond to the calculation results obtained without regard for the boundary layer on the Earth's surface.

We now compare the data of the calculation and of the flight experiment carried out in 1995 in the Memphis airport (USA) for a Boeing-727 airplane under the following conditions: the flight altitude, flight velocity V_∞, wind velocity u_w, angle of attack α, and flap inclination angle were, respectively, 34.8 m; 72 m/s; –1.3 m/s, 5.6°, and 25° [11]. The satisfactory consistency of the calculated results with the experimental data for the vertical position of the vortex bundles (see Fig. 1c) is notable.

We now present the calculation results for the far vortex wake of the Boeing-727 airplane in the presence and the absence of a side wind. The flight conditions were the same as in Figs. 1a and 1b, except for the elevated degree $\frac{q}{V_0} = 0.75$ of the atmosphere turbulence, where $V_0 = 1.44$ m/s is the dropping rate of the vortex pair at the initial instant $t = 0$. The conventional determination of the turbulence degree yields $\frac{q}{V_\infty} \approx 1.5\%$. Figures 2a and 2b illustrate the relevant dependences. From this it follows that the elevated atmospheric turbulence leads to a decrease in both the height of the vortex's upward jump near the Earth's surface and the transverse distance between the vortex bundles.

ACKNOWLEDGMENTS

This work was performed under the financial support of the Russian Foundation for Basic Research, project no. 99-01-00131.

REFERENCES

1. V. V. Vyshinskiĭ, in *Flight* (Tsentr. Aerogidrodin. Inst., Moscow, 1958), pp. 12–19.
2. T. O. Aubakirov, A. I. Zhelannikov, P. E. Ivanov, and M. I. Nisht, *Wakes and Their Action on an Aircraft. Computer Simulation* (Mariya, Almaty, 1999).
3. T. Sarpkaya, J. Aircr. **37** (1), 53 (2000).
4. A. N. Pakin, Tr. TsAGI, No. 2627, 79 (1997).
5. M. Shur, M. Strelets, A. Travin, and P. K. Spalart, AIAA Pap., No. 595 (1998).
6. G. G. Soudakov, Tr. TsAGI, No. 2641, 95 (1999).
7. S. M. Belotserkovskiĭ and M. I. Nisht, *Detached Flow and Flow without Separation around Thin Wings for Ideal Fluids* (Nauka, Moscow, 1978).
8. G. Greene, J. Aircr. **23**, 566 (1986).
9. N. A. Baranov, Al. S. Belotserkovskiĭ, S. M. Belotserkovskiĭ, and A. S. Ginevskiĭ, Preprint No. 109, TsAGI (Zhukovsky Central Institute of Aerohydrodynamics, Moscow, 1997).
10. K. K. Fedyaevskiĭ, A. S. Ginevskiĭ, and A. V. Kolesnikov, *Calculation of Turbulent Layer of Incompressible Fluid* (Sudostroenie, Leningrad, 1973).
11. S. D. Campbell, T. J. Dasey, R. E. Freehart, *et al.*, in *Technical Notes. Data Guide. Project Report ATC-250* (Lincoln Laboratory, Lexington, 1996).

Translated by G. Merzon

Doklady Physics, Vol. 46, No. 10, 2001, pp. 751–755. Translated from Doklady Akademii Nauk, Vol. 380, No. 6, 2001, pp. 765–769.

MECHANICS

On the Nonlocal Stability of Periodic Motion of a Hamiltonian System at the Third-Order Resonance

A. P. Markeev

Presented by Academician D.M. Klimov May 23, 2001

Received May 24, 2001

1. PROBLEM STATEMENT

We assume that a 2π-periodic motion exists in an autonomous Hamiltonian system with two degrees of freedom and that Hamiltonian function in the vicinity of the trajectory corresponding to this motion is analytic. With a proper choice of the canonically conjugate variables ξ_i and η_i (i =1, 2), the solution corresponding to undisturbed motion can be represented in the form [1] $\xi_1(t) = t + \xi_1(0)$, $\eta_1 = \xi_2 = \eta_2 = 0$, and the Hamiltonian function will also be 2π-periodic in ξ_1.

Two characteristic indices of the linearized equations of disturbed motion are always equal to zero, while two others, $\pm i\lambda$, are assumed to be imaginary. When the value of 3λ is integer, i.e., a third-order resonance takes place, the orbit of the periodic motion is, as a rule, unstable [2]. However, this instability may happen to be only local, because trajectories of disturbed motion can perpetually stay in a certain restricted vicinity of the trajectory of undisturbed motion. In this study, we obtained asymptotic estimates for the size of this vicinity in the case when the equations of motion contain a small parameter.

2. HAMILTONIAN OF DISTURBED MOTION

Let Hamiltonian function depend on the parameter ε and be analytic for sufficiently small values of this parameter, while the value of 3λ differs from an integer n by the value on the order of ε^2. We set

$$n - 3\lambda = \varepsilon^2\alpha$$

and assume that for $\varepsilon = 0$ Hamiltonian function is independent of ξ_1. This assumption is acceptable for many problems of mechanics. It holds, for example, for the circular restricted three-body problem.

We represent the Hamiltonian H of disturbed motion as a series in powers of η_1, ξ_2, η_2, and ε. Thereafter, using the real, analytical with respect to η_1, ξ_2, η_2, and ε, canonical change of variables, $\xi_1, \eta_1, \xi_2, \eta_2 \longrightarrow \varphi_1$, r_1, q_2, p_2 (obtained, for example, by the Deprit–Hori method [2]), we bring H to the form

$$H = r_1 + \frac{1}{2}\lambda(q_2^2 + p_2^2)$$
$$+ \varepsilon[(a\cos n\varphi_1 - b\sin n\varphi_1)q_2(q_2^2 - 3p_2^2)$$
$$+ (a\sin n\varphi_1 + b\cos n\varphi_1)p_2(p_2^2 - 3q_2^2)] + c_{20}r_1^2 \quad (1)$$
$$+ \frac{1}{2}c_{11}r_1(q_2^2 + p_2^2) + \frac{1}{4}c_{02}(q_2^2 + p_2^2)^2 + \sum_{k=1}^{\infty}\varepsilon^k H_4^{(k)} + O_5.$$

Here, $H_4^{(k)}$ is the form of the fourth power with respect to $|r_1|^{1/2}$, q_2, and p_2 and coefficients that are 2π-periodic in φ_1, and O_5 is the sum of terms whose power is no less than 5. The quantities a, b, c_{20}, c_{11}, and c_{02} are the constant coefficients, among which a and b are representable by the convergent series $a = a_1 + \varepsilon a_2 + \ldots$ and $b = b_1 + \varepsilon b_2 + \ldots$. The canonical transformation

$$\varphi_1 = \tilde{\varphi}_1, \quad r_1 = \tilde{r}_1 - \frac{1}{6}n(\tilde{q}_2^2 + \tilde{p}_2^2),$$
$$q_2 = \tilde{q}_2\cos\varphi + \tilde{p}_2\sin\varphi, \quad (2)$$
$$p_2 = -\tilde{q}_2\sin\varphi + \tilde{p}_2\cos\varphi \quad \left(\varphi = \frac{1}{3}n\tilde{\varphi}_1\right)$$

ceases the dependence of third-power terms on the angular variable φ_1, bringing Hamiltonian (1) to the form

$$H = \tilde{r}_1 - \frac{1}{2}\varepsilon^2\alpha(\tilde{q}_2^2 + \tilde{p}_2^2) + \varepsilon[a\tilde{q}_2(\tilde{q}_2^2 - 3\tilde{p}_2^2)$$
$$+ b\tilde{p}_2(\tilde{p}_2^2 - 3\tilde{q}_2^2)] + a_{20}\tilde{r}_1^2 + \frac{1}{2}a_{11}\tilde{r}_1(\tilde{q}_2^2 + \tilde{p}_2^2)$$
$$+ \frac{1}{4}a_{02}(\tilde{q}_2^2 + \tilde{p}_2^2)^2 + \sum_{k=1}^{\infty}\varepsilon^k\tilde{H}_4^{(k)} + O_5,$$

Institute of Problems in Mechanics,
Russian Academy of Sciences,
pr. Vernadskogo 101, Moscow, 117526 Russia

1028-3358/01/4610-0751$21.00

$$a_{20} = c_{20}, \quad a_{11} = c_{11} - \frac{2}{3}nc_{20},$$

$$a_{02} = \frac{1}{9}n^2c_{20} - \frac{1}{3}nc_{11} + c_{02}.$$

Let $a_{02} \neq 0$. By making another canonic transformation

$$\tilde{\varphi}_1 = \sigma w_1, \quad \tilde{r}_1 = \varepsilon^2\kappa^2 a_{02}^{-2} I_1,$$
$$\tilde{q}_2 = \varepsilon\kappa|a_{02}|^{-1}\sqrt{2\rho_2}\sin(\psi + \psi_0),$$
$$p_2 = \varepsilon\kappa|a_{02}|^{-1}\sqrt{2\rho_2}\cos(\psi + \psi_0),$$
$$\kappa = 2\sqrt{2(a_1^2 + b_1^2)}, \quad \psi = \sigma\theta_2 + \frac{1}{6}\pi(1-\sigma), \tag{3}$$
$$\sigma = \operatorname{sgn} a_{02}, \quad a_1 = -\frac{\sqrt{2}}{4}\kappa\sin 3\psi_0,$$
$$b_1 = \frac{\sqrt{2}}{4}\kappa\cos 3\psi_0$$

and going to the new independent variable $\tau = \kappa^2|a_{02}|^{-1}t$, we obtain the Hamiltonian of disturbed motion in the following form:

$$H = H^{(0)}(I_1) + \varepsilon^2 H^{(2)}(I_1, \rho_2, \theta_2) + \varepsilon^3 H^{(3)}(I_1, \rho_2, w_1, \theta_2, \varepsilon),$$
$$H^{(0)} = a_{02}\kappa^{-2} I_1,$$
$$H^{(2)} = -\nu\rho_2 + \rho_2^{3/2}\cos 3\theta_2 + \rho_2^2 + b_{11}I_1\rho_2 + b_{20}I_1^2, \tag{4}$$
$$\nu = \alpha a_{02}\kappa^{-2}, \quad b_{11} = a_{11}a_{02}^{-1}, \quad b_{20} = a_{20}a_{02}^{-1}.$$

The quantity I_1 can have arbitrary sign, while $\rho_2 \geq 0$.

3. TRAJECTORIES OF AN APPROXIMATE SYSTEM

We now consider an approximate system with Hamiltonian function $H^{(0)} + \varepsilon^2 H^{(2)}$. In this system, the quantity I_1 is constant, while the variables θ_2 and ρ_2 are described by the equations

$$\frac{d\theta_2}{d\tau} = \varepsilon^2\frac{\partial\gamma}{\partial\rho_2}, \quad \frac{d\rho_2}{d\tau} = -\varepsilon^2\frac{\partial\gamma}{\partial\theta_2}, \tag{5}$$

in which

$$\gamma = -\tilde{\nu}\rho_2 + \rho_2^{3/2}\cos 3\theta_2 + \rho_2^2. \tag{6}$$

Here, we introduced the notation

$$\tilde{\nu} = \nu - b_{11}I_1. \tag{7}$$

The system of equations (5) has the integral $\gamma = h = \text{const}$. The behavior of its trajectories has been examined in detail (see, e.g., [3] and references therein). Phase portraits of system (5) are shown in Fig. 1. The singular point $x_1 = x_2 = 0$ corresponds to the unperturbed periodic motion. Next, we will be interested solely in the trajectories that envelop all singular points of system (5). From the results obtained in [3] it follows that for such trajectories, a point with coordinates $\tilde{\nu}$ and h must be located in the region D of the plane $\tilde{\nu}, h$, which is defined by the following conditions. When $\tilde{\nu} < -\frac{9}{32}$, then $h > 0$; when $\tilde{\nu} \geq -\frac{9}{32}$, $h > f(\tilde{\nu})$, where

$$f = \frac{27 - 18u + 8u^{3/2} - u^2}{4096}, \quad u = 32\tilde{\nu} + 9. \tag{8}$$

The region D is shown schematically in Fig. 2.

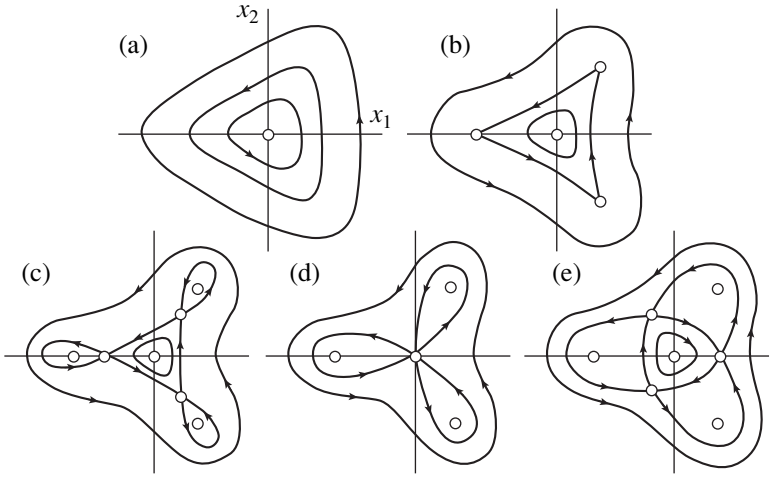

Fig. 1. Phase portraits of system (5) in the plane $x_1 = \sqrt{2\rho_2}\cos\theta_2$, $x_2 = \sqrt{2\rho_2}\sin\theta_2$ for the cases (a) $\tilde{\nu} < -\frac{9}{32}$, (b) $\tilde{\nu} = -\frac{9}{32}$, (c) $-\frac{9}{32} < \tilde{\nu} < 0$, (d) $\tilde{\nu} = 0$, and (e) $\tilde{\nu} > 0$.

On the trajectories being considered, the inequalities $0 < r \le \rho_2 \le R$ are satisfied. The quantities $r(\tilde{\nu}, h)$ and $R(\tilde{\nu}, h)$ are real positive roots of the equations

$$r^2 + r^{3/2} - \tilde{\nu}r - h = 0, \quad R^2 - R^{3/2} - \tilde{\nu}R - h = 0. \quad (9)$$

When $h \ge 0$, we have a single real positive root for each of these equations. However, when $h < 0$, each of the equations has two real roots; in this case r and R are equal, respectively, to the maximum real roots of the first and second equations (9).

If the condition $\rho_2(0) < r$ is satisfied at the initial moment $\tau = 0$, then the inequality $\rho_2(\tau) < R$ is valid for all $\tau \ge 0$.

We will write Hamiltonian (4) for equations of undisturbed motion in new variables I_i and w_i ($i = 1, 2$), which, for the approximate system, are the action–angle variables in the regions filled with trajectories enveloping all singular points of system (5). Since w_1 is a cyclic coordinate in the approximate system, one of these pairs of variables is the pair I_1, w_1. Hamiltonian (4) written out in variables I_i and w_i is denoted by

$$F = F^{(0)}(I_1) + \varepsilon^2 F^{(2)}(I_1, I_2) + \varepsilon^3 F^{(3)}(I_1, I_2, w_1, w_2, \varepsilon). \quad (10)$$

Here $F^{(0)}$ is the function $H^{(0)}$ from (4), $F^{(2)} = b_{20}I_1^2 + \Phi(I_1, I_2)$, and Φ is function (6) represented in new variables. This function is inverse to the function

$$I_2(h) = \oint \rho_2(\theta_2, h)d\theta_2, \quad (11)$$

where $\rho_2(\theta_2, h)$ is the value of the momentum ρ_2 on the considered closed trajectories of the approximate system (the dependence of ρ_2 on I_1 in (11) is not indicated).

Hamiltonian function (10) is 6π-periodic in w_1 and 2π-periodic in w_2, and is analytic for $I_2 > 0$ with respect to its arguments. When $\varepsilon = 0$, function (10) depends only on one of the action variables (on I_1). Therefore, in the problem at hand the case of the degeneracy of this problem is realized [4].

4. ESTIMATES OF THE VALUES OF $r_1(t)$ AND $q_2^2(t) + p_2^2(t)$

We can verify that Hamiltonian (10) satisfies the conditions

$$\frac{\partial F^{(0)}}{\partial I_1} \ne 0, \quad \frac{\partial F^{(2)}}{\partial I_2} \ne 0, \quad \frac{\partial^2 F^{(2)}}{\partial I_2^2} \ne 0. \quad (12)$$

Therefore, according to [4], in the case of disturbed motion the quantities $I_i(\tau)$ ($i = 1, 2$) perpetually stay near their initial values:

$$|I_i(\tau) - I_i(0)| < c\varepsilon, \quad c = \text{const}. \quad (13)$$

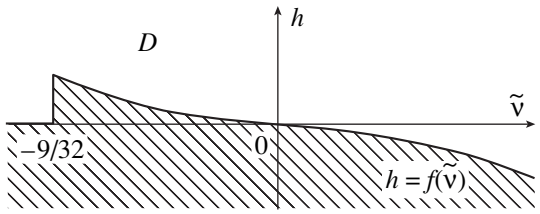

Fig. 2. Region D of the existence of trajectories enveloping all singular points of the system of equations (5). Part of the plane lying outside the region D is hatched.

It follows from (13) and from formulas (2) and (3), which describe a change of variables, that for all $t \ge 0$ the equality

$$r_1 + \frac{1}{6}n(q_2^2 + p_2^2) = \varepsilon^2\kappa^2 a_{02}^{-2}(I_1(0) + O(\varepsilon))$$

is valid. Therefore, the quantity $r_1 + \frac{1}{6}n(q_2^2 + p_2^2)$ may be called an almost integral of the equations of disturbed motion. This implies that for all $t > 0$ this quantity differs from its initial value by at least 3 orders of magnitude with respect to ε if $r_1(0)$ and $q_2^2(0) + p_2^2(0)$ have an order no less than 2.

The presence of this integral makes it possible to reduce the problem of estimation of the size of the region where trajectories of disturbed motion are concentrated to finding the estimate of the quantity $q_2^2(t) + p_2^2(t)$.

First, we consider the case where the coefficient b_{11} in Hamiltonian (4) is equal to zero. From (7), it follows that $\tilde{\nu} = \nu$; i.e., the quantity $\tilde{\nu}$ does not depend on initial conditions and is completely determined by the parameters of the system under consideration. Taking into account the fact that, according to (13), $I_2(t) = I_2(0) + O(\varepsilon)$ for all initial conditions, we obtain, using the results of Sections 2 and 3, the following asymptotic estimates. When

$$q_2^2(0) + p_2^2(0) < 2\varepsilon^2\kappa^2 a_{02}^{-2}[r(\nu, h) - \delta_1], \quad (14)$$

the inequality

$$q_2^2(t) + p_2^2(t) < 2\varepsilon^2\kappa^2 a_{02}^{-2}[R(\nu, h) + \delta_2] \quad (15)$$

is satisfied for all $t \ge 0$. Here r and R are determined by Eqs. (9), and positive values of δ_i are infinitesimal for small ε and tend to zero more slowly than ε. It can be assumed, e.g., that $\delta_1 = \delta_2 = O(\chi)$, where $\chi = \varepsilon^{1-\beta}(0 < \beta < 1)$.

For the given ν, inequalities (14) and (15) define a one-parameter family of estimates. The parameter in this family is the quantity h, which is chosen so that the point (ν, h) falls in the region D (Fig. 2). When $b_{11} \ne 0$,

estimates (14) and (15) remain valid, but the quantity ν must be replaced by the quantity $\tilde{\nu}$ defined by Eq. (7), which depends on initial conditions. Using (13), we can represent this equality in the form

$$\tilde{\nu} = \nu - b_{11}I_1(0) + O(\varepsilon).$$

Taking (2) and (3) into account and introducing the notation

$$r_1(t) = \varepsilon^2\kappa^2 a_{02}^{-2}x(t), \quad q_2^2(t) + p_2^2(t) = \varepsilon^2\kappa^2 a_{02}^{-2}y(t),$$
$$x(0) = x_0, \quad \text{and} \quad y(0) = y_0,$$

we obtain, with an accuracy on the order of ε,

$$\tilde{\nu} = \tilde{\nu}(x_0, y_0) = \nu - b_{11}\left(x_0 + \frac{1}{6}ny_0\right). \qquad (16)$$

The quantity x can have arbitrary sign, and $y \geq 0$.

Let the values of ν, b_{11}, and n appearing in the right-hand side of (16) be known. We fix a certain value of the parameter h exceeding $\frac{27}{4096}$ (with such a choice, a point with coordinates h and $\tilde{\nu}$ lies in the region D of Fig. 2 at any $\tilde{\nu}$), and consider the inequality

$$y_0 < 2r(\tilde{\nu}, h), \qquad (17)$$

in which r is determined by the first equation in (9) and $\tilde{\nu}$ is given by formula (16). In the half-plane $y_0 > 0$, inequality (17) holds in a certain region G. Let $x_0 = x_0^*$, $y_0 = y_0^*$, and the point (x_0^*, y_0^*) lies in the region G together with its χ-vicinity. Then for these initial data (and for sufficiently small ε), trajectories of disturbed motion satisfy the condition that, for all $t \geq 0$, inequality (15) is valid in which ν is the value ν^* of function (16) at the point (x_0^*, y_0^*).

The algorithm described here can be slightly refined if we divide the half-plane $y_0 > 0$ into the regions $\tilde{\nu} < -\frac{9}{32}$ and $\tilde{\nu} > -\frac{9}{32}$ and take into account that in this case $h > 0$ for the first region and $h > f(\tilde{\nu})$ for the second, where the function $f(\tilde{\nu})$ is determined by equality (8).

5. EXAMPLE

As an example, we consider the problem of boundedness of asteroid trajectories in the Cassini gap of Minerva. The ratio of the mean motion of asteroids in this gap to Jupiter's mean motion is close to the rational number 5 : 2; i.e., it corresponds to the third-order resonance [5]. We model the orbits of asteroids using the Poincaré first-order periodic solutions for the restricted three-body problem.

Units of measure are chosen in such a manner that Jupiter's revolution period, the distance between the Sun and Jupiter, and the sum of their masses are equal to unity. Jupiter's mass is denoted by ε. For $\varepsilon = 0$, the Poincaré orbits become circular orbits with a radius ρ; the value $\rho = \rho_0 = \sqrt[3]{\frac{4}{25}} = 0.54288$ corresponds to the above 5 : 2 commensurability.

The quantity λ is calculated by the formula

$$\lambda = \omega(\rho) + \varepsilon\lambda_1(\rho) + O(\varepsilon^2),$$

where $\omega = (1 - \rho^{3/2})^{-1}$; the expression for λ_1 is given in [6]. Assuming that

$$\rho = \rho_0 - \varepsilon\lambda_1(\rho_0)\left(\frac{d\omega(\rho_0)}{d\rho_0}\right)^{-1},$$

we obtain $\lambda = \frac{5}{3} + O(\varepsilon^2)$.

The calculations show that in Hamiltonian (1),

$$a_1 = -1.21567, \quad b_1 = 0,$$
$$c_{20} = \frac{1}{2}c_{11} = c_{02} = -3.39302.$$

According to formulas of Section 2, we find

$$a_{20} = -\frac{3}{4}a_{11} = \frac{9}{4}a_{02} = -3.39302,$$
$$\kappa = 3.43842, \quad b_{11} = -3$$

and expression (16) takes the form

$$\tilde{\nu} = \tilde{\nu}(x_0, y_0) = \nu + 3x_0 + \frac{5}{2}y_0. \qquad (18)$$

The region G is specified by the inequalities

$$y_0 > 0, \quad x_0 > -\frac{2h}{3y_0} + \frac{\sqrt{2y_0}}{6} - \frac{2y_0}{3} - \frac{\nu}{3}.$$

Let the initial disturbances of the quantities r_1, q_2, and p_2 be chosen so that the point (x_0^*, y_0^*) with

$$x_0^* = 0.192349\varepsilon^{-2}r_1(0),$$
$$\text{and} \quad y_0^* = 0.192349\varepsilon^{-2}(q_2^2(0) + p_2^2(0)), \qquad (19)$$

lies in the interior of the region G at a distance no smaller than χ from its boundary. Then for all $t \geq 0$ we obtain the estimate

$$q_2^2(t) + p_2^2(t) < 10.39779\varepsilon^2[R(\nu^*, h) + \delta_2],$$

where ν^* is the quantity defined by formula (18) and calculated at the point with coordinates (19).

ACKNOWLEDGMENTS

This study was supported in part by the Ministry of Education of the Russian Federation, project no. E 00-11.0-28.

REFERENCES

1. G. D. Birkhoff, *Dynamical Systems* (American Mathematical Society, New York, 1927; Gostekhizdat, Moscow, 1941).
2. A. P. Markeev, *Libration Points in Celestial Mechanics and Cosmodynamics* (Nauka, Moscow, 1978).
3. O. V. Kholostova, Prikl. Mat. Mekh. **61** (4), 556 (1997).
4. V. I. Arnol'd, V. V. Kozlov, and A. I. Neĭshtadt, *Mathematical Aspects of Classical Celestial Mechanics. Itogi Nauki Tekh., Ser. Sovrem. Probl. Mat. Fundam. Napravl.* **3** (VINITI, Moscow, 1985).
5. V. G. Demin and S. G. Zhuravlev, Itogi Nauki Tekh., Ser. Astron. **15**, 3 (1979).
6. A. P. Markeev, Dokl. Akad. Nauk **377**, 335 (2001) [Dokl. Phys. **46**, 210 (2001)].

Translated by A. Kozlenkov

Doklady Physics, Vol. 46, No. 10, 2001, pp. 756–759. Translated from Doklady Akademii Nauk, Vol. 380, No. 6, 2001, pp. 770–773.

MECHANICS

Saint-Venant Problems for a Bar with a Screw Anisotropy

Yu. A. Ustinov

Presented by Academician V.V. Vorovich May 7, 2001

Received May 30, 2001

In [1], Saint-Venant problems for anisotonic bars with rectilinear and cylindrical anisotropy were thoroughly studied on the basis of a semi-inverse method. In the present paper, the results of an analysis of Saint-Venant problems for a bar with a screw anisotropy are given. These results are based on the method of homogeneous solutions and spectral operator theory [2, 3]. In particular, we can imagine a material with the screw anisotropy obtained as a result of a helical winding of thin fiber layers made of a stiff material with their simultaneous covering with a polymeric material. Thus we deal with a fibrous composite having screw anisotropy with respect to the cylinder axis. Homogenization methods [4, 5] lead to transversely isotropic materials with their symmetry axis aligned along the tangents to the screw spirals. Bars with the screw anisotropy, and also naturally twisted ones, can be used as transformers of longitudinal strains into longitudinal-torsional strains and, vice versa, as transformers of longitudinal vibrations into flexure-torsion vibrations. At present, there exist examples of devices based on these phenomena that are used in engineering practice.

BASIC RELATIONSHIPS

We consider a cylindrical body occupying the volume $V = S \times [0, l]$, where S and l are the cylinder cross section and length, respectively. We denote the side surface of the cylinder as $\Gamma = \partial S \times [0, l]$, where ∂S is the boundary of S. We associate the origin of the Cartesian coordinate system $x_1, x_2, x_3 = z$ with the center of gravity of one of the cylinder end walls. In order to describe mechanical properties of the body, we introduce a concomitant cylindrical coordinate system r, θ, z, which is linked with the basic coordinate system by the relations

$$\begin{aligned} x_1 &= r\cos\theta\cos\tau z - r\sin\theta\sin\tau z, \\ x_2 &= r\cos\alpha\sin\tau z + r\sin\theta\cos\tau z. \end{aligned} \tag{1}$$

Here, $\tau = \dfrac{2\pi}{h}$ is the relative twisting angle (twist) of the screw spiral, and h is its step. Furthermore, these quantities are considered to be constant at all points of the cylinder.

For r = const, θ = const, relationships (1) are parametric equations of a screw line. The radius vector for points of the screw line can be represented in the form

$$\mathbf{R} = r\mathbf{e}_1' + z\mathbf{e}_3'.$$

Here, $\mathbf{e}_1' = \mathbf{e}_r$, $\mathbf{e}_2 = \mathbf{e}_\theta'$, $\mathbf{e}_3' = \mathbf{e}_z$ are unit vectors of the concomitant coordinate system. We associate with points of a screw line a natural frame $\mathbf{e}_1 = \mathbf{n}$, $\mathbf{e}_2 = \mathbf{b}$, $\mathbf{e}_3 = \mathbf{t}$, where $\mathbf{n}$, $\mathbf{b}$, and $\mathbf{t}$ are the unit vectors of the principal normal, of the binormal, and of the tangent, respectively. The orthogonal matrix for the transition from the $\mathbf{e}_j$ basis to the $\mathbf{e}_i'$ basis has the form

$$A = \begin{bmatrix} -1 & 0 & 0 \\ 0 & -1/g & x/g \\ 0 & x/g & 1/g \end{bmatrix}, \quad g^2 = 1 + x^2, \quad x = \tau r.$$

We consider the material of the cylinder to be locally transversely isotropic, with the symmetry axis of mechanical properties directed along the tangent to the screw line. We determine the properties in the $\mathbf{e}_j$ basis by five elasticity moduli c_{11}, c_{12}, c_{13}, c_{33}, and c_{44} [1]. As a result of the passage from the $\mathbf{e}_j$ basis to the $\mathbf{e}_i'$ basis, we arrive at the following relations for the generalized Hooke's law:

$$\begin{aligned} \sigma_{rr} &= c_{11}e_{rr} + c_{12}e_{\theta\theta} + c_{13}e_{zz} + 2c_{15}e_{\theta z}, \\ \sigma_{\theta\theta} &= c_{12}e_{rr} + c_{22}e_{\theta\theta} + c_{23}e_{zz} + 2c_{25}e_{\theta z}, \\ \sigma_{zz} &= c_{13}e_{rr} + c_{23}e_{\theta\theta} + c_{33}e_{zz} + 2c_{35}e_{\theta z}, \\ \sigma_{\theta z} &= 2c_{44}e_{\theta z}, \quad \sigma_{rz} = 2(c_{55}e_{rz} + c_{56}e_{r\theta}), \\ \sigma_{r\theta} &= 2(c_{56}e_{rz} + c_{66}e_{r\theta}); \end{aligned} \tag{2}$$

$$c_{11}' = c_{11}, \quad c_{12}' = (c_{12} + c_{13}x^2]/g^2,$$

$$c_{13}' = (c_{13} + c_{12}x^2]/g^2, \quad c_{14}' = x(c_{13} - c_{12})/g^2,$$

Rostov State University,
ul. Fridrikha Engel'sa 105, Rostov-on-Don, 344711 Russia

1028-3358/01/4610-0756$21.00

$$c'_{22} = [c_{11} + (2c_{13} + 4c_{44})x^2 + c_{33}x^4]/g^4,$$
$$c'_{23} = [c_{13} + (c_{11} + c_{33} - 4c_{44})x^2 + c'_{13}x^4]/g^4,$$
$$c'_{24} = [(c_{13} + 2c_{44} - c_{11})x + (c_{33} - c_{13} - 2c_{44})x^3]/g^4,$$
$$c'_{33} = [c_{33} + 2(c_{13} + 2c_{44})x^2 + c_{11}x^4]/g^4, \quad (3)$$
$$c'_{34} = [(c_{33} - c_{13} - 2c_{44})x + (c_{44} + 2c_{13} - 2c_{11})x^3]/g^4,$$
$$c'_{44} = [c_{44} + (-2c_{13} + c_{11} + c_{33} - 2c_{44})x^2 + c_{44}x^4]/g^4,$$
$$c'_{55} = [c_{44} + 2(c_{11} - c_{12})x^2]/g^2,$$
$$c'_{56} = x[c_{44} - 2(c_{11} - c_{12})]/g^2,$$
$$c'_{66} = [2(c_{11} - c_{12}) + c_{44}x^2]/g^2.$$

The components of the strain tensor ε and the equations of equilibrium in the basis of the concomitant coordinate system can be obtained with the help of the relations

$$2\varepsilon = \nabla \otimes \mathbf{u} + (\nabla \otimes \mathbf{u})', \quad (4)$$
$$\nabla \cdot \sigma = 0, \quad \nabla = \mathbf{e}_r\partial_r + \mathbf{e}_\theta r^{-1}\partial_\theta + \mathbf{e}_z(\partial_z - \tau\partial_\theta). \quad (5)$$

Here, $\mathbf{u} = \{u_r, u_\theta, u_z\}$ is the displacement vector; σ is the stress tensor; and ∂_r, ∂_z, and ∂_θ are derivatives with respect to the corresponding variables.

ELEMENTARY SOLUTIONS AND THE GENERAL REPRESENTATION OF THE SOLUTION

We assume that the side surface Γ is free of stresses:

$$n_r\sigma_{rr} + n_\theta\sigma_{r\theta} = 0, \quad n_r\sigma_{r\theta} + n_\theta\sigma_{\theta\theta} = 0, \quad n_r\sigma_{rz} + n_\theta\sigma_{\theta z} = 0, \quad (6)$$

where n_r and n_θ are the projections of the vector corresponding to the unit normal to the surface Γ.

Using relationships (2)–(5), we can represent the equilibrium equations with respect to the displacement vector and boundary conditions (6) in the form

$$L(\partial_z)\mathbf{u} \equiv \partial_z^2 C\mathbf{u} + \partial_z B\mathbf{u} + A\mathbf{u} = 0,$$
$$N(\partial_z)\mathbf{u}|_\Gamma \equiv (\partial_z G + E)\mathbf{u} = 0. \quad (7)$$

Here A, B, C, E, and G are the 3×3 matrix differential operators expressed in terms of the variables r and θ with the coefficients depending only on r.

While searching for the solution to problem (7) in the form $\mathbf{u} = e^{\lambda z}\mathbf{a}(r, \theta)$, this property of the matrix coefficients makes it possible to reduce the solution to the spectral problem on the cross section

$$Z(\lambda)\mathbf{a} = \{L(\lambda)\mathbf{a}, N(\lambda)\mathbf{a}\} = 0. \quad (8)$$

Three following statements are valid.

Statement 1. The spectrum of problem (8) $\Lambda = \Lambda_0 \cup \Lambda_1$, where Λ_0 consists of four-fold eigenvalues, namely, $\lambda_0 = 0$, $\lambda_1 = i\tau$, and $\lambda_{-1} = -i\tau$; Λ_1 is the countable symmetric set of eigenvalues λ_k for which $\mathrm{Re}(\lambda_k) \neq 0$.

Statement 2. Eigenvalues from Λ_0 corresponds to 12 elementary solutions to problem (7):

$$\mathbf{u}_1 = \mathbf{a}_1, \quad \mathbf{u}_2 = \mathbf{a}_2, \quad \mathbf{u}_3 = e^{i\tau z}\mathbf{a}_3, \quad \mathbf{u}_4 = \mathbf{u}_3^*,$$
$$\mathbf{u}_5 = e^{i\tau z}(z\mathbf{a}_3 + \mathbf{a}_5), \quad \mathbf{u}_6 = \mathbf{u}_5^*,$$
$$\mathbf{u}_7 = z\mathbf{a}_1 + \mathbf{a}_7, \quad \mathbf{u}_8 = z\mathbf{a}_2 + \mathbf{a}_8, \quad (9)$$
$$\mathbf{u}_9 = e^{i\tau z}\left(\frac{z^2\mathbf{a}_3}{2} + z\mathbf{a}_5 + \mathbf{a}_9\right), \quad \mathbf{u}_{10} = \mathbf{u}_9^*,$$
$$\mathbf{u}_{11} = e^{i\tau z}\left(\frac{z^3\mathbf{a}_3}{6} + \frac{z^2\mathbf{a}_5}{2} + z\mathbf{a}_9 + \mathbf{a}_{11}\right), \quad \mathbf{u}_{12} = \mathbf{u}_{11}^*.$$

Here, the superscript * corresponds to the complex conjugate quantity;

$$\mathbf{a}_1 = \mathbf{e}_r, \quad \mathbf{a}_2 = r\mathbf{e}_\theta, \quad \mathbf{a}_3 = e^{i\theta}(\mathbf{e}_r + i\mathbf{e}_\theta), \quad \mathbf{a}_5 = -\frac{rze^{i\theta}\mathbf{e}_z}{R};$$

the vector functions $\mathbf{a}_7$, $\mathbf{a}_8$, $\mathbf{a}_9$, and $\mathbf{a}_{11}$ are the solutions to the following two-dimensional problems on the cylinder cross section:

$$A\mathbf{a}_{j+6} = \mathbf{F}_j, \quad E\mathbf{a}_{j+6} = \mathbf{f}_j, \quad j = 1, 2, \quad (10)$$

$$\mathbf{F}_1 = \left\{-\partial_r c'_{13} - \frac{c'_{13} + c'_{23}}{r}, 0, 0\right\},$$
$$\mathbf{f}_1 = \{-n_r c'_{13}, -n_\theta c'_{23}, 0\}, \quad (11)$$
$$\mathbf{F}_2 = \{-c'_{44}\tau r, 0, 0\}, \quad \mathbf{f}_2 = \{0, 0, -n_\theta c'_{44}\tau r\},$$
$$L(i\tau)\mathbf{a}_{j+6} = \mathbf{F}_j, \quad E\mathbf{a}_{j+6} = \mathbf{f}_j, \quad j = 3, 5,$$
$$\mathbf{F}_3 = -(2i\tau C + B)\mathbf{a}_5 - C\mathbf{a}_3, \quad \mathbf{f}_3 = -G\mathbf{a}_5,$$
$$\mathbf{F}_5 = -(2i\tau C + B)\mathbf{a}_9 - C\mathbf{a}_5, \quad \mathbf{f}_5 = -G\mathbf{a}_9;$$

and R is a certain characteristic linear scale.

The next statement follows from the theorem on the completeness of the system of elementary solutions [2].

Statement 3. Any solution to problem (7) can be represented in the form

$$\mathbf{u} = \mathbf{u}_s + \mathbf{u}_p,$$
$$\mathbf{u}_s = \sum_{m=1}^{6} X_m\mathbf{u}_m + \sum_{m=1}^{6} C_m\mathbf{u}_{m+6}, \quad \mathbf{u}_p = \sum_k C_k\mathbf{u}_k. \quad (12)$$

Here, X_m, C_m, and C_k are arbitrary constants; the summation in the expression for $\mathbf{u}_s$ is performed over elementary solutions (9); finally, in the expression for $\mathbf{u}_p$, the summation is performed over all elementary solutions corresponding to eigenvalues from Λ_1. The first sum in the expression for $\mathbf{u}_s$ describes an arbitrary displacement of the cylinder as a solid body; the second sum describes the stress-strain state with the nonzero principal vector and the nonzero principal moment in

the cross section z = const. The stress state corresponding to $\mathbf{u}_p$ is self-balanced and localized near the cylinder end walls.

It is natural to call the vector functions $\mathbf{u}_s$ and $\mathbf{u}_p$ the Saint-Venant solution and the boundary layer, respectively. For the latter, the attenuation rate is described in the general case by the expression $\exp(-\alpha y)$, where y is the distance to the nearest cylinder end wall and $\alpha = \inf(\mathrm{Re}\lambda_k)$. (The value of the parameter α depends on mechanical properties and on cross-section geometry of the bar.)

The determination of X_m, C_m, and C_k can be reduced to the solution of infinite systems of equations, which are obtained when the boundary conditions on the cylinder end walls are satisfied with the help of the relationships for the generalized orthogonality [2, 6]. In this case, the constants C_m are determined exactly on the basis of an algebraic system whose matrix coincides in its structure with that obtained in [3].

SAINT-VENANT SOLUTION FOR A CIRCULAR CYLINDER

For a circular cylinder ($r_1 \le r \le r_2 = R$), $n_r = 1$ and $n_\theta = 0$. Thus, the construction of the Saint-Venant elementary solutions $\mathbf{u}_{m+6}$ is reduced to the integration of boundary value problems for ordinary differential equations. Here, we restrict our consideration by the results obtained in solving the Saint-Venant problem on the tension–torsion of a cylinder. In this case, analysis of solution (10) yields the following expressions for displacements and stresses:

$$u_r = C_1 a_{r1} + C_2 a_{r2}, \quad u_\theta = \frac{X_2 r}{R} + \frac{C_2 z r}{R}, \quad u_z = X_1 + C_1 z,$$

$$\sigma_{rr} = C_1[c'_{11}\partial_r a_{r1} + r^{-1}c'_{12}a_{r1} + c'_{13}] + C_2\left[c'_{11}\partial_r a_{r2} + r^{-1}c'_{12}a_{r2} + \frac{c'_{14}r}{R}\right],$$

$$\sigma_{\theta\theta} = C_1[c'_{12}\partial_r a_{r1} + r^{-1}c'_{22}a_{r1} + c'_{23}] + C_2\left[c'_{12}\partial_r a_{r2} + r^{-1}c'_{22}a_{r2} + \frac{c'_{24}r}{R}\right], \qquad (13)$$

$$\sigma_{zz} = C_1[c'_{13}\partial_r a_{r1} + r^{-1}c'_{23}a_{r1} + c'_{33}] + C_2\left[c'_{13}\partial_r a_{r2} + r^{-1}c'_{23}a_{r2} + \frac{c'_{34}r}{R}\right],$$

$$\sigma_{z\theta} = C_1[c'_{14}\partial_r a_{r1} + r^{-}c'_{24}a_{r1} + c'_{34}] + C_2\left[c'_{14}\partial_r a_{r2} + r^{-1}c'_{24}a_{r2} + \frac{c'_{44}r}{R}\right].$$

Here, $a_{rj} = a_{rj}(r)$ are the solutions to the following boundary value problems:

$$\partial_r[c'_{11}\partial_r a_{rj} + r^{-1}c'_{12}a_{rj}] + r^{-1}(c'_{11} - c'_{12})\partial_r a_{rj} + r^{-2}(c'_{12} - c'_{22})a_{rj} = F_{rj},$$

$$(c'_{11}\partial_r a_{rj} + r^{-1}c'_{12}a_{rj})(r_\alpha) = f_{r\alpha j}, \qquad (14)$$

$$F_{r1} = -\partial_r c'_{13} - r^{-1}(c'_{13} - c'_{23}), \quad f_{r\alpha 1} = -c'_{13}(r_\alpha),$$

$$F_{r2} = \frac{(-c'_{14} + c'_{24})r}{R}, \quad f_{r\alpha 2} = 0.$$

The constants C_1 and C_2 are determined in terms of the principal vector and of the principal stress moment $\sigma_{z\theta}$, σ_{zz} by the relations

$$d_{11}C_1 + d_{12}C_2 = Q_z, \quad d_{21}C_1 + d_{22}C_2 = \frac{M_z}{R}. \qquad (15)$$

The exact values for the coefficients d_{11}, d_{12}, d_{21}, and d_{22} of the stiffness matrix are expressed by the quadratures

$$d_{11} = 2\pi\int_{r_1}^{R}(c'_{33} + c'_{13}\partial_r a_{r1} + r^{-1}c'_{23}a_{r1})r\,dr,$$

$$d_{12} = 2\pi R^{-1}\int_{r_1}^{R}(c'_{14}\partial_r a_{r1} + r^{-1}c'_{24}a_{r1})r^2\,dr,$$

$$d_{21} = 2\pi\int_{r_1}^{R}(c'_{13}\partial_r a_{r2} + r^{-1}c'_{23}a_{r2})r\,dr,$$

$$d_{22} = 2\pi\int_{r_1}^{R}(c'_{44}r/R + c_{14}\partial_r a_{r2} + r^{-1}c_{14}a_{r2})r^2\,dr.$$

Relationships (15) make it possible to present the following interpretation of the quantities appearing in them: d_{11} is the bar stiffness for tension–compression; d_{22} is the stiffness for torsion; $d_{12} = d_{21}$ (this equality follows from the Betti theorem) is the correlation coefficient for the tension–compression and torsion; C_1 is the bar longitudinal strain; and C_2 is the relative twisting angle normalized to R.

Assuming that the cylinder is rigidly fixed at $z = 0$, we can determine the exact values of the constants X_1 and X_2 only by solving infinite systems of equations, which were mentioned above. For sufficiently long cylinders, these constants may be put equal to zero [with the asymptotic error $O\left(\frac{R}{l}\right)$].

ASYMPTOTIC SOLUTIONS FOR SMALL AND LARGE τ

The construction of the solutions to problems (14) at arbitrary values of the dimensionless parameter $\tau_0 = \tau R$ can be realized by numerical methods. However, the asymptotic behavior of the solutions to these problems at small and large τ_0 is of certain importance. The possibility to reconstruct this behavior follows from the analysis of expression (3).

In the case $\tau_0 < 1$, the straightforward simplifications of expressions (3) and subsequent integration of problems (14) lead, in the first approximation, to the following results:

$$a_{r1} = -\nu' r,$$

$$a_{r2} = \frac{\tau_0}{8c_{11}}\left\{\frac{A_0 r^3}{R^2} + A\left[\frac{(1+\rho^2)r}{c_{11}+c_{12}} + \frac{\rho^2 R^2}{r(c_{11}-c_{12})}\right]\right\},$$

$$d_{11} = SE', \quad d_{12} = \frac{\tau_0 J_p}{R^2}[E' - 2(1+\nu')G'], \quad d_{22} = \frac{c_{44}J_p}{R^2},$$

$$S = \pi(1-\rho^2)R^2, \quad J_p = \frac{\pi}{2}(1-\rho^4)R^4, \quad \rho = \frac{r_1}{R},$$

$$\nu' = \frac{c_{13}}{c_{11}+c_{12}}, \quad E' = c_{33} - 2\nu' c_{13}, \quad G' = c_{44},$$

$$A_0 = 3c_{12} - 2c_{13} - c_{11} + 2c_{44},$$

$$A_1 = -3c_{12}^2 + 3c_{11}^2 - 2c_{13}(c_{11}-c_{12}) - 2c_{44}(2c_{12}+6c_{11}).$$

These formulas are valid for both solid and hollow cylinders. The symbols E' and ν' correspond to the Young's modulus and Poisson's ratio that determine the longitudinal and transverse strains of a trustropic material in the case of tension–compression along the symmetry axis [1]. The formula for d_{12} provides an idea of the interaction of torsion and tension–compression as a function of the anisotropy degree for small values of τ_0. It should be noted, therewith, that $2(1+\nu')G' = E'$ only in the case of an isotropic material.

The formulas given below for large values of τ_0 are valid only for hollow cylinders under the condition $\rho\tau_0 > 1$. In this case, we have in the first approximation:

$$a_1 = -Rc_{13}$$

$$a_2 = -\tau_0^{-1} R(c_{13}-c_{12})\left[B(p)\left(\frac{r}{R}\right)^p + B(-p)\left(\frac{r}{R}\right)^{-p}\right],$$

$$d_{11} = c_{11}S + 2\pi R^2[B_{11}(p) + B_{11}(-p)], \quad d_{22} = c_{44}J_p,$$

$$d_{12} = \tau_0^{-1}(2c_{44} + c_{13} - c_{11})S + \tau_0^{-1} 2\pi R^2[B_{12}(p) + B_{12}(-p)],$$

$$B_{11}(p) = -c_{13}(pc_{12} + c_{13})(1-\rho^{p+1})\frac{B(p)}{p+1},$$

$$B_{12}(p) = -c_{13}(pc_{13} - pc_{12} + c_{33} - c_{13} - 2c_{44}) \times (1-\rho^{p+1})\frac{B(p)}{p+1},$$

$$B(p) = \frac{1-\rho^{p+1}}{(pc_{11}+c_{12})(1-\rho^{2p})}, \quad p = \left(\frac{c_{33}}{c_{11}}\right)^{1/2}.$$

We now may conclude that, on the basis of the method proposed, the Saint-Venant solutions can be constructed for an inhomogeneous (along the radius) cylinder, as well as for the case of $\tau = \tau(r)$. The case $\tau(r) = kr^{-1}$ leads to differential equations with constant coefficients and corresponds to the condition of a constant angle between the unit vectors $\mathbf{t}$ and $\mathbf{e}_z$.

ACKNOWLEDGMENT

This work was supported in part by the Russian Foundation for Basic Research, project no. 01-01-00454.

REFERENCES

1. S. G. Lekhnitskiĭ, *Theory of Elasticity for an Anisotropic Body* (Nauka, Moscow, 1977).
2. I. P. Getman and Yu. A. Ustinov, *Mathematical Theory of Solid Irregular Waveguides* (Rostov. Gos. Univ., Rostov-on-Don, 1993).
3. A. N. Druz', N. A. Polyakov, and Yu. A. Ustinov, Prikl. Mat. Mekh. **60** (4), 660 (1996).
4. R. M. Christensen, *Mechanics of Composite Materials* (Wiley, New York, 1979; Mir, Moscow, 1982).
5. B. E. Pobedrya, *Mechanics of Composite Materials* (Mosk. Gos. Univ., Moscow, 1984).

Translated by G. Merzon

Doklady Physics, Vol. 46, No. 10, 2001, pp. 760–764. Translated from Doklady Akademii Nauk, Vol. 380, No. 6, 2001, pp. 774–778.

MECHANICS

On the Theory of Solitary Waves in the Flowing-Down Layer of Viscous Fluid

V. Ya. Shkadov and G. M. Sisoev

Presented by Academician G.G. Chernyĭ April 25, 2001

Received May 3, 2001

The maximum possible finite spacing between principal humps in a sequence of solitary waves is shown to exist in a flowing-down layer. For small values of the wave number $s < s_*$, the spacing between the humps reduces spontaneously due to the hydrodynamic instability. Bifurcations of a new type, $s \longrightarrow 2s$, $s \longrightarrow 3s$, are found, and a critical value s_* is estimated.

1. Solitary waves in a thin viscous-fluid layer flowing down along a vertical surface were first experimentally studied by P.L. Kapitsa and S.P. Kapitsa [1]. If perturbing pulses in the initial cross section are fairly rare, a set of identical two-dimensional waves is formed in the initial cross section down stream, with the layer thickness being constant on a significant interval between their humps. In essence, a periodic sequence of solitary waves is formed. Their velocity exceeds the velocity of propagation of linear perturbations and varies depending on the spacing between the humps. Increasing the frequency of perturbing pulses, it is possible to attain a stable wave mode, in which the humps are close to each other and an intermediate type of wave flow is realized. In the subsequent experiments [2], it was found that the inverse process of increasing the spacings between the humps by decreasing the frequency of perturbing pulses is of limited nature. Indeed, for a given fluid flow rate, there exists a boundary frequency such that the mean spacing between the humps in the wave mode, which is being developed downstream, does not increase with a subsequent decrease in frequency.

As a result of the interaction between the principal humps and the newly arising intermediate humps, either their coalescence or decomposition takes place. Curve *1* in Fig. 1 specifies the experimental limit for the existence of waves with the largest wavelength L [2]. In this study, we give the theoretical interpretation of the experiments on the formation of a chain of solitary waves.

Moscow State University,
Vorob'evy gory, Moscow, 119899 Russia

2. The investigation is carried out on the basis of numerical solutions to the set of equations [3] for the thickness $h(x, t)$ of a layer and the fluid flow rate $q(x, t)$:

$$h_t + q_x = 0,$$

$$q_t + \frac{6}{5}\left(\frac{q^2}{h}\right) = \frac{1}{5\delta}\left(hh_{xxx} + h - \frac{q}{h^2}\right), \qquad (1)$$

$$\delta = \frac{(3\mathrm{Re})^{11/9}}{45\gamma^{1/3}}, \quad \mathrm{Re} = \frac{gH_c^3}{3\nu^2}, \quad \gamma = \frac{\sigma}{\rho(\nu^4 q)^{1/3}}.$$

Here, H_c is the characteristic thickness of the layer; ρ is the fluid density; ν and σ are the coefficient of viscosity

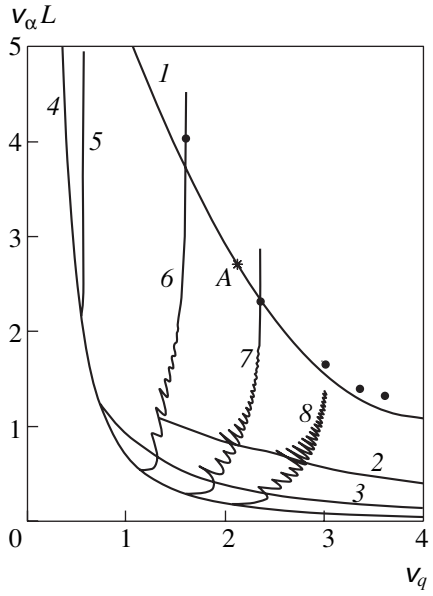

Fig. 1. Curves *1–4* are the boundaries of wave modes in the experiments [2]. The parameters used are $\nu_q = (45\delta)^{9/11}\frac{q_0}{3}$ and $\nu_\alpha = (30\pi\delta q_0^{4/3})^{-1}$. Curves *5–8* show the dominating waves for $\delta = 0.04$, 0.1, 0.15, and 0.2, respectively. The dots correspond to the waves of the second family with the maximum flow rate for $\delta = 0.1$, 0.15, 0.2, 0.225, and 0.247.

1028-3358/01/4610-0760$21.00

and surface tension coefficient, respectively; and g is the gravitational acceleration.

The system involves one similarity parameter δ introduced in [4]. This allows the results to be suitable for an arbitrary fluid. In studies [2, 5, 6] and many others, solutions to Shkadov equations (1) provided a comprehensive description of all principal experimental data on spatially periodic nonlinear waves in a flowing-down thin layer. With an increase in the wavelengths L $\left(\text{or with decreasing the wave number } \alpha \equiv \frac{2\pi}{L}\right)$, special features of the instability of the periodic waves become pronounced and do not allow stable sequences of solitary waves to be obtained from such waves.

Together with a wave-free solution $h = 1$ and $q = 1$, we will consider the solutions for solitary and periodic waves. The steady motion of a wave having the velocity c in the coordinate system t and $\xi = x - ct$ is determined by the equation following from Eq. (1):

$$h^3h''' + \delta[6(q_0 - c)^2 - c^2h^2]h' + h^3 - q_0 - c(h-1) = 0. \quad (2)$$

A local flow rate in the steady wave can be found from its profile:

$$q = c(h-1) + q_0. \quad (3)$$

In the case of a solitary wave, the following asymptotic boundary conditions should be added to condition (3):

$$\xi \longrightarrow \pm\infty: h \longrightarrow 1. \quad (4)$$

The phase velocity c can be found as an eigenvalue for boundary value problem (2), (4) for $q_0 = 1$. The solution is numerically constructed by the method of matching the corresponding asymptotic expansions at points at infinity $\xi = \pm\infty$ [4].

In the case of a spatially periodic wave, Eq. (2) should be complemented by the periodicity conditions

$$h(\xi) = h(\xi + L), \quad h'(\xi) = h'(\xi + L), \quad h''(\xi) = h''(\xi + L), \quad \frac{1}{L}\int_{\xi}^{\xi+L} h\,d\xi = 1. \quad (5)$$

While solving the equations numerically, it is convenient to use the normalized wave number $s = \frac{\alpha}{\alpha_n}$, $\alpha_n = \sqrt{15\delta}$. In this case, the instability region for a basic wave-free flow is $s \in (0, 1)$. The phase velocity c and the mean flow rate q_0 for a nonlinear periodic wave are found as eigenvalues of boundary value problem described by Eq. (2) and conditions (5).

As was proved in [7], for every fixed δ, boundary value problem described by Eq. (2) with condition (4) has two denumerable sets of solutions $\gamma_{\pm m, j}$. Here, the sign in the subscript stands for a subset of fast (+) or slow (–) waves, $m = 1, 2, \ldots$, is the number of the solution, and $j = 1, 2$, denotes one of two possible varieties of the solitary wave with the number m, namely, with one or two principal humps.

The single-hump solitary wave of the elevation $\gamma_{+1, 1}$ has the highest phase velocity, and the single-hump solitary wave of indentation $\gamma_{-1, 1}$ has the lowest one. The solution to the boundary value problem described by Eq. (2) and condition (5) can be found in the form of the finite Fourier series:

$$h(x, t) = \sum_{k=-N}^{N} h_k \exp ik\xi, \quad h_k = \overline{h_{-k}}, \quad h_0 = 1,$$
$$q(x, t) = \sum_{k=-N}^{N} q_k \exp ik\xi, \quad q_k = \overline{q_{-k}}. \quad (6)$$

There are two denumerable sets of the periodic solutions $\gamma^n_{\pm m, j}$ for a given value of δ. Each family is represented by a smooth curve in the (s, c) plane. The family arises at the bifurcation point s_n and extends to $s \longrightarrow 0$, being transformed into the corresponding solitary wave $\gamma_{\pm m, j}$. In [8], two principally distinguishing families of solutions were selected and named the first and second families.

The first family $\gamma^1_{-1, 1}$ begins from a soft bifurcation at the point $s = 1$ and is finishes by the slowest single-hump solitary wave $\gamma_{-1, 1}$ as $s \longrightarrow 0$. The second family $\gamma^n_{+1, 1}$ branches as a rigid bifurcation at the point $s = s_b$ and ends with the fastest single-hump solitary wave. For small values of $\delta \le 0.096$, the bifurcation point of the second family is in the vicinity of $s \approx 1/2$; when δ increases, this point displaces to $s \longrightarrow 0$. There exists an ascending sequence of critical values of δ, above which a jump transition of s_b to the next lower value from the sequence $s \approx 1/3, 1/4, \ldots$ occurs. In this case, the solution of the second family is interchanged by the bifurcation point with the next family of the slow waves $\gamma^n_{-m, 1}$, which leads to the formation of families of intermediate bifurcations.

We now pay attention to the excitation of nonlinear waves by means of small perturbations at an initial time moment:

$$t = 0: h_k = h_k(0), \quad q_k = q_k(0). \quad (7)$$

The solution to Cauchy problem described by formulas (1), (5), and (7), is sought in the form of Fourier series (6), whose coefficients depend on t. The use of the Galerkin method leads to the formation of a dynamic system for h_k and q_k. In [9], on the basis of systematic numerical experiments for $s \ge 0.1$, we established a set of dominating waves composing a global attractor of periodic solutions to system (1). Every dominating wave is characterized by the fact that its

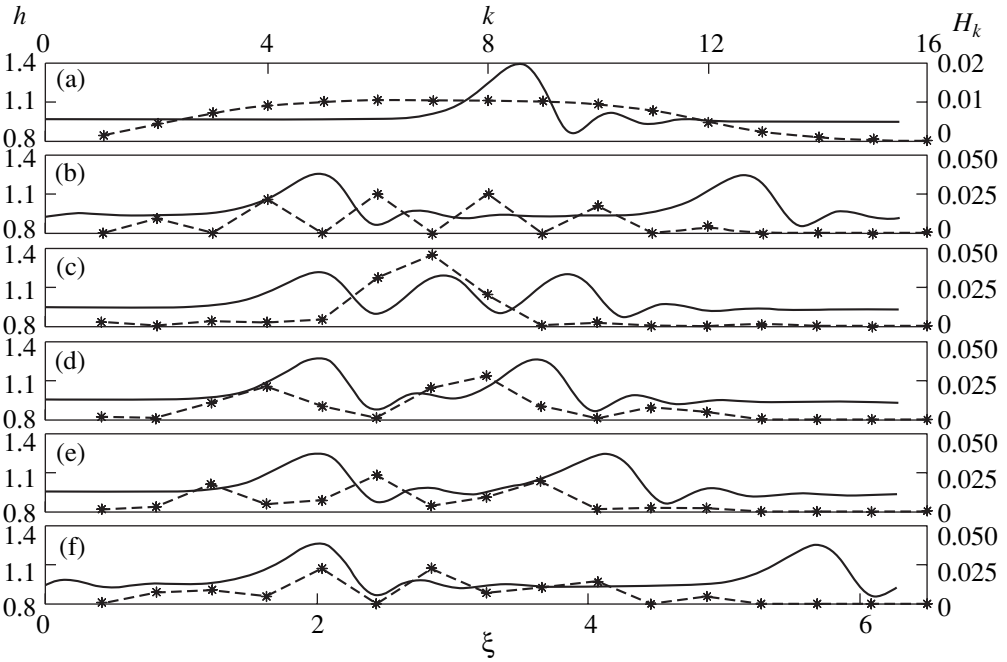

Fig. 2. Wave profiles for $\delta = 0.04$, $s = 0.15$: (a) $\gamma^{2}_{+1,1}$, $c = 3.7740$, $q_0 = 1.0327$; (b) $\gamma^{2,2}_{+1,1}$, $c = 3.3941$, $q_0 = 1.0319$; (c) Γ_1, $c = 3.2858$, $q_0 = 1.0275$; (d) Γ_2, $c = 3.4127$, $q_0 = 1.0317$; (e) Γ_3, $c = 3.3518$, $q_0 = 1.0310$; and (f) Γ_4, $c = 3.3909$, $q_0 = 1.0317$.

velocity, amplitude, and mean flow rate have maximum values among all regular waves existing for the values of (δ, s) under consideration.

The projection of the attractor onto the (s, c) plane represents a piecewise continuous curve with its pieces belonging to the different families, namely (in order of decreasing s) to the first, intermediate, and second families. In Fig. 1, we show the dominating waves for δ = 0.04, 0.1, 0.15, and 0.2, and the experimental boundaries of wave modes. The waves belonging to the second, intermediate, and first families are observed between curves *1* and *2*, *2* and *3*, and *3* and *4*, respectively.

3. The second-family solutions $\gamma^{n}_{+1,1}$ correspond to the solitary waves observed in experiments (Fig. 2). The translation along the branch of this family to $s \longrightarrow 0$ corresponds to the passage to a periodic sequence of solitary waves with the increasing spacings between their principal humps. The question is whether the attracting properties of the family $\gamma^{n}_{+1,1}$ are conserved for all small values of s. By virtue of these properties, the solutions of this family develop spontaneously from small initial perturbations of the wave-free flow.

The calculations of unsteady solutions to Eqs. (1) show that the attracting properties of the second solution are weakened for sufficiently small values $s < s_*(\delta)$ and that the global attractor consisting of the dominating waves is destroyed. The attracting solutions turn out to be waves of another type. In Fig. 3, we show two examples of the regular waves developing with time from small initial perturbations. For $s = 0.1125$ and $s = 0.165$, a small harmonic perturbation and a periodic wave with random small Fourier coefficients are used as initial conditions, respectively. The spontaneous transition from a wave with a period of $\frac{2\pi}{s}$ to shorter wavelengths with periods of $\frac{2\pi}{2s}$ and $\frac{2\pi}{3s}$ is a new observed phenomenon. It is possible to verify by the direct comparison that the principal parameters of the formed nonlinear waves, such as the phase velocity c, maximum height $h_{\max}$, and fluid flow rate q_0, differ slightly from the parameters of the corresponding dominating wave with the wave number $2s$ or $3s$. The similar evolutions of unsteady solutions arise only for $s < s_*(\delta)$. It was found that the critical values are $s_*(0.04) \approx 0.22$ [with $s_*(0.1) \approx 0.1$] and $s_*(0.04) \approx 0.115$ for the transitions $s \longrightarrow 2s$ and $s \longrightarrow 3s$, respectively.

The effect discovered manifests itself in the fact that the periodic sequence of waves, which is specified by the initial conditions and corresponds to the number s, is inconsistent with the flow, and the solution is spontaneously reconstructed into a sequence of waves with two shorter spacings between the humps, which are specified by the wave numbers $2s$ and $3s$.

Because the steady nonlinear waves with the wave numbers $2s$ and $3s$ represent invariant solutions, they must also be solutions to the nonlinear eigenvalue problem described by Eq. (2) and condition (5).

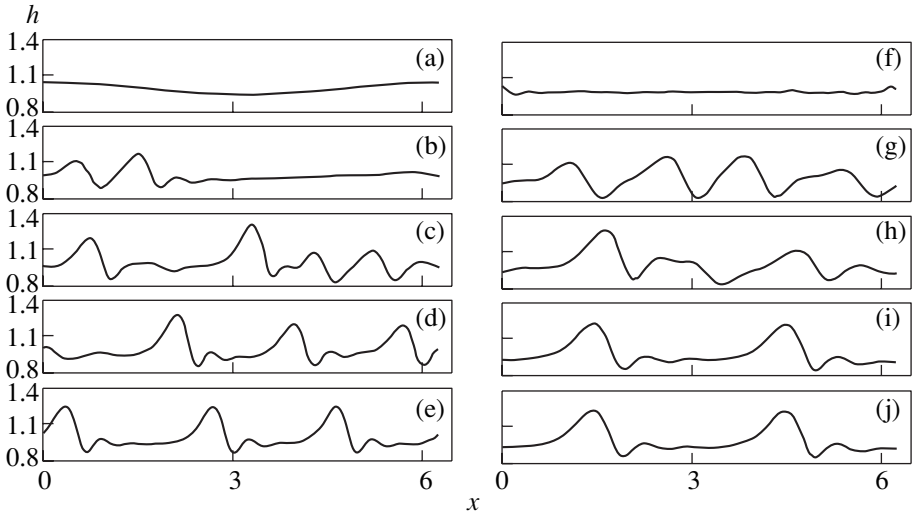

Fig. 3. Formation of solitary waves for δ = 0.04. Figures 3a to 3e correspond to $s = 0.1125$ and $t = 0$, 5, 10, 20, and 80; Figs. 3f to 3j correspond to $s = 0.165$ and $t = 0$, 10, 20, 40, and 80, respectively.

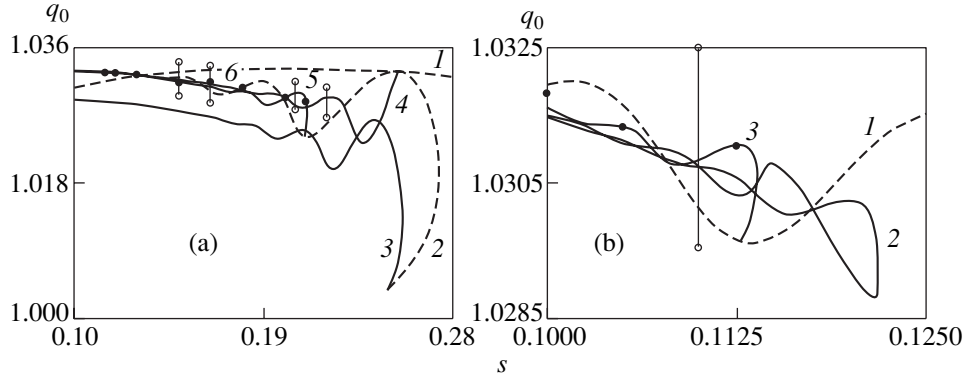

Fig. 4. Families of bifurcations of the second sequence for δ = 0.04. (a): (*1*) $\gamma^{2}_{+1,1}$, (*2*) $\gamma^{2,2}_{+1,1}$, (*3*) Γ_1, (*4*) Γ_2, (*5*) Γ_3, and (*6*) Γ_4. (b): (*1*) $\gamma^{2,3}_{+1,1}$, (*2*) Γ_5, and (*3*) Γ_6.

It should be noted that the foregoing branches of solutions bifurcate at the points s_n from the first family. This is associated with the existence of doubled solutions for this family. The solution with wave number s is repeated n times for the wave number $\frac{s}{n}$. Different branches of solutions originate in the vicinity of these points. We will refer to them as families of the first kind. The doubled families are possible also for other families of regular waves. In order to identify them, it is convenient to use the denotation $\gamma^{n,l}_{\pm m,j}$, where the additional superscript l implies the fact that an arbitrary solution $\gamma^{n}_{\pm m,j}$ calculated for a wave-number value s is considered over the period of $\frac{2\pi l}{s}$. In Fig. 4, we show the results of the bifurcation analysis of the second family in the (s, q_0) plane for δ = 0.04. The new families denoted as Γ_k, $k = 1, 2, \ldots, 6$, branch from the doubled families $\gamma^{2,l}_{+1,1}$, whose bifurcation points are $s = \frac{0.4961}{l}$ for $l = 1, 2$. For the doubled families and the families branching from them, the phase velocities and maximum heights of waves differ only slightly; their fluid flow rates are also very close, but these waves are different. In Fig. 3, we also show the spectral distributions $H_k = k^2|h_k|^2$, which are of importance for the identification of the families. The waves belonging to the families Γ_3 and Γ_4 have very similar shapes, differing only in the spacings between the principal humps, but their spectra are significantly different. In particular, the maximum values of H_k are attained for various harmonics. The important role of the spectral analysis in processing experimental results was indicated even in [1]; here, this idea turned out also to be fruitful for the numerical investigations of waves.

The circles in Fig. 4 show the attractors of system (1) for small parameters defining initial conditions. The closed circles mark the ultimate solutions whose integral characteristics, for example, the fluid flow rate and the wave velocity, attain constant values under the prolonged integration of Eq. (1). In the phase space h_k, $k = 1, 2, \ldots$, such solutions to the dynamic system obtained from Eq. (1) by the Galerkin method correspond to ultimate cycles. We note that the solutions belonging to the various families Γ_2, Γ_3, Γ_4, Γ_6, and $\gamma_{+1,1}^{2,3}$ serve as attractors for nearly equal small values of the wave number, but not the waves of the second family as is the case for finite values of s (see Fig. 2). The competition between close regular waves can lead to the formation of biperiodic and quasiperiodic oscillatory solutions, which are shown in Fig. 4 by connected open circles corresponding to the maximum and minimum values of the fluid flow rate. The alternation of almost coherent localized wave structures and disordered periodic waves is intrinsic to quasiperiodic solutions [10]. The trajectories on the invariant tori in the phase space h_k correspond to the biperiodic oscillating solutions.

4. Thus, while decreasing the wave number s, the passage to shorter structures corresponding to the wave numbers $2s$ and $3s$ takes place in the developing wave. In the formed sequence of solitary waves, the spacing between their humps is, on the average, less than a certain critical value corresponding to the wave number $s_*(\delta)$.

The calculation of the critical value $s_*(\delta)$, which can be principally carried out by numerically solving Eq. (1), encounters considerable calculational difficulties when δ increases. For estimating $s_*(\delta)$, we use an idea of [3] on optimal wave modes, which provide the maximum flow rate for a given mean thickness of the layer (or the maximum mean thickness for a given flow rate). We assume that the maximum value of $q_0(s)$ along the second family $\gamma_{+1,1}^{n}$ is attained at the point $s_*(\delta)$. This assumption is quite consistent with the numerical results obtained for two values of δ: $s_*(0.04) = 0.195$, $s_*(0.1) = 0.087$, and $s_*(0.15) = 0.080$.

In Fig. 1, the dots mark the parameters of the wave flow corresponding to the critical value $s_*(\delta)$ for $\delta = 0.1, 0.15, 0.2, 0.225$, and 0.247. For the two last values, s_* was found by extrapolation. It can be seen that all the points are placed virtually at the curve that specifies the upper experimental boundary of the existence of steady-state modes, with their wavelengths determined by periodic pulses in the initial cross section of the layer. In [5], Shkadov equations (1) in the formulation simulating the experimental conditions [1, 2] were numerically solved for given input perturbations with random frequencies. A unique cumbersome calculation concerns the variant $\delta = 0.217 q_0^{-11/9}$. The estimate of the maximum spacing between the humps in the wave chain formed downstream amounts to $L = 65$. This value correlates with the theory developed here; the corresponding point A is shown in Fig. 1.

ACKNOWLEDGMENTS

This work was supported by the Russian Foundation for Basic Research, project no. 00-01-00645.

REFERENCES

1. P. L. Kapitsa and S. P. Kapitsa, Zh. Éksp. Teor. Fiz. **19** (2), 105 (1949).
2. S. V. Alekseenko, V. E. Nakoryakov, and B. T. Pokusaev, *Wave Flows of Fluid Films* (Nauka, Novosibirsk, 1992).
3. V. Ya. Shkadov, Izv. Akad. Nauk SSSR, Mekh. Zhidk. Gaza, No. 1, 43 (1967).
4. V. Ya. Shkadov, Izv. Akad. Nauk SSSR, Mekh. Zhidk. Gaza, No. 1, 63 (1977).
5. H.-C. Chang, E. A. Demekhin, and E. Kalaidin, J. Fluid Mech. **294**, 123 (1995).
6. V. Ya. Shkadov and G. M. Sisoev, in *Proceedings of the IUTAM Symposium on Nonlinear Waves in Multi-Phase Flows, Notre Dame, USA, 1999*, pp. 1–10.
7. A. V. Bunov, E. A. Demekhin, and V. Ya. Shkadov, Vestn. Mosk. Univ., Ser. 1: Mat., Mekh., No. 2, 73 (1986).
8. A. V. Bunov, E. A. Demekhin, and V. Ya. Shkadov, Prikl. Mat. Mekh. **48** (4), 691 (1984).
9. G. M. Sisoev and V. Ya. Shkadov, Izv. Akad. Nauk, Mekh. Zhidk. Gaza, No. 6, 30 (1997).
10. G. M. Sisoev and V. Ya. Shkadov, Dokl. Akad. Nauk **363** (4), 489 (1998).

Translated by V. Bukhanov